Multipactor and long-pulse phenomena

Benito Gimeno Martínez[1,2] and co-workers

[1]Department of Applied Physics and Electromagnetics – ICMUV, University of Valencia (Spain)

[2] European Space Agency - Val Space Consortium, Valencia (Spain)

International Workshop on Breakdown Science and High Gradient Technology
HG2017 - June 13-16, 2017 - Valencia, Spain

Index

- Introduction
- Objectives
- Multipactor simulation algorithm
- Results

Index

- Introduction
- Objectives
- Multipactor simulation algorithm
- Results

1. Introduction

What is the multipactor effect?

Multipactor breakdown is an electron avalanche-like discharge occurring in components operating under vacuum conditions and high-power RF electromagnetic fields.

Galileo constellation satellite

INTA-NASA center (Madrid)

DESY (Hamburg, Germany)

TWT = Traveling Wave Tube

1. Introduction

- Solar activity causes a continuous flux of high energy elemental particles towards the spaceships.
- These particles can penetrate in the satellites, reaching the electromagnetic field region of the passive RF components and leading to a very harmful multipactor discharge.

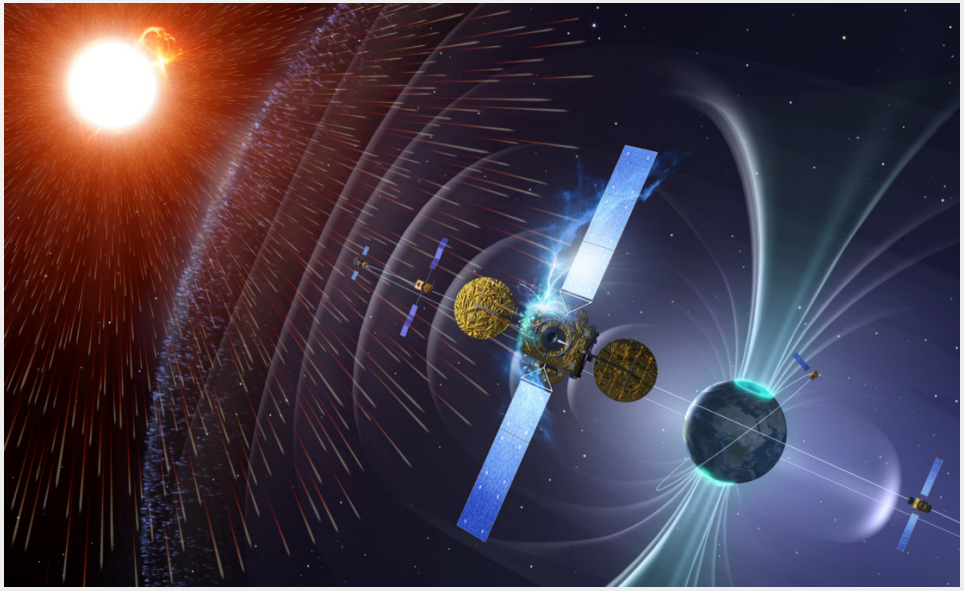

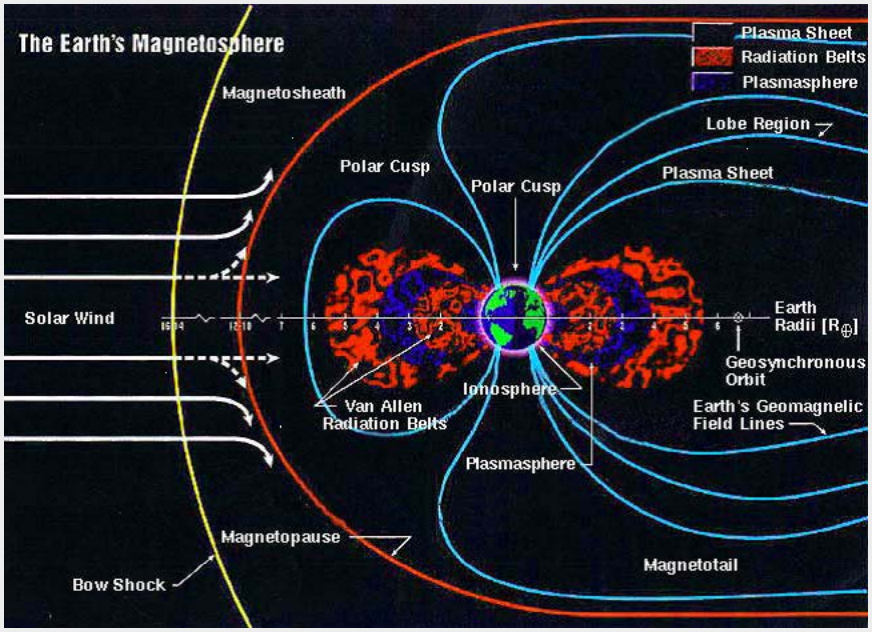

I. Introduction

How is the discharge produced?

Basic steps:

- Free electrons reach the RF electromagnetic field zone.
- Electrons are accelerated by the RF electric field towards metallic walls of the device.
- Each colliding electron may release one or more secondary electrons from the metallic surface.
- RF electric field changes polarity and those new electrons released are pushed towards opposite wall.
- This chain reaction causes an exponential growth in the electron population inside the device leading to a multipactor discharge .

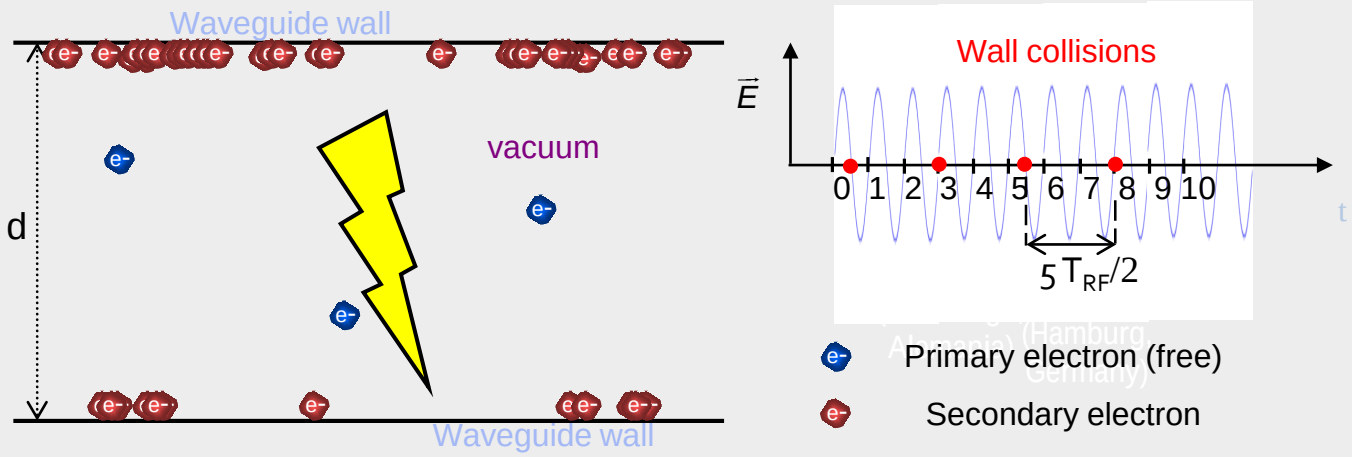

I. Introduction

Effects of a multipactor discharge on the device

- Increase of signal noise
- Increase of reflected power
- Heating up of device walls
- Detuning of resonant cavities
- Physical damages

→ Degradation of the device performance

↓

Limitation of the managed RF power

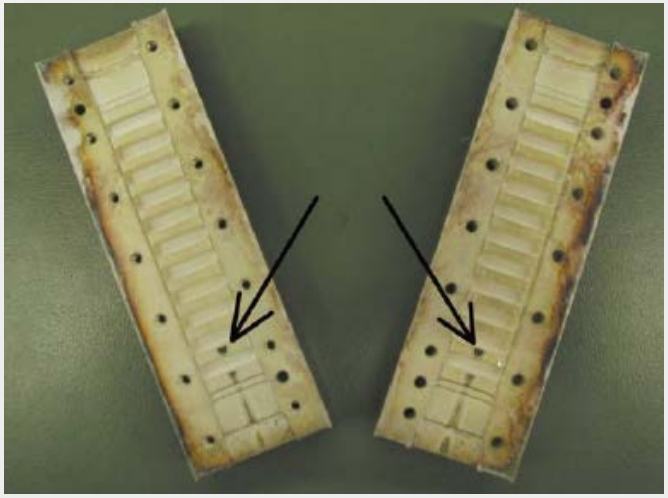

Low-pass filter

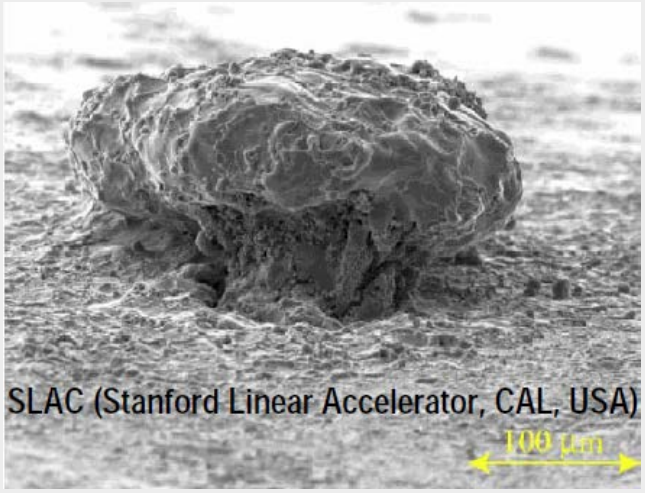

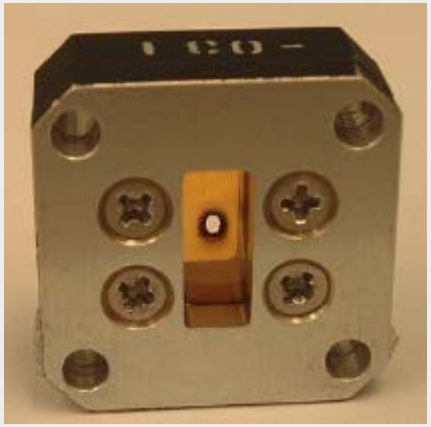

Kapton window

1. Introduction

- In this undesired scenario the space agencies have to control and predict the possible existence of a multipactor discharge occurring within on-board microwave sub-systems: replacement of equipments is NOT POSSIBLE in a satellite…

- Due to this, assessment of the multipactor risk in the design process of satellite devices is crucial to avoid the appearance of the discharge during its operation.

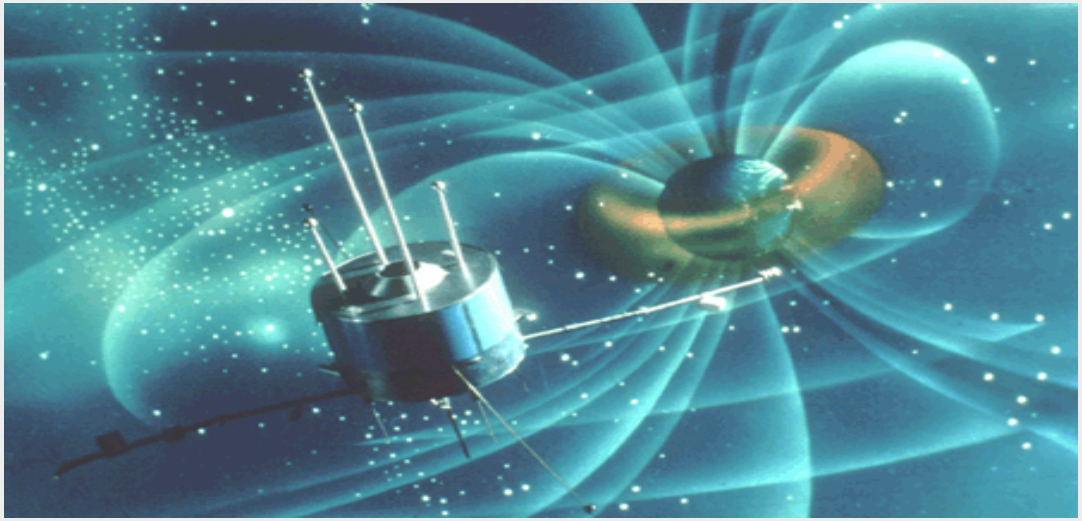

I. Introduction

Multipactor theory in parallel-plate waveguide ("constant-v" theory)

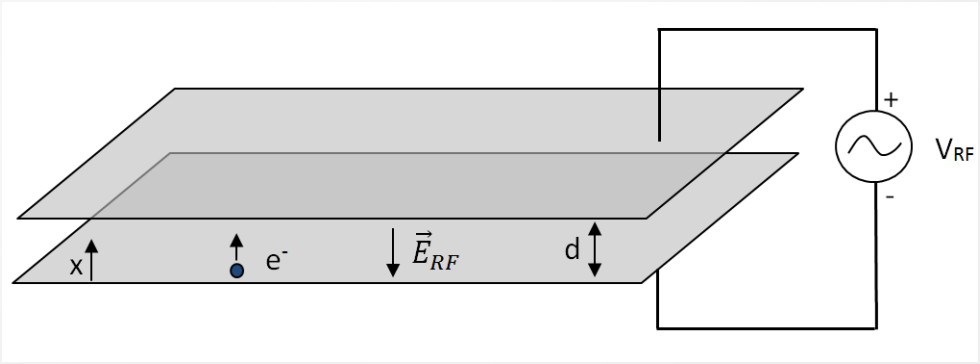

Scheme of a parallel plate waveguide

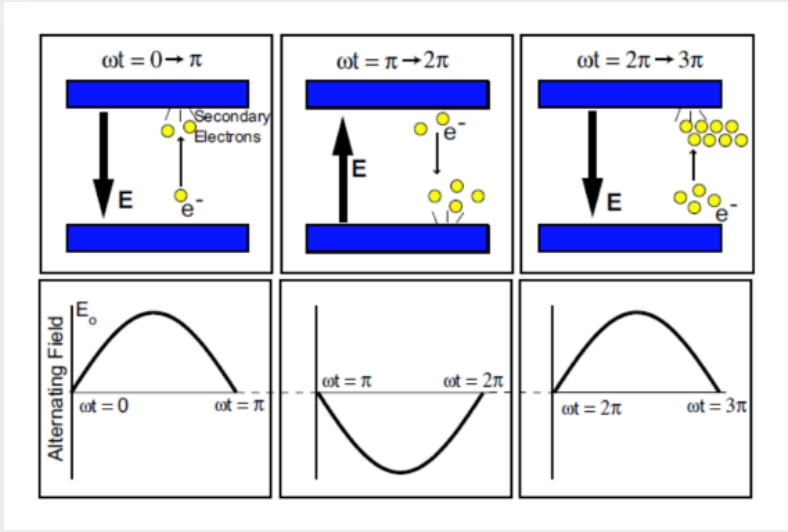

Basics steps of the multipactor discharge

Excitation field $\vec{E}_{RF} = -\frac{V_0}{d}\sin\omega t\,\hat{x}$

Non-relativistic Lorentz force $\vec{F}_L = -e\vec{E}_{RF}$

Differential equation of motion $\ddot{x} = \frac{eV_0}{m_e d}\sin\omega t$

$\omega = 2\pi f$ f is the RF frequency

$-e$ is the electron charge

m_e is the electron mass

Initial conditions

$$\left.\begin{array}{l}\omega t_0 = \phi \\ \dot{x}(t_0) = v_0 \\ x(t_0) = x_0\end{array}\right\} \Longrightarrow$$

$$x = x_0 + \frac{v_0}{\omega}(\omega t - \phi) + \frac{eV_0}{m_e\omega^2 d}[(\omega t - \phi)\cos\phi - \sin\omega t + \sin\phi]$$

$$v = v_0 + \frac{eV_0}{m_e\omega d}(\cos\phi - \cos\omega t)$$

1. Introduction

Multipactor theory in parallel-plate waveguide (II)

Conditions for the multipactor discharge:

1. Synchronism between the electron and the RF electric field. ⟶ $\omega t_i = \phi + m\pi \;;\; m = 1, 3, 5, 7, \ldots$

2. Proper impacting energy to release secondary electrons.

$$W_1 < W < W_2$$

t_i , impacting time

m , multipactor order (number of half-periods that takes the electron to cross the gap)

Secondary electron emission coefficient

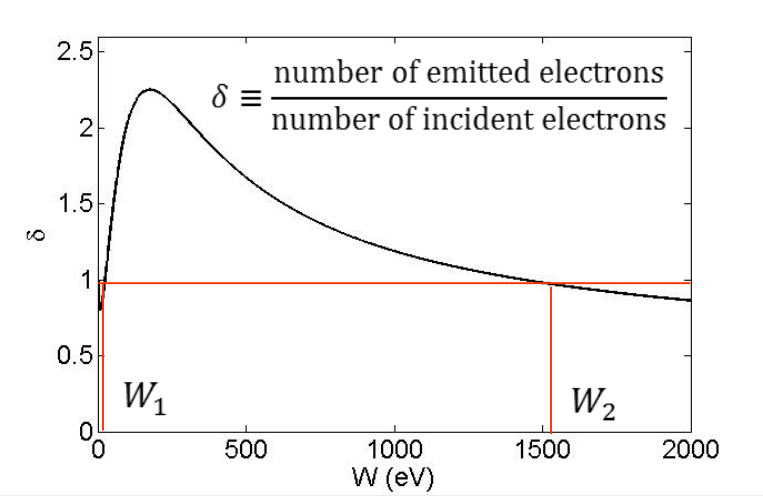

Example of electron trajectory and velocity for m = 1

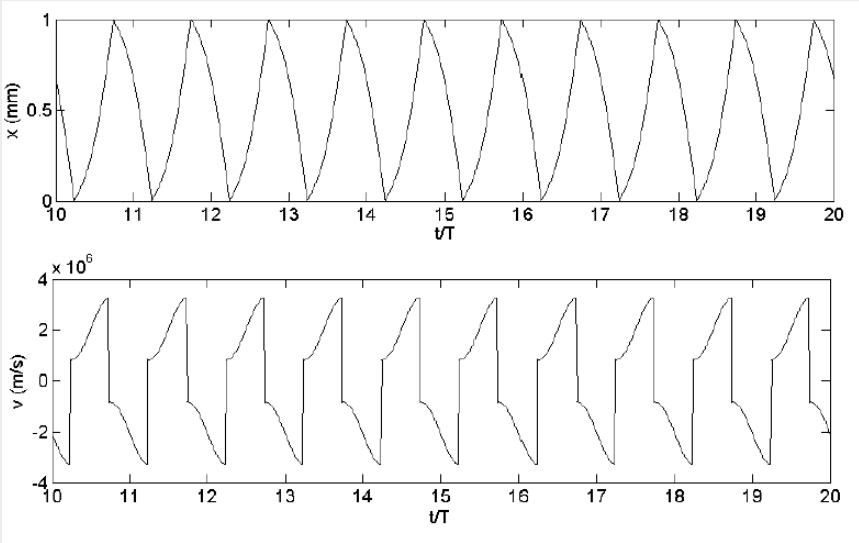

1. Introduction

Multipactor theory in parallel-plate waveguide (III)

$$x = x_0 + \frac{v_0}{\omega}(\omega t - \phi) + \frac{eV_0}{m_e \omega^2 d}[(\omega t - \phi)\cos\phi - \sin\omega t + \sin\phi]$$

$$v = v_0 + \frac{eV_0}{m_e \omega d}(\cos\phi - \cos\omega t)$$

$$\omega t_i = \phi + m\pi \quad ; m = 1, 3, 5, 7, \ldots \Rightarrow V_0 = \frac{m_e}{e}\frac{\omega d(\omega d - m\pi v_0)}{m\pi\cos\phi + 2\sin\phi}$$

$$v_f = v_0 + \frac{2eV_0}{m_e \omega d}\cos\phi$$

In order to ensure the synchronism the RF phase must be within a certain range $\phi_{min} \leq \phi \leq \phi_{max}$

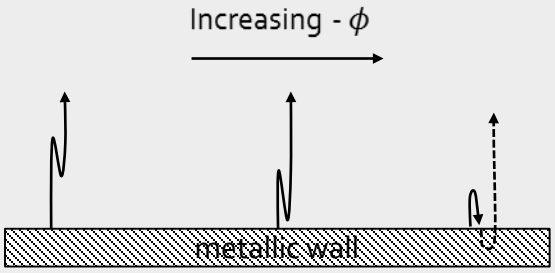

Non-return limit

$$\left.\begin{matrix} x = 0 \\ v = 0 \end{matrix}\right\} \rightarrow \phi_{min}$$

The system has not analytical solution

ϕ_{max} is chosen as the value that minimizes the resonant voltage V_0

$$\phi_{max} = \tan^{-1}\left(\frac{2}{m\pi}\right)$$

1. Introduction

Multipactor theory in parallel-plate waveguide (IV)

$$W_1 < W < W_2 \quad \Rightarrow \quad (v_1 - v_0)\frac{m_e \omega d}{2e\cos\phi} \leq V_0 \leq (v_2 - v_0)\frac{m_e \omega d}{2e\cos\phi}$$

After imposing the conditions for the onset of the multipactor discharge it is possible to obtain the multipactor susceptibility chart

For the parallel-plate waveguide the multipactor zones only depend on the frequency gap product

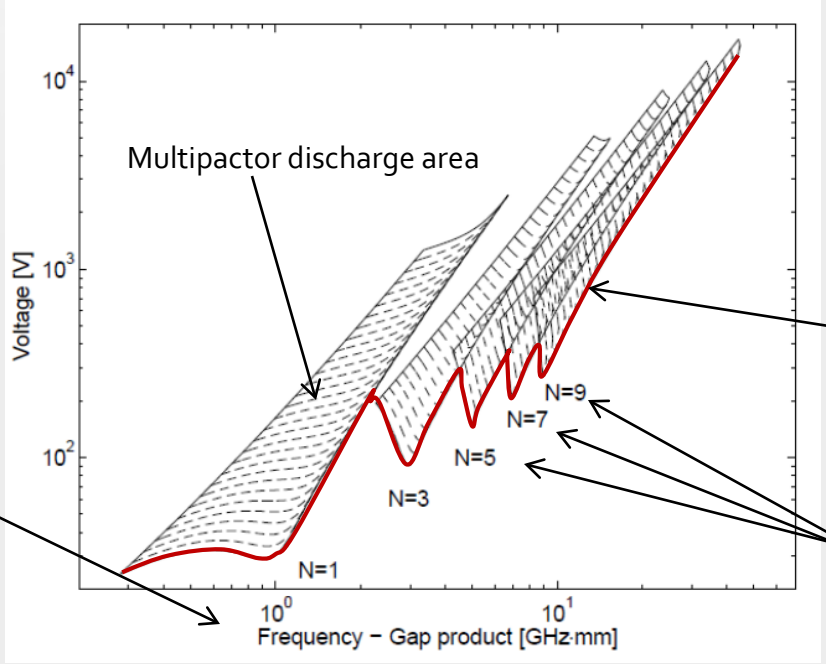

Multipactor susceptibility chart extracted from [1]

The lower envelope of the multipactor zones is named as the multipactor voltage threshold

Higher multipactor modes appear when the frequency gap increases

[1] R. Udiljak, "Multipactor in low pressure gas", Master's thesis, Chalmers University of Technology, Goteborg, Sweden, 2004.

1. Introduction

Multipactor growth model for parallel-plates

As we have just seen for parallel-plate waveguides:

- The multipactor resonant electrons cross the gap between surfaces in an odd number of half-periods of the RF signal (m = 1, 3, 5, 7…)
- The value of the SEY coefficient δ will be the same in the successive impacts due to periodic trajectory and velocity of the resonant electron

Under these assumptions, the evolution of the electron population with time can be obtained as follows:

N_0, electron population at t = 0
N_n electron population after the *n*-th impact
δ SEY at the collisions

$$N_1 = N_0\delta$$

$$N_2 = N_1\delta = N_0\delta^2$$

$$N_n = N_0\delta^n = N_0 e^{n\ln\delta}$$

$$t_n = n\frac{m}{2f}$$

Time of the n-th impact

$$N(t_n) = N_0 e^{t_n\frac{2f}{m}\ln\delta} = N_0 e^{\alpha t_n}$$

$$\alpha = \frac{2f}{m}\ln\delta$$

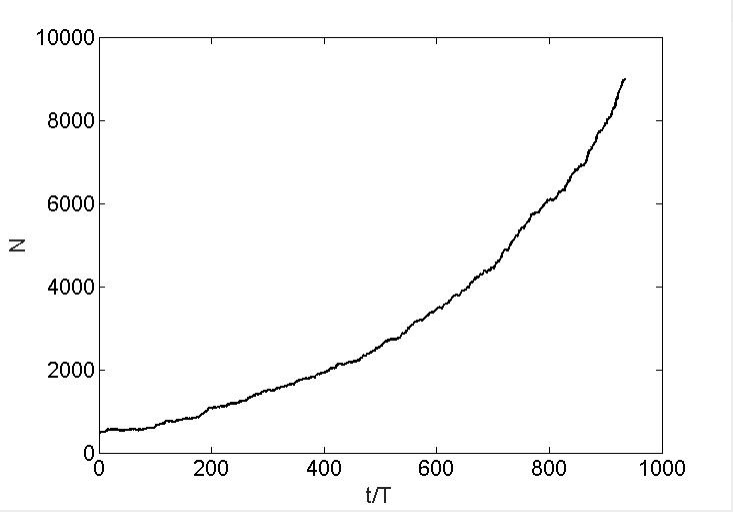

Results for numerical simulations for the electron population as a function of the normalized time

1. Introduction

Multipactor experimental set-up

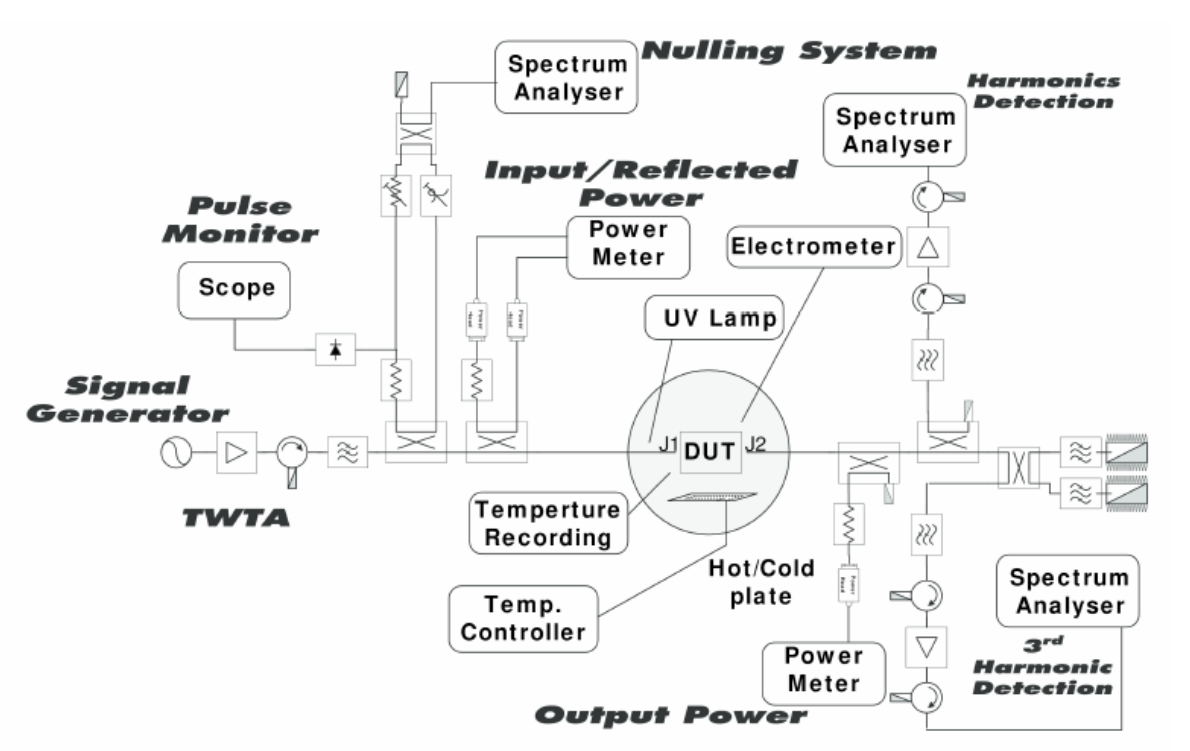

Nulling system

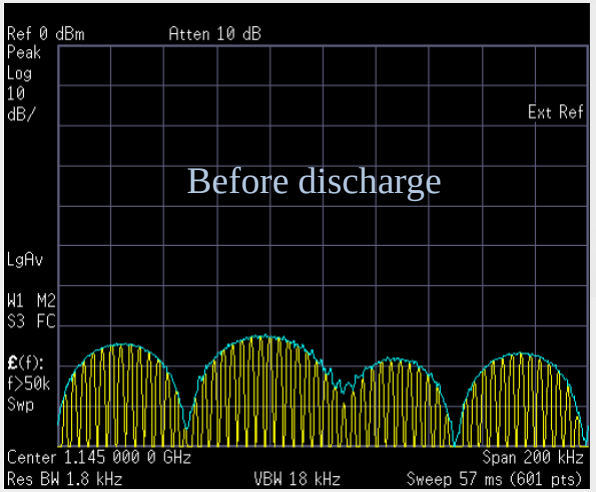

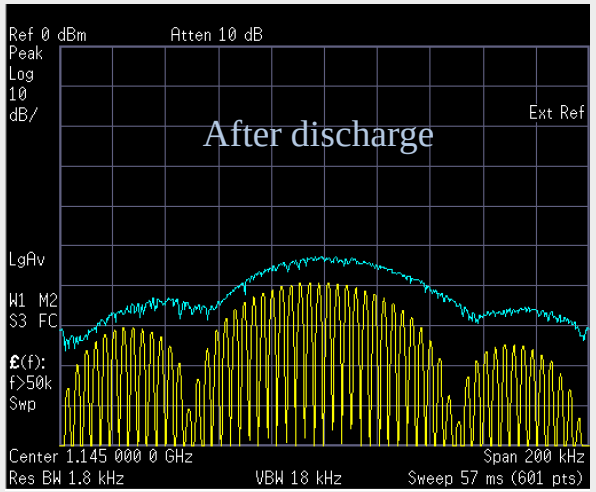

Free electrons sources:

- UV lamp
- Radioactive source
- Regulated electron gun

Multipactor detection methods:

- Electron probe
- Nulling system
- Third harmonic detection

Index

- Introduction
- Objectives
- Multipactor simulation algorithm
- Results

II. Objectives

The objective of this presentation is to study the multipactor effect in microwave waveguides. Concretely the following topics will be considered:

- Mitigation of the multipactor discharge in coaxial transmission lines by means of an external magnetostatic field
- Study of the multipactor effect in ridge and multi-ridge waveguides
- Analysis of the multipactor breakdown in coaxial lines excited with digital modulated signals
- Multipactor with ferrite materials: parallel-plate waveguide loaded with a magnetized ferrite slab

Index

- Introduction
- Objectives
- Multipactor simulation algorithm
- Results

III. Multipactor simulation algorithm

Basic block diagram of the Monte-Carlo multipactor prediction tool

Input data:

- Waveguide dimensions
- RF frequency
- Signal type
- Initial number of electrons
- Maximum simulation time
- Discharge criteria
- RF voltage

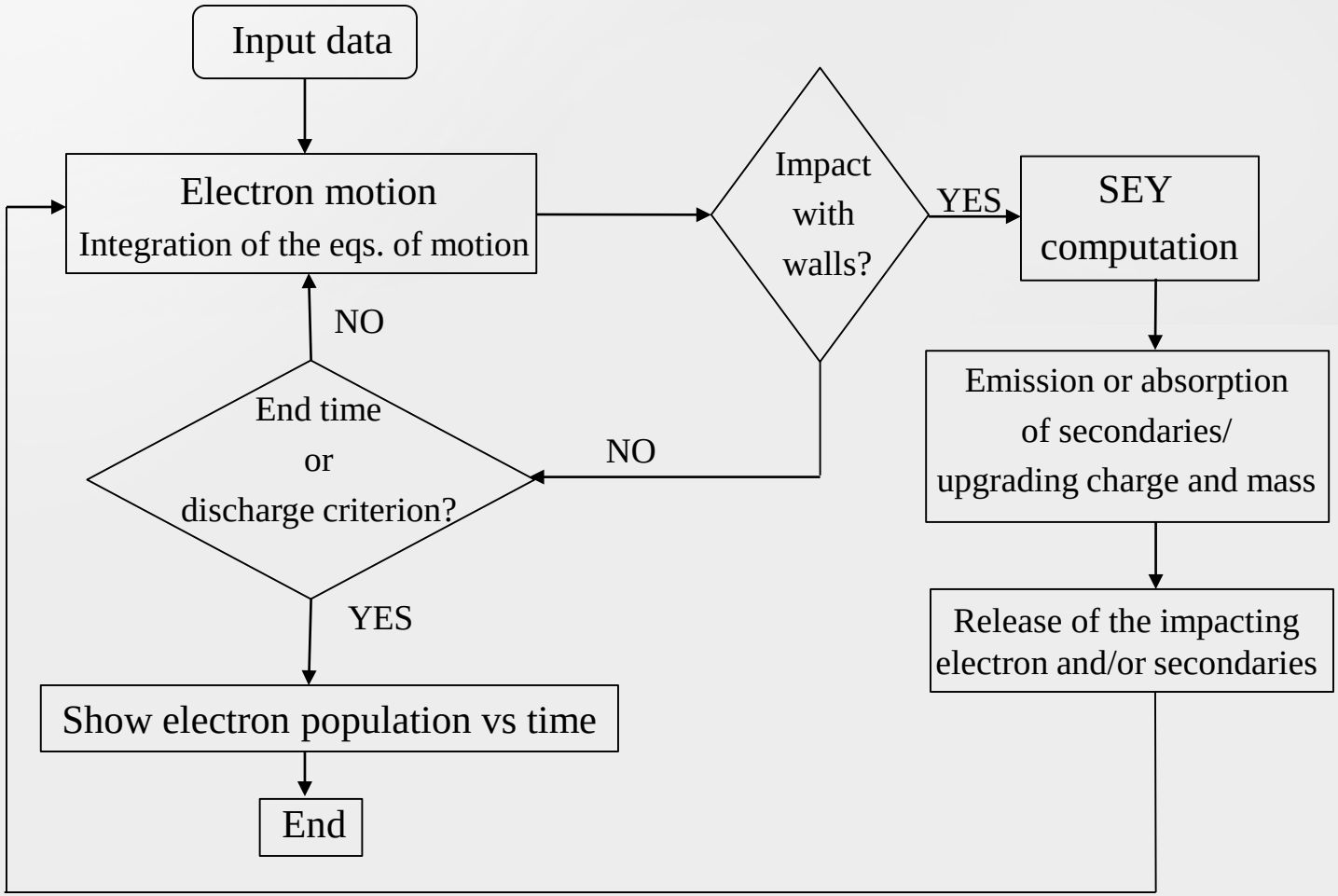

III. Multipactor simulation algorithm

Electron dynamics

- The electron dynamics is described by the relativistic Lorentz Force:

$$\vec{F}_L = q\left(\vec{E} + \vec{v} \times \vec{B}\right) = \frac{d\vec{p}}{dt} \qquad \vec{p} = m_0 \gamma \vec{v} \qquad \gamma = 1/\sqrt{1-(v/c)^2}$$

where m_o is the electron mass at rest, q=-e is the electron charge, *v* is the magnitude of the velocity vector, γ is the relativistic factor, $\vec{E}$ and $\vec{B}$ are the total electric and magnetic field existing within the device

$$\vec{E} = \vec{E}_{RF} + \vec{E}_{sc} + \vec{E}_{pol} \qquad \vec{B} = \vec{B}_{RF} + \vec{B}_{dc}$$

where $\vec{E}_{RF}$ and $\vec{B}_{RF}$ are the RF electric and magnetic field, $\vec{E}_{sc}$ arises due to the space charge effect of the electron cloud, $\vec{E}_{pol}$ appears when a dielectric surface emits or absorbs electrons in an unbalanced way, $\vec{B}_{dc}$ is an external magnetic field applied in certain circumstances (e. g. for magnetize a ferrite or for multipactor mitigation purposes

III. Multipactor simulation algorithm

Electron dynamics (II)

- The typical electron velocities in the spacial communication systems are quite below the value of the speed of light in vacuum and, as a consequence, the relativistic formulation can be approximated considering that $\gamma \approx 1$,

$$\vec{F}_L = q\left(\vec{E} + \vec{v} \times \vec{B}\right) = m_0 \vec{a}$$

Finally, the problem can be expressed as a linear system of coupled second order differential equations:

$$\vec{F}_L = q\left(\vec{E} + \vec{v} \times \vec{B}\right) = m_0 \frac{d\vec{v}}{dt} = m_0 \frac{d^2\vec{r}}{dt^2}$$

which has to be numerically solved.

- To do that, a Velocity-Verlet algorithm was employed to solve the differential equations (≈ 300 integration steps per RF carrier period):

  - Accurate
  - Efficient
  - Stable

L. Verlet, "Computer 'experiments' on classical fluids. I. Thermodynamical properties of Lennard–Jones molecules," Phys. Rev., vol. 159, no. 1, pp. 98–103, Jul. 1967.

III. Multipactor simulation algorithm

Space charge and polarization electric field (parallel-plate waveguide)

- The coulombian repulsion among the electrons (space charge effect) is taken into account by considering that the electric charge due to the increase in the electron population is accumulated in a single electron sheet of negligible thickness placed in the middle-gap of the waveguide.
- The polarization electric field in the ferrite slab appears when it becomes electrically charge as a consequence of the emission/absorption of secondary electrons.

$$\vec{E}_{sc} = \begin{cases} -\dfrac{\rho_{sc}}{2\varepsilon_0\left(1+\dfrac{h}{\varepsilon_r d}\right)}\hat{y} & h \le y \le h + {}^{d}/_{2} \\ \dfrac{\rho_{sc}}{\varepsilon_0}\left[1-\dfrac{1}{2\left(1+\dfrac{h}{\varepsilon_r d}\right)}\right]\hat{y} & h + {}^{d}/_{2} \le y \le h + d \end{cases}$$

$$\vec{E}_{pol} = \frac{\rho_{sd}}{\varepsilon_0}\left[1-\frac{1}{\left(1+\dfrac{h}{\varepsilon_r d}\right)}\right]\hat{y} \qquad h \le y \le h + d$$

$$\rho_{sc} = -\frac{eN(t)}{A}$$

$$\rho_{sd} = \frac{eN_{ext}(t)}{A}$$

A: multipactor discharge area

N: electron population within the waveguide

N_{ext}: number of electrons extracted from the ferrite slab

Gauss's Law in the vacuum $\longrightarrow$ $\oint_{\partial V} \vec{E}\cdot d\vec{A} = \frac{1}{\epsilon_o}\int_V \rho\, dV$

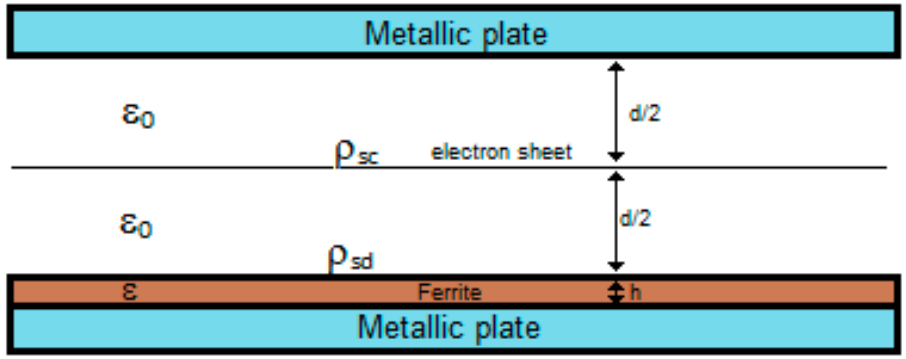

Scheme of the ferrite loaded parallel-plate waveguide with the space charge electron sheet

III. Multipactor simulation algorithm

Space charge electric field (coaxial line)

- Similarly as for the parallel-plate waveguide, it is assumed that the electric charge is accumulated in a single electron sheet of negligible thickness located in the center of the gap of the coaxial waveguide and charged with a surface electron density $\rho_s(t)$.

Gauss's Law in the vacuum $\longrightarrow$ $\oint_{\partial V} \vec{E} \cdot d\vec{A} = \frac{1}{\epsilon_o} \int_V \rho \, dV$

$\Downarrow$

Electric field due to the space-charge $\rightarrow$

$$\vec{E}_{sc}(\vec{r},t) = \begin{cases} -\frac{r_s}{r}\frac{\rho_s(t)}{\varepsilon_0}\frac{\ln\left(\frac{b}{r_s}\right)}{\ln\left(\frac{b}{a}\right)}\hat{r} & a \le r \le r_s \\ \frac{r}{r_s}\frac{\rho_s(t)}{\varepsilon_0}\frac{\ln\left(\frac{r_s}{a}\right)}{\ln\left(\frac{b}{a}\right)}\hat{r} & r_s \le r \le b \end{cases}$$

Surface charge electrical density of the electron sheet $\longrightarrow$ $\rho_s(t) = \frac{eN(t)}{2\pi r_s h}$

$r_s = (a+b)/2$: radius of the electron sheet

N(t): electron population at time t

h: sheet height

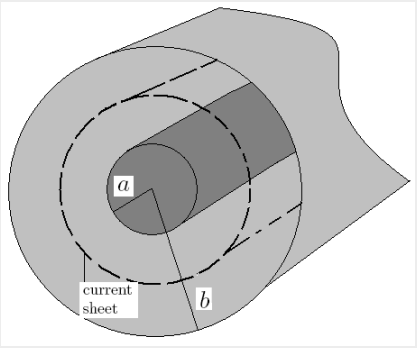

Scheme of the coaxial transmission line and the single electron sheet

III. Multipactor simulation algorithm

Interaction electron-surface

- When an electron collides with the devices surfaces, the interaction between them is modelled by means of the Secondary Electron Yield (SEY) coefficient δ, which is defined as

$$\delta \equiv \frac{\text{number of emitted electrons}}{1\,\text{impacting electron}}$$

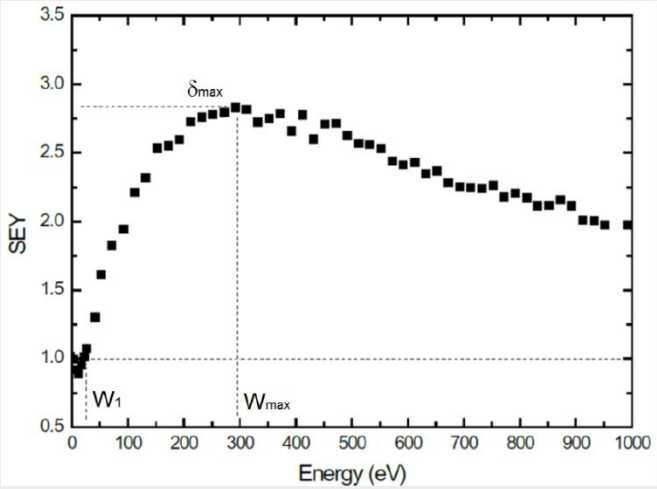

Experimental SEY curve

- The SEY coefficient depends on:
  - Kinetic energy of the primary electron (W)
  - Incidence angle of primary electron (ξ)
  - Surface roughness

- Despite the concrete values of the SEY coefficient are different for each material, the shape of the SEY curve is universal for all of them (metal, dielectrics, ferrite).

- There are several models to parameterize the SEY curve. In this work, depending on the multipactor scenario, two different models have been employed: the Furman and Pivi model and the modified Vaughan's model.

III. Multipactor simulation algorithm

Furman and Pivi SEY model[1,2]

When an electron individual collides with a surface it can be:

- Elastically backscattered
- Inelastically backscattered
- Absorbed
- Generate true secondaries

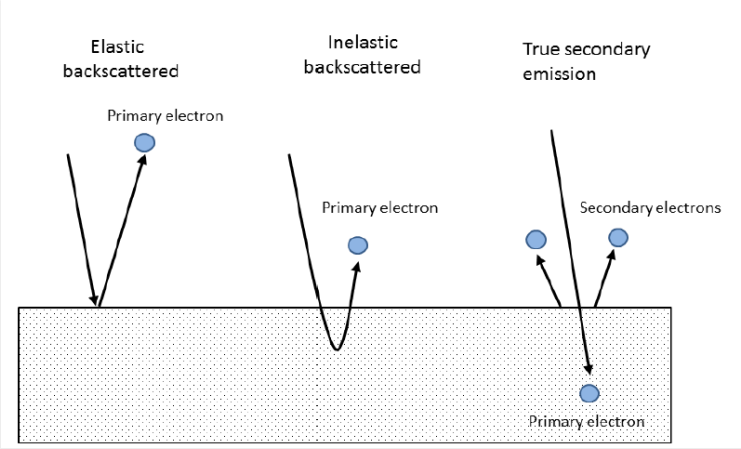

Different components of the secondary electron emission

Contribution of elastically backscattered electrons

$$\varepsilon(E_p) = \frac{\varepsilon_1}{1+\frac{E_p}{E_{e1}}} + \frac{\varepsilon_2}{1+\frac{E_p}{E_{e2}}}$$

Contribution of true secondaries

$$\delta(E_p) = \delta_m \frac{s\frac{E_p}{E_m}}{s-1+\left(\frac{E_p}{E_m}\right)^s}$$

Contribution of inelastically backscattered electrons

$$\eta(E_p) = a(1-bE_p){E_p}^{\gamma} exp\left(-\left(\frac{E_p}{E_m}\right)^{\mu}\right)$$

E_p is the primary electron energy

$E_b = c + Zd \;\; b = 3.0 \times 10^{-5}, c = 300, d = 175$

$\gamma = 0.56 \;\; \mu = 0.70$

$a \in [7 \times 10^{-3}, 10 \times 10^{-3}]$

$\varepsilon_1 = \varepsilon_0 - \varepsilon_2$

$\varepsilon_2 = 0.07, E_{e1} = g/\sqrt{Z}\,, E_{e2} = hZ^2$

$g = 50, h = 0.25$

ε_0 elastic contribution for $E_p = 0$

Z is the atomic number

$\delta_m, E_m,$ and s are parameters of the material

[1] M. A. Furman and M. T. Pivi, "Probabilistic model for the simulation of secondary electron emission", Physical Review Special Topics- Accelerators and Beams, vol. 5, 124404 (2002).

[2] J. de Lara, F. Perez, M. Alfonseca, L. Galan, I. Montero, E. Roman, D.R. Garcia-Baquero, "Multipactor prediction for on-board spacecraft RF equipment with the MEST software tool", IEEE Transactions on Plasma Science, vol. 34, no. 2, pp. 476-484, April 2006.

III. Multipactor simulation algorithm

Furman and Pivi SEY model (II)

Angular dependence for the different contributions:

$$\eta(E_p,\varphi) = \eta(E_p)^{\cos\varphi} {C_1}^{1-\cos\varphi}$$

$$\varepsilon(E_p,\varphi) = \varepsilon(E_p)^{\cos\varphi} {C_2}^{1-\cos\varphi}$$

$$\delta(E_p,\varphi) = \delta(E_p)\frac{k+1}{k+\cos\varphi}$$

$$C_1 = \chi\frac{\eta(E_p)}{\eta(E_p)+\varepsilon(E_p)}$$

$$C_2 = \chi\frac{\varepsilon(E_p)}{\eta(E_p)+\varepsilon(E_p)}$$

$$C_1 + C_2 = \chi$$

$\chi = 0.89$

$k = pZ + r, p = 0.0027$ For a clean flat surface, $r = 0$

Z= atomic number

The probability for each kind of emission is given by:

- Elastic $P_e(E_p,\varphi) = \varepsilon(E_p,\varphi)$
- Inelastic $P_b(E_p,\varphi) = \eta(E_p,\varphi)$
- True Secondaries $P_s(E_p,\varphi) = 1 - P_e(E_p,\varphi) - P_b(E_p,\varphi)$

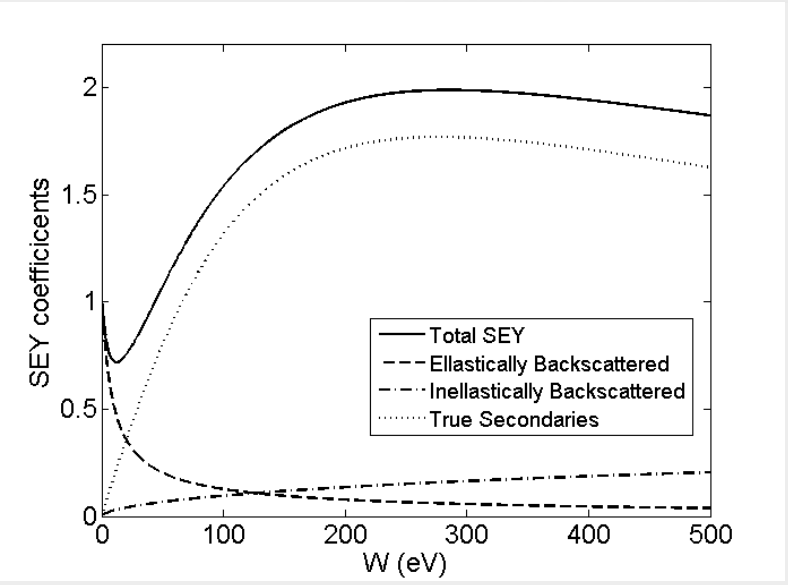

Different contributions to the SEY coefficient

III. Multipactor simulation algorithm

Modified Vaughan's SEY model

This model does not distinguish among the different contributions or interactions, only provides the total SEY coefficient

Kinetic energy of impacting electron

Incidence angle measured from the normal to the surface

$$\delta(W,\xi) = \begin{cases} \delta_{low} & \text{if} \quad \gamma < 1 \\ \delta_{max}(\xi)\left(\gamma e^{(1-\gamma)}\right)^{0.25} & \text{if} \quad 1 < \gamma \leq 3.6 \\ \delta_{max}(\xi)\dfrac{1.125}{\gamma^{0.35}} & \text{if} \quad \gamma \geq 3.6 \end{cases}$$

Parameter obtained from continuity conditions of SEY

Maximum SEY value at normal incidence

$$\gamma = \frac{W - W_0}{W_{max}(\xi) - W_0}$$

Factors related to the surface roughness

$$\delta_{max}(\xi) = \delta_{max}(0)\left(1 + \frac{k_W \xi^2}{2\pi}\right)$$

$$W_{max}(\xi) = W_{max}(0)\left(1 + \frac{k_\xi \xi^2}{2\pi}\right)$$

$$0 \leq \delta_{low} \leq 1$$

Kinetic impact energy at $\delta_{max}(0)$

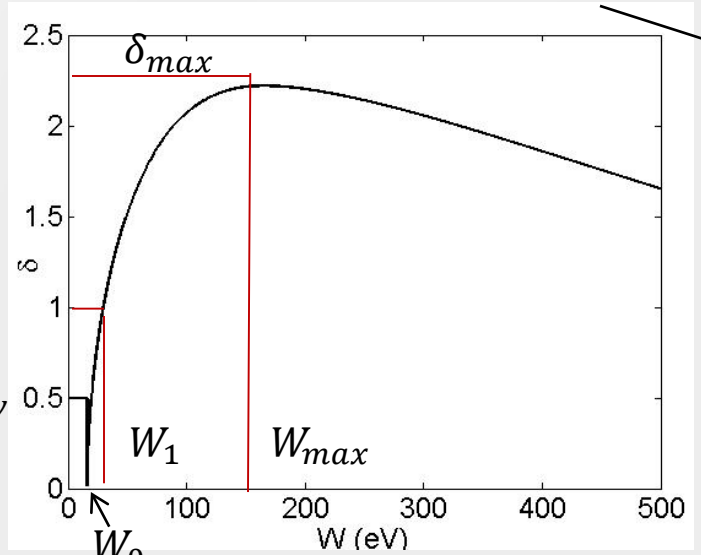

III. Multipactor simulation algorithm

Electron model

In this work, it has been considered two different electron models depending on the specific scenario: the effective and the individual electron models.

Effective electron:

- This model consists of the 3D tracking of a set of N_e effective electrons
- Each effective electron has associated an electron population N_i which is upgraded when the electron collides with the device walls

$$N_i(t + \Delta t) = N_i(t)\delta_i$$

i-th electron population after the impact

electron population before the impact

$$N_i(t) = \prod_{j=1}^{k} \delta_i{}^{(j)}$$

$\delta_i{}^{(j)}$ is the SEY value of the j−th impact of the i−th electron

Total electron population within the device $\longrightarrow$ $N(t) = \sum_{i=1}^{N_e} N_i(t)$

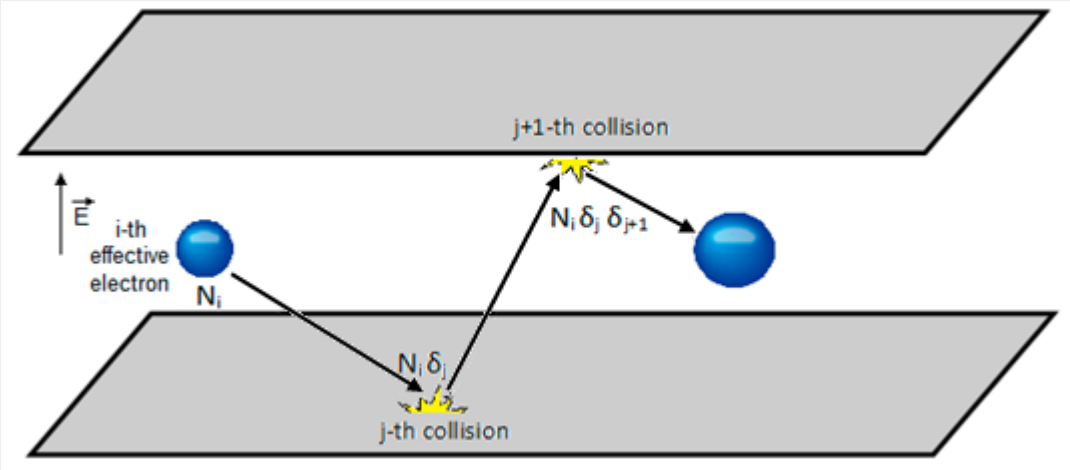

Scheme of the effective electron model

III. Multipactor simulation algorithm

Effective electron (II)

- The modified Vaughan's SEY model is implemented with the effective electron model
- After the collision, the effective electron is launched back from the impact point. The velocity and angle of the released electron depends on the impact kinetic energy of the primary electron:
  - If the impact kinetic energy $W < W_0$: effective electron is elastically reflected as in a specular reflection (the magnitude and the angle of the velocity vector with regard the normal plane to the impact surface do not change).
  - If the impact kinetic energy $W \geq W_0$: the effective electron is treated as a true secondary electron. It implies that:
    1. The output kinetic energy of the effective electron is calculated by means of a Rayleigh probability distribution density:

$$\eta(W_s) = \frac{W_s}{{W_g}^2} exp\left(-\frac{{W_s}^2}{2{W_g}^2}\right)$$

Normalization condition $\longrightarrow$ $\int_0^\infty \eta(W_s)\, dW_s = 1$

W_s = Departure energy of the secondary electron

$\eta(W_s)$ = Probability of release a secondary electron with a departure energy of W_s

W_g = Standard deviation value

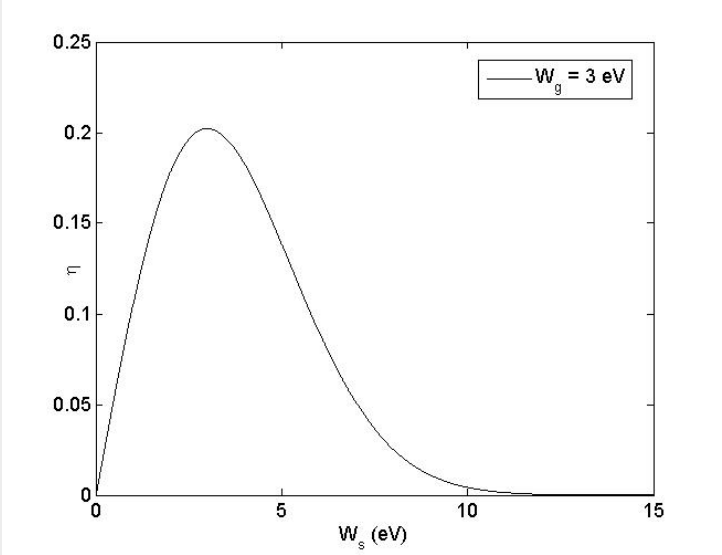

Rayleigh distribution

III. Multipactor simulation algorithm

Effective electron (III)

In order to implement this concept in the Monte-Carlo method, the algorithm generates a random real number $u \in [0,1]$, and the departure energy is calculated:

$$W_s = W_g\sqrt{-2\ln u}$$

Note the Energy Conservation Principle has to be satisfied. It implies that the output energy cannot exceed the value of the impacting energy.

2. The direction of the velocity vector of the electron is calculated in a local spherical coordinate system centred at the impact point:

- The azimuthal angle $\varphi \in [0,2\pi[$ is easily calculated by means of a uniform probability density:

$$\varphi = 2\pi u$$

- The elevation angle θ has to be computed by means of the cosine law:

$$\theta = \sin^{-1}(\sqrt{u})$$

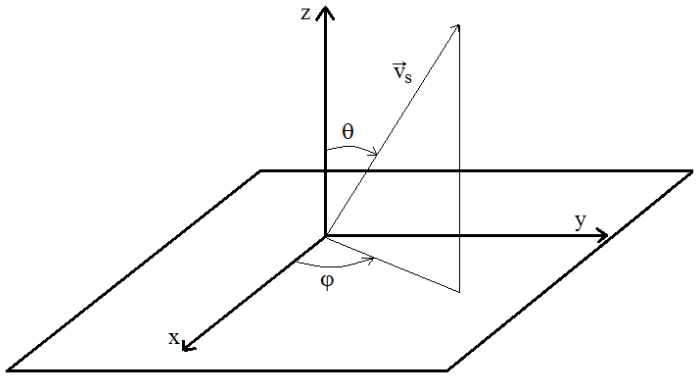

J. Greenwood, "The correct and incorrect generation of a cosine distribution of scattered particles for Monte-Carlo modelling of vacuum systems" , Vacuum, vol. 67, pp. 217–222, 2002

III. Multipactor simulation algorithm

Individual electron

- In this model, the number of tracked particles varies with the ongoing of the simulation and each particle represents only a real electron.
- The Furman and Pivi SEY model is implemented allowing to distinguish the following types of interactions: elastic backscattering, inelastic backscattering and true secondary electrons.
- When an electron impacts a surface the interaction type is obtained by means of the Monte-Carlo method:

$u \in [0,1]$ real random number

Elastic backscattered
$u < P_e(E_p, \varphi)$

Inelastic backscattered
$P_e(E_p, \varphi) \leq u < P_e(E_p, \varphi) + P_b(E_p, \varphi)$

True secondary
$u \geq P_e(E_p, \varphi) + P_b(E_p, \varphi)$

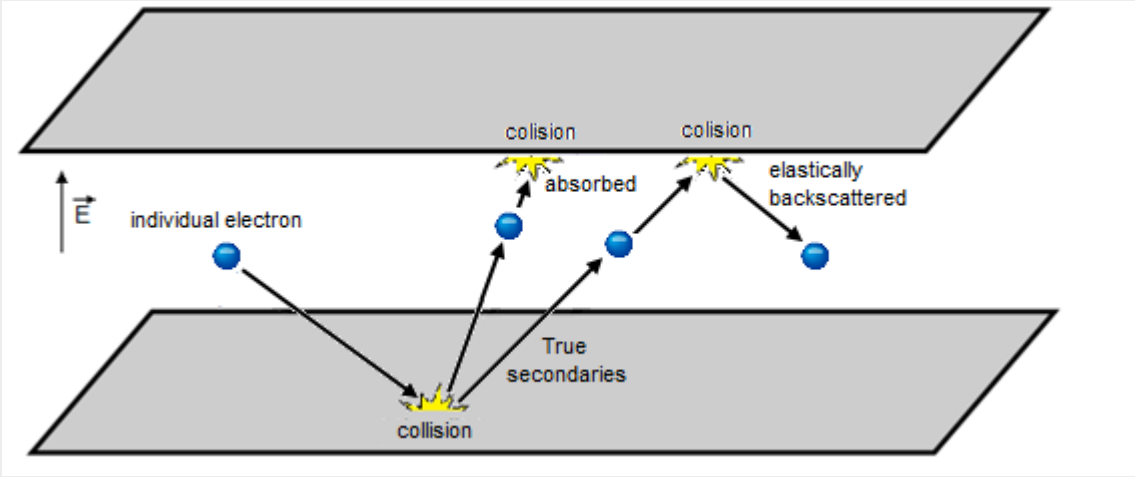

Scheme of the individual electron model

III. Multipactor simulation algorithm

Individual electron (II)

After the collision, if not absorbed, the electron is re-emitted from the impacting point. The magnitude and angle (with regard the normal of the impacting surface) of the output velocity depend on the collision type of the primary electron:

- Elastic collision. The output energy is equal to the impacting energy, W = W_i. The departure angle is equal to the incidence angle (specular reflection).
- Inelastic collision. The output energy is less than the impacting energy W < W_i. The departure angle is equal to the incidence angle.
- Collision generating true secondaries:

Mean number of true secondaries per impacting electron $\longrightarrow$ $\lambda(E_p,\varphi) = \dfrac{\delta(E_p,\varphi)}{1-\varepsilon(E_p,\varphi)-\eta(E_p,\varphi)}$

The exact number of true secondaries *n* is determined as:

$$\mathrm{n} = \begin{cases} \lambda_i & \text{if} \quad u < \lambda_f \\ \lambda_i + 1 & \text{if} \quad u > \lambda_f \end{cases}$$

(Note that if n = o then the impacting electron is absorbed)

$u \in [0,1]$ real random number

λ_i integer part of λ

λ_f fractional part of λ

The true secondary electrons are released with an output energy given by the Raileigh distribution and an angle following the Cosine Law, similarly as described in the effective electron case

III. Multipactor simulation algorithm

Multipactor criteria

A multipactor criterion must be established in the simulations in order to decide if the discharge has taken place. Mainly, the are two possibilities:

- The number of electrons exceeds a threshold value, typically a certain number of times the initial population value.
- It is reached a steady state in the electron population due to the space charge effect when the electron number becomes very high.

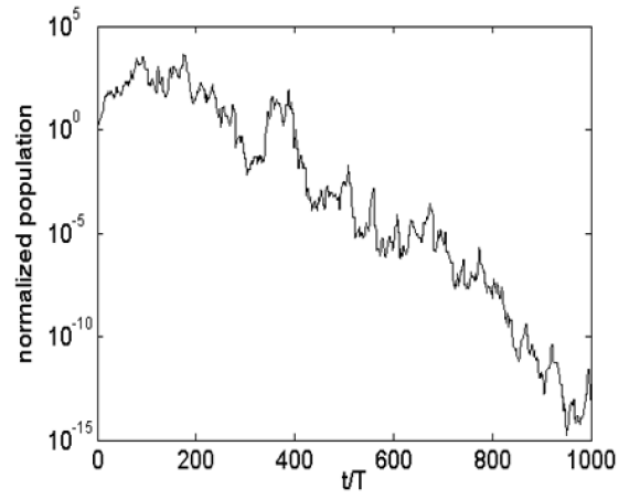

The electron population diminishes and no discharge is expected

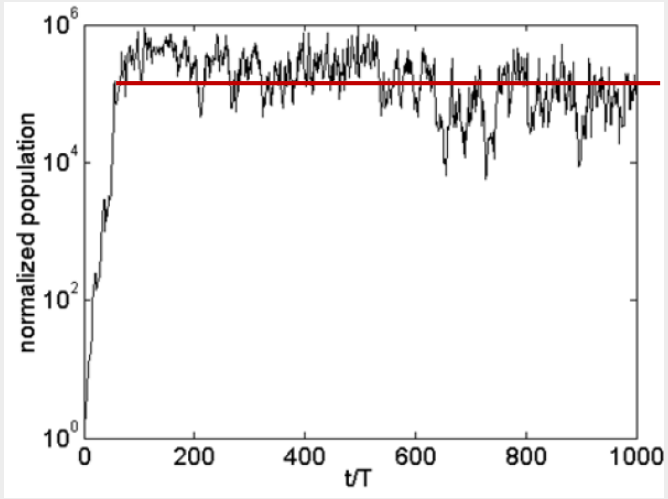

Electron population quickly grows and saturation is observed

Index

- Introduction
- Objectives
- Multipactor simulation algorithm
- Results

Mitigation of the multipactor discharge in coaxial transmission lines by means of an external magnetostatic field

IV. Results

Multipactor mitigation techniques

There are several techniques in order to avoid the onset of the multipactor discharge:

- Surface treatments aimed to reduce the SEY coefficient of the surfaces. For example: chemical polishing, groove insertions, surface coatings, etc. Inconveniences: surface treatments degrade with time, grooves can impair the RF performance.
- External DC electric and/or magnetic fields are applied to the device in order to disturb the electron resonant trajectories.

In this chapter, we explore the multipactor mitigation when an axial DC magnetic field is applied to a coaxial transmission line

$$\vec{B}_{DC}(\vec{r},t) = B_{DC}\hat{z}$$

TEM fundamental mode of the coaxial line $\longrightarrow$

$$\vec{E}_{RF}(\vec{r},t) = \frac{V_0}{r\ln\left(\frac{b}{a}\right)}\cos(2\pi f t - \beta z)\hat{r}$$

$$\vec{B}_{RF}(\vec{r},t) = \frac{V_0}{r\,c\ln\left(\frac{b}{a}\right)}\cos(2\pi f t - \beta z)\hat{\varphi}$$

f is the RF frequency
(r, φ, z) are the cylindric coordinates
β is the propagation factor

a and b are the inner and outer coaxial radii
c is the speed of light in vacuum
V_0 is the RF voltage amplitude

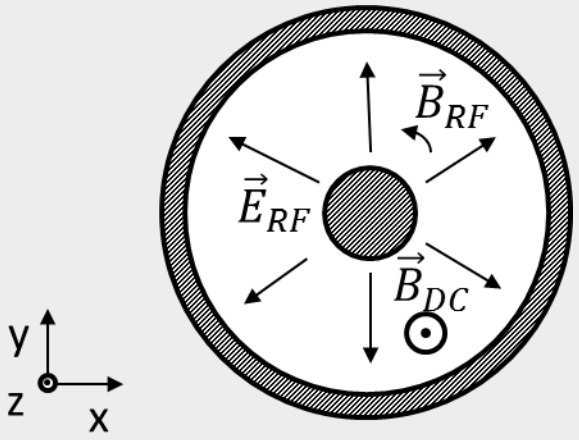

Transversal cross section of a coaxial line

IV. Results

Magnetic field implementation

We consider two different posibilities:

Solenoid: uniform DC magnetic field

Permanent magnet: non-uniform DC magnetic field

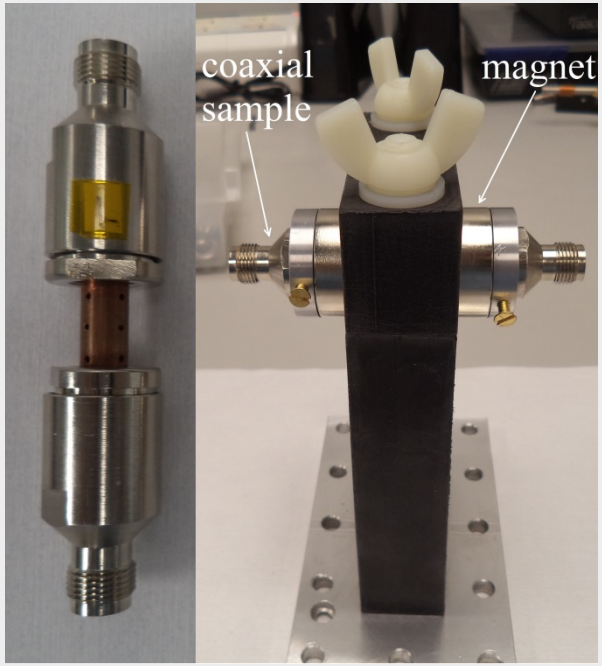

IV. Results

Solenoid: uniform DC magnetic field

A solenoid was designed and manufactured to provide an uniform axial DC magnetic field along the coaxial sample when it is fed by a DC electric current

Support: Aluminium hollow cylinder
- Inner radius $r_i = 15.80$ mm
- Outer radius $r_e = 19.05$ mm
- Length $h = 300$ mm

Winding: copper wire
- Wire diameter Ø = 0.8 mm
- 22 turn layers
- Aprox. 375 turns/layer
- Total turns = 8250

Solenoid

Inner conductor radius → a = 1.515 mm

Outer conductor radius → b = 3.490 mm

Gap → d = b-a = 1.975 mm

Impedance → Z = 50 Ω

Material → Copper

W_1 = 25 eV

W_{max} = 175 eV

δ_{max} = 2.25

Coaxial sample

IV. Results

Solenoid: uniform DC magnetic field (II)

Solenoid calibration set-up based on the electromagnetic induction phenomenon

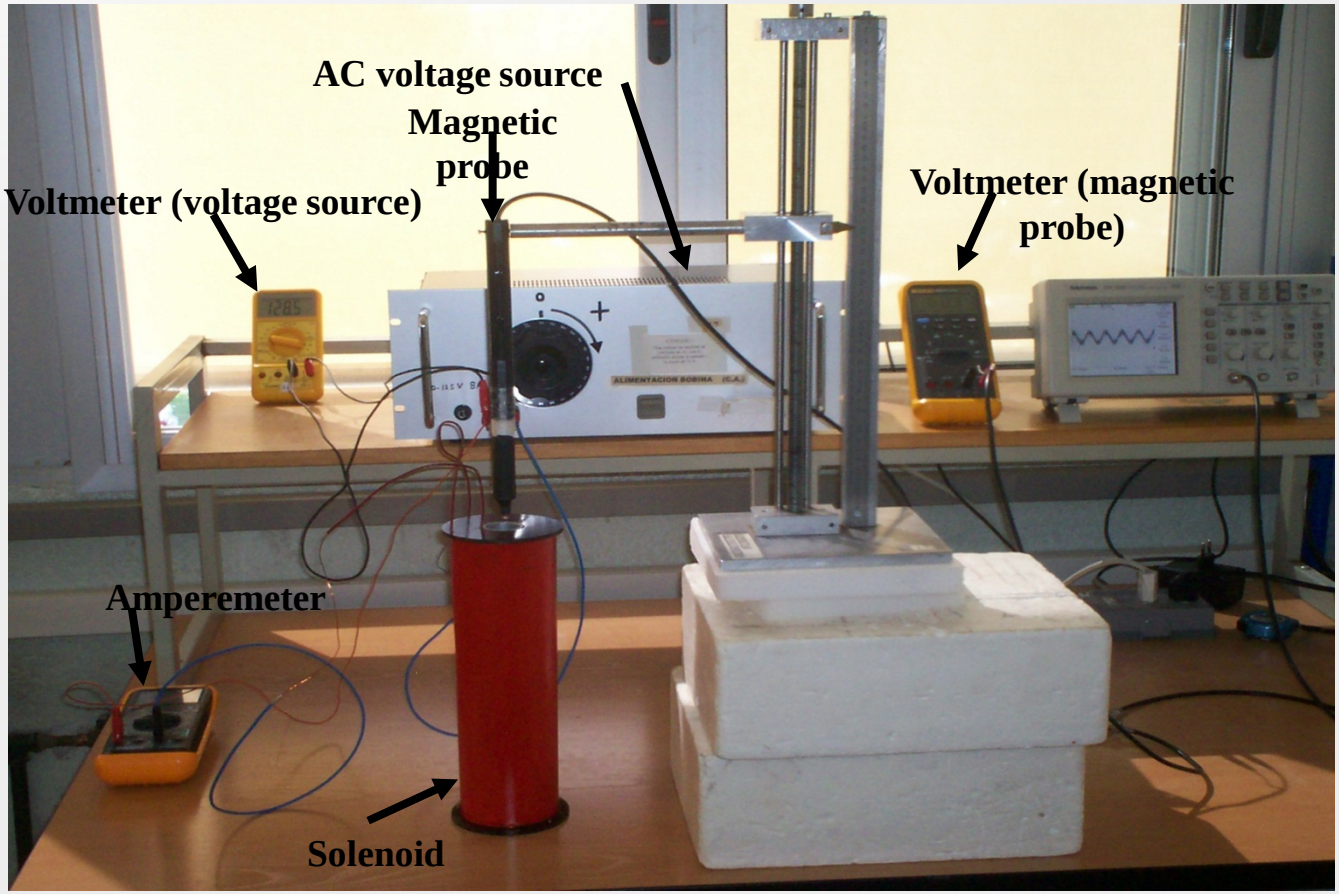

IV. Results

Solenoid: uniform DC magnetic field (III)

Results of the solenoid calibration

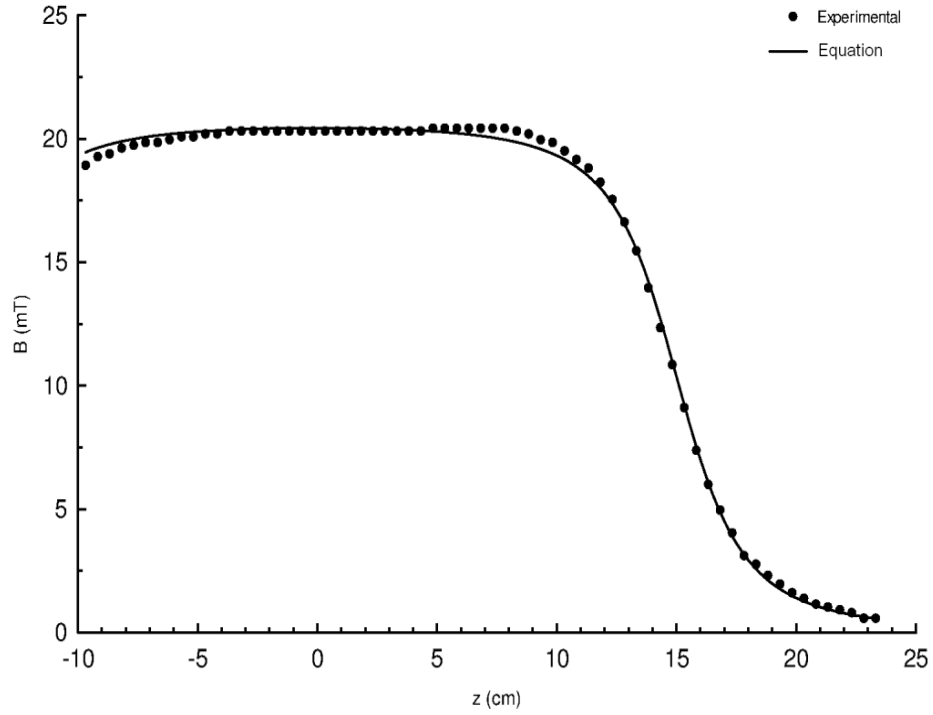

Fit of the experimental data

$$B_z(0,0,z) = \frac{\mu_0}{2}\frac{N \cdot I}{h}\left\{\frac{z+\frac{h}{2}}{\left[a^2+\left(z+\frac{h}{2}\right)^2\right]^{\frac{1}{2}}} - \frac{z-\frac{h}{2}}{\left[a^2+\left(z-\frac{h}{2}\right)^2\right]^{\frac{1}{2}}}\right\}$$

I: DC current feeding the solenoid

z: axial coordinate in the axis

a: mean radius = 29.3 mm

h: length = 300 mm

N: number of turns = 8250

In the center of the solenoid a DC magnetic field of 3.8 mT for I=100 mA is detected.

IV. Results

Solenoid: uniform DC magnetic field (IV)

Multipactor RF power threshold as a function of the cyclotron to RF frequency ratio

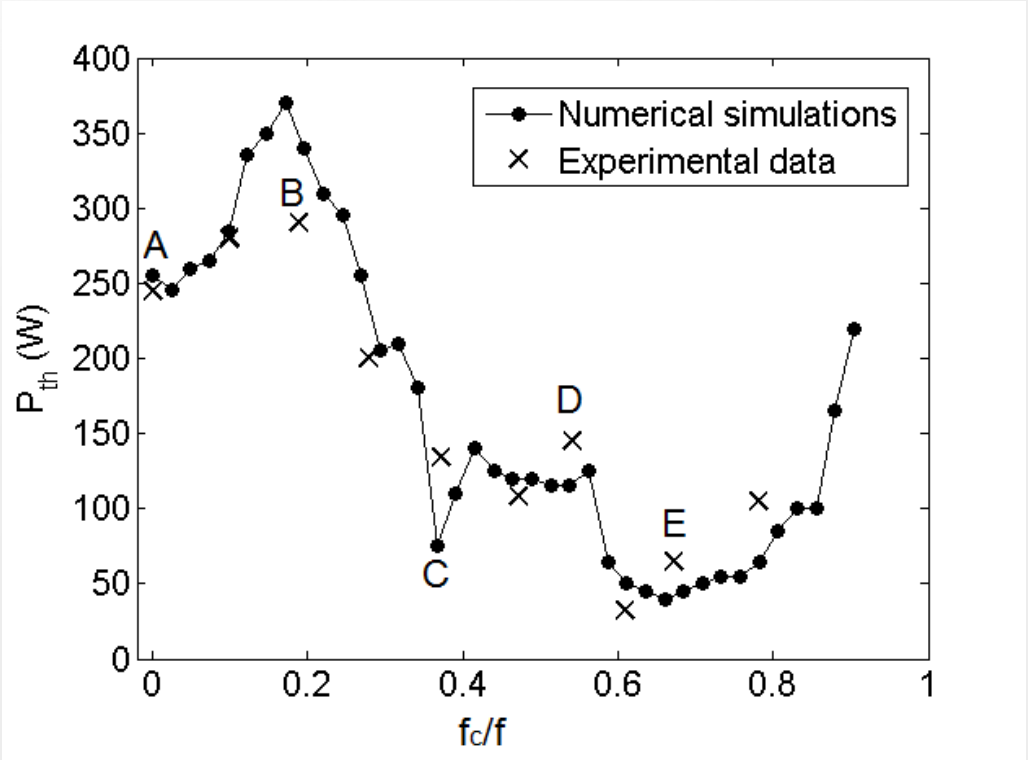

RF frequency → 1.145 GHz

- Good agreement between theoretical and experimental data.
- Within a certain range of f_c/f, the multipactor RF voltage threshold drops below the without magnetic field case.
- Experimentally no discharge was detected for $f_c/f > 0.8$. Theoretical simulations predict no multipactor above $f_c/f > 0.9$
- Small differences can be related to inaccuracies in the SEY data used in theoretical simulations.

cyclotron frequency $f_c = \frac{e}{m_e}\frac{B_{DC}}{2\pi}$

IV. Results

Solenoid: uniform DC magnetic field (V)

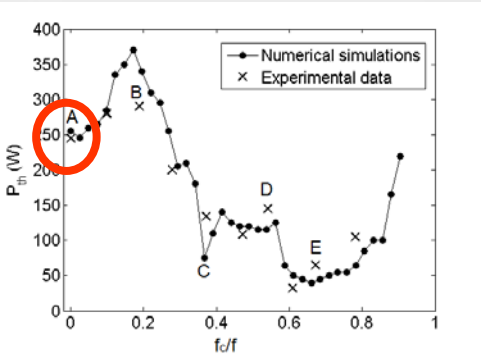

Point A $\quad f_c / f = 0 \quad P = 245\ \mathrm{W}$

Double surface multipactor

From outer to inner conductor → Order 3

From inner to outer conductor → Order 1

Inner conductor mean SEY value → $SEY_i = 2.0$

Outer conductor mean SEY value → $SEY_o = 1.1$

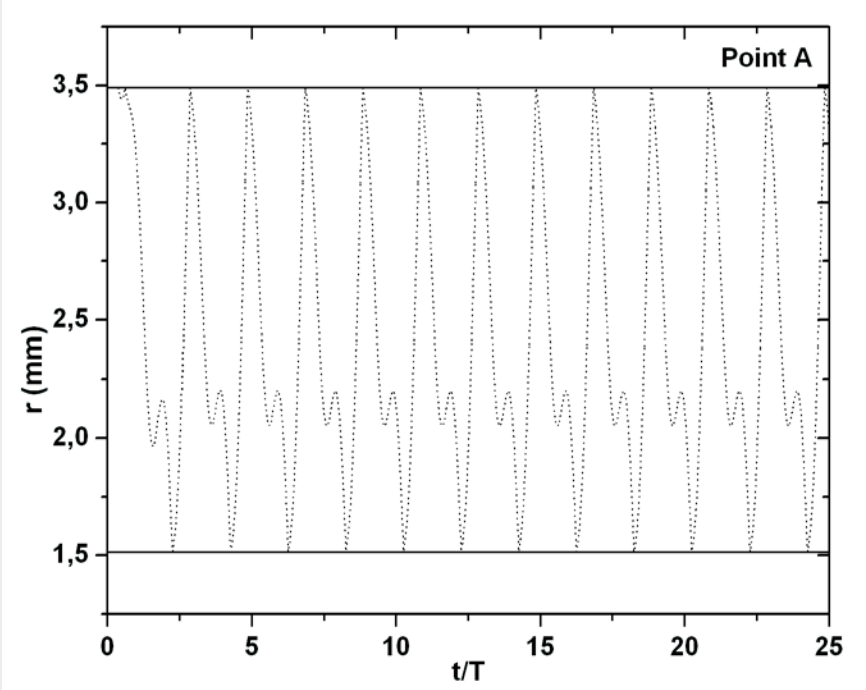

IV. Results

Solenoid: uniform DC magnetic field (VI)

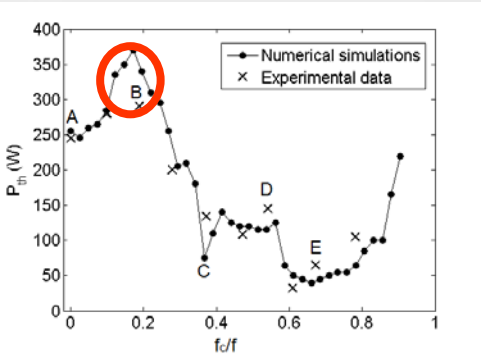

Point B $\quad f_c / f = 0.197 \quad P = 290\ \mathrm{W}$

Mix between double surface and single surface multipactor:

the DC magnetic field tends to bend the electron orbits around the magnetic field flux lines.

Multipactor threshold is higher than for point A !

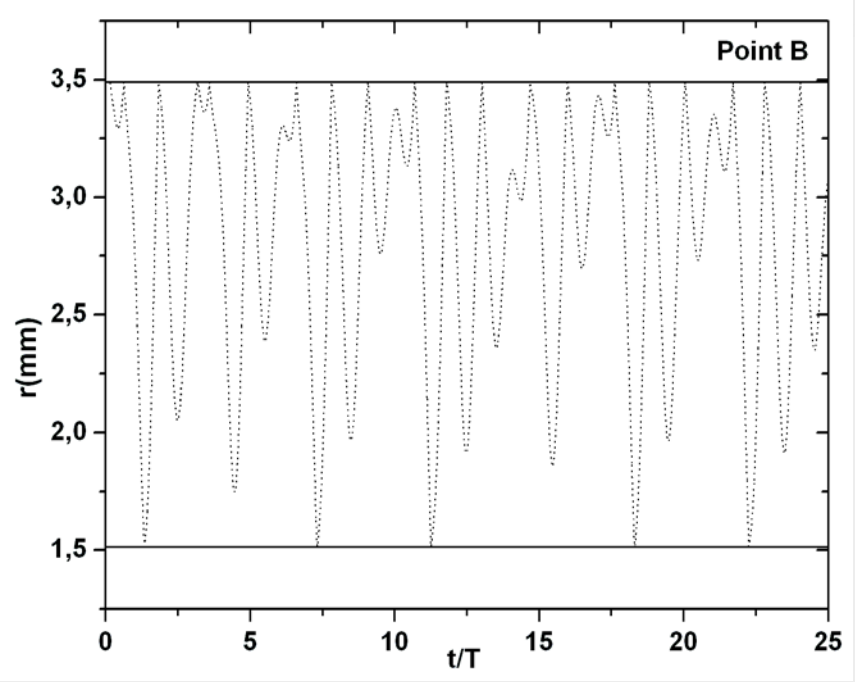

Inner conductor mean SEY value → $SEY_i = 2.9$

Outer conductor mean SEY value → $SEY_o = 2.9$

IV. Results

Solenoid: uniform DC magnetic field (VII)

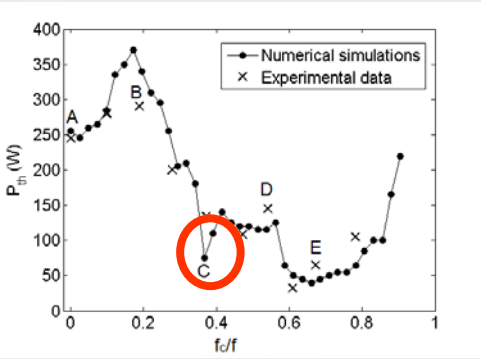

Point C $\quad f_c / f = 0.367 \quad P = 86\ \mathrm{W}$

The DC magnetic field is strong enough to avoid electrons reaching the opposite conductor so that there are only single-surface orbits.

- Electrons launched from the inner conductor:

  Discharge is generated only on the inner wall. Multipactor of order 4.

- Electrons launched from the outer conductor:

  Low energetic impacts, there is no release of secondary electrons.

Inner conductor mean SEY value → $SEY_i = 1.2$

Outer conductor mean SEY value → $SEY_o = 0.5$

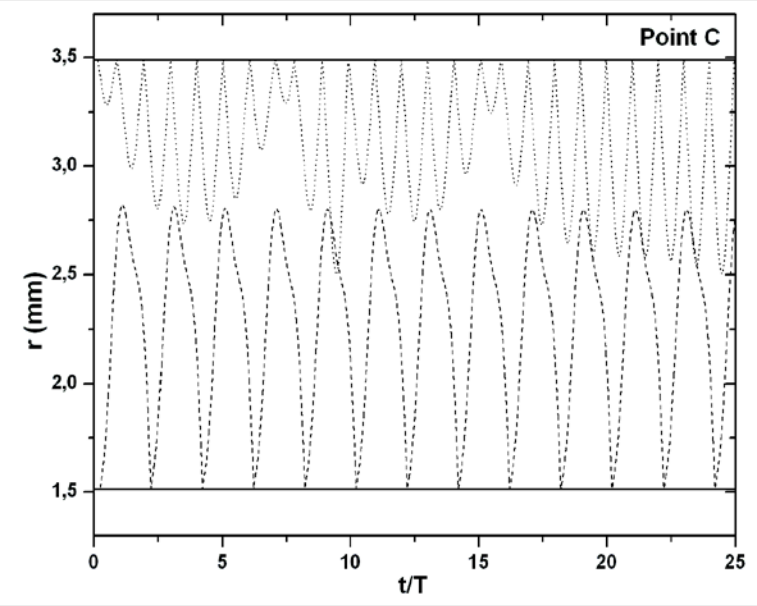

IV. Results

Solenoid: uniform DC magnetic field (VIII)

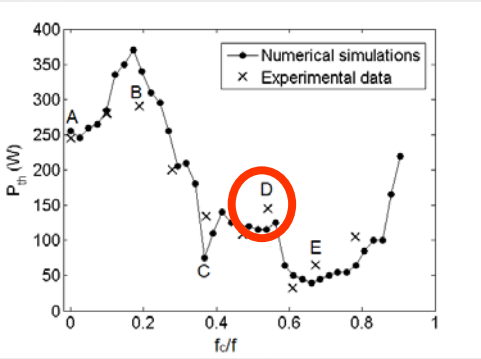

Point D $\quad f_c / f = 0.538 \quad P = 145\ \mathrm{W}$

- Electrons launched from the inner conductor:

  Multipactor cannot occur on the inner wall because of a lack of resonance and low energetic impacts.

- Electrons launched from the outer conductor:

  A single-surface discharge of order 2 can be generated. Significant local increase in the threshold of point D is explained in terms of the variation with the radial coordinate of the applied RF electric field.

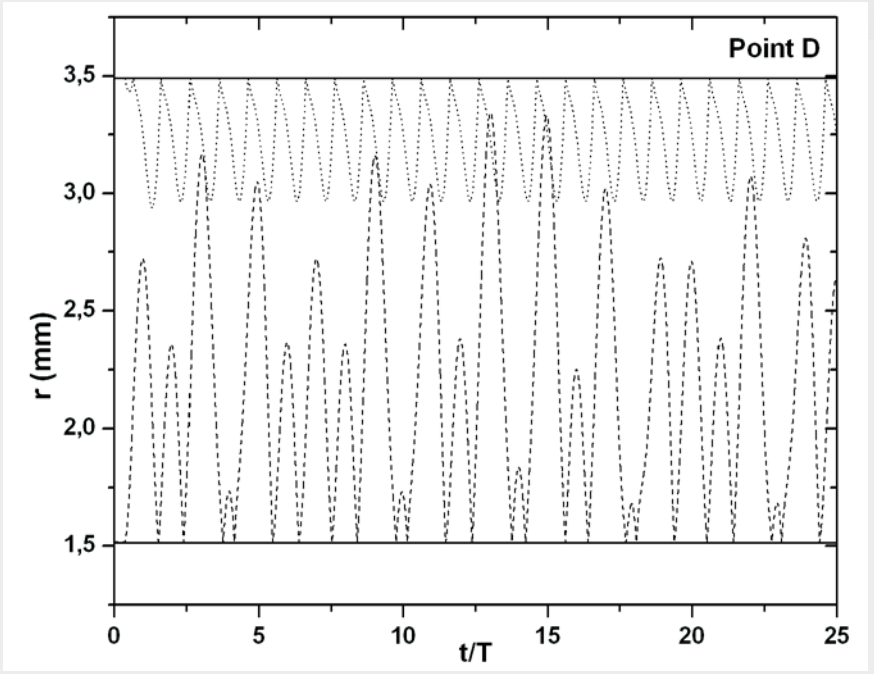

Inner conductor mean SEY value → $SEY_i = 0.4$

Outer conductor mean SEY value → $SEY_o = 1.1$

IV. Results

Solenoid: uniform DC magnetic field (IX)

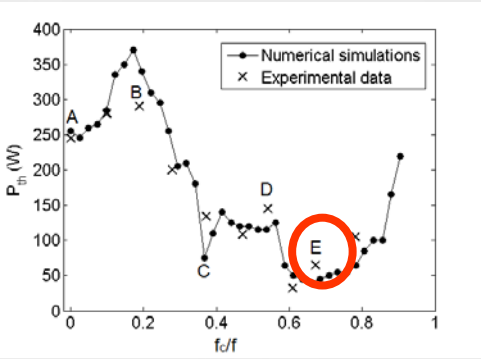

Point E $\quad f_c / f = 0.660 \quad P = 65\ \mathrm{W}$

- Electrons launched from the inner conductor:

  Single-surface discharge of order 2 on inner wall, local decrease in the threshold of point E is explained in terms of the variation with the radial coordinate of the applied RF electric field.

- Electrons launched from the outer conductor:

  Multipactor cannot occur on the inner wall because of a lack of resonance and low energetic impacts.

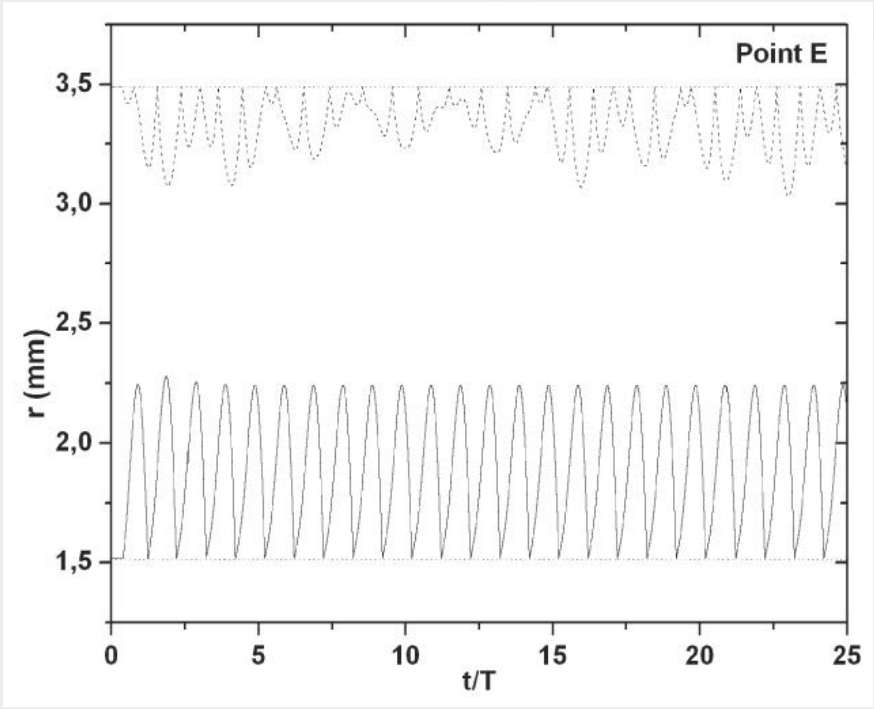

Inner conductor mean SEY value → $SEY_i = 2.2$

Outer conductor mean SEY value → $SEY_o = 0.9$

IV. Results

Solenoid: uniform DC magnetic field (X)

Why for high external magnetic fields does the multipactor disappear?

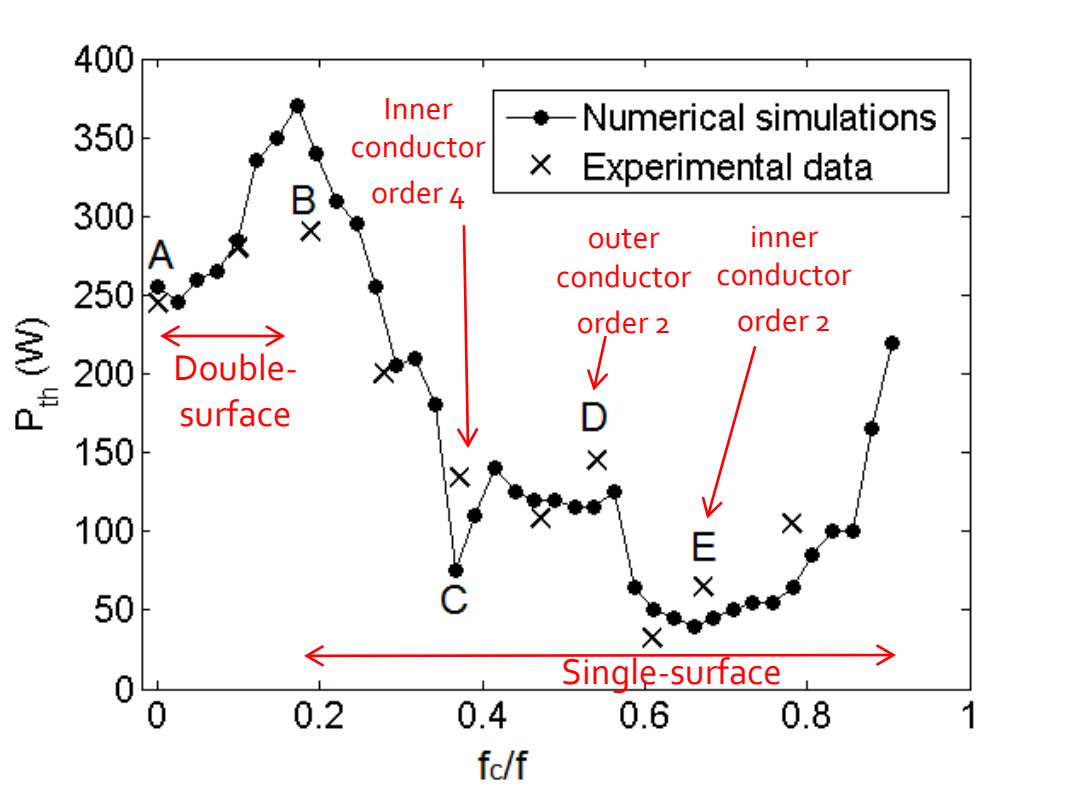

- As the magnetic field increases it bends the electron orbits forcing single-surface multipactor regimes.
- The increase of the magnetic field also implies that the electron time of flight between successive impacts becomes shorter as a consequence of the orbit bending.
- Single-surface multipactor orders must be an even number (m = 2,4,6…) to ensure the resonance with the RF electric field.
- The impossibility of single-surface multipactor orders below 2 and the reduction of the time of flight of the electron due to the magnetic field justifies the mitigation of the multipactor for high magnetic fields.

IV. Results

Solenoid: uniform DC magnetic field (XI)

Can be multipactor mitigated at any RF frequency?

Theoretical results for other RF frequencies predict multipactor mitigation when f_c/f increases above a threshold which depends on the specific RF frequency but it is approximately within the range $f_c/f \in [0.7, 1]$

f = 0.435 GHz

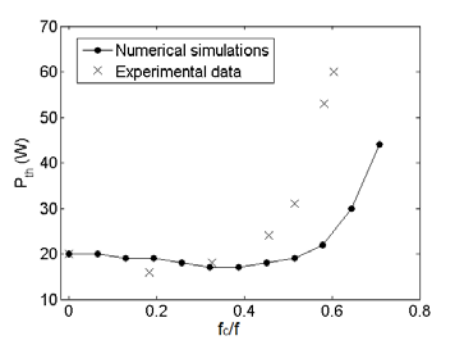

f = 1.145 GHz

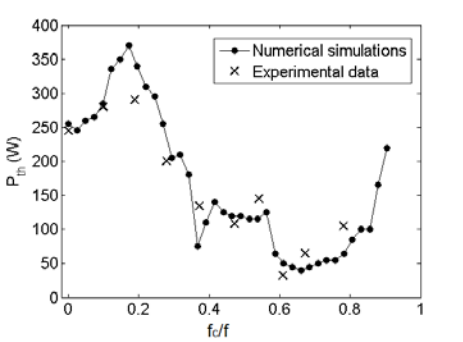

f = 2.000 GHz

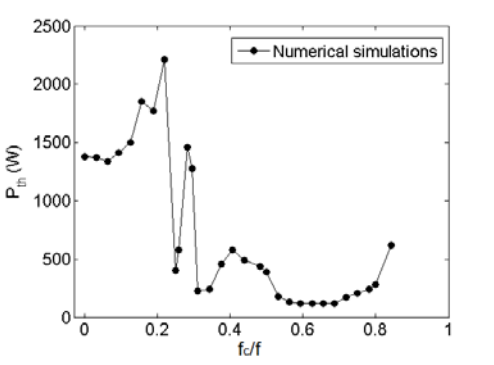

f = 3.000 GHz

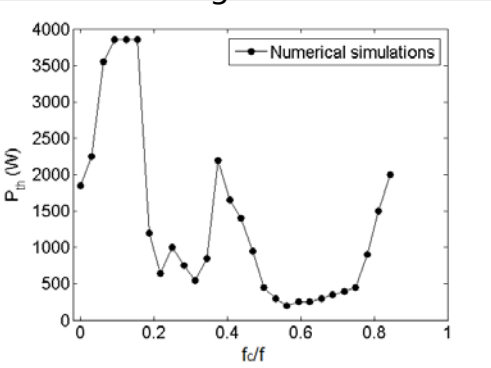

IV. Results

Permanent magnet: non-uniform DC magnetic field

- A hollow cylindrical neodymium permanent magnet was employed to generate a non-uniform magnetic field over the coaxial sample.
- Expressions for the magnetic field generated by a permanent magnet are derived from the equivalent volume and surface currents. These expressions are required for the multipactor numerical simulations.

Volume magnetization $\vec{M} = M\hat{z}$

Equivalent surface current $\vec{K}_M = \vec{M} \times \vec{n}$

Equivalent volume current $\vec{J}_M = \nabla \times \vec{M}$

$$\sigma = \frac{4rr_0}{(r+r_0)^2}$$

$$k_1 = \sqrt{\frac{4rr_0}{(r+r_0)^2 + \left(z - {}^{h}/_{2}\right)^2}}$$

$$k_2 = \sqrt{\frac{4rr_0}{(r+r_0)^2 + \left(z + {}^{h}/_{2}\right)^2}}$$

Elliptical integral of the First Kind

Elliptical integral of the Second Kind

$$B_r(r,z) = \frac{\mu_0 M}{2\pi\sqrt{rr_0}\left(1+\frac{r}{r_0}\right)^2}\left[\frac{E(k_2)}{k_2} - \frac{E(k_1)}{k_1} + \frac{1}{{k_1}^2}\left(1-\frac{{k_1}^2}{2}\right)K(k_1) - \left(1-\frac{{k_2}^2}{2}\right)K(k_2)\right]$$

$$B_z(r,z) = \frac{\mu_0 M}{2\pi\sqrt{rr_0}\left(1+\frac{r}{r_0}\right)^2}\left[\left(z+\frac{h}{2}\right)k_2\Pi(k_2,\sigma) - \left(z-\frac{h}{2}\right)k_1\Pi(k_1,\sigma)\right] - \frac{r}{r_0}B_r(r,z)$$

Elliptical integral of the Third Kind

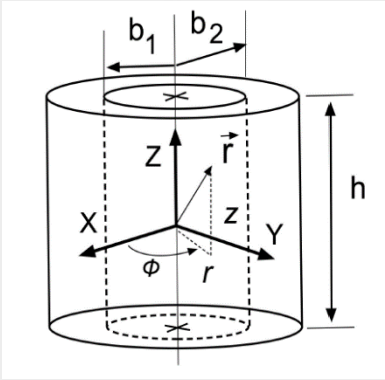

Scheme of the hollow magnet with height *h*, and *b1* and *b2* radii.

$M = 1.153 \times 10^6$ A/m

$b_1 = 12.5$ mm

$b_2 = 16.5$ mm

$h = 44$ mm

IV. Results

Permanent magnet: non-uniform DC magnetic field (II)

Multipactor simulations and an experimental test campaign was carried out to assess the multipactor mitigation capabilities of the magnet prototype

Inner conductor radius → a = 1.238 mm
Outer conductor radius → b = 2.850 mm
Gap → d = b-a = 1.612 mm
Impedance → Z = 50 Ω

Material → Copper
W_1 = 19.5 eV
W_{max} = 219.7 eV
δ_{max} = 2.61

- According to the simulations, multipactor is inhibited below 4.030 GHzmm, which corresponds to $f_c/f = 1.12$
- Firstly, it was explored the multipactor threshold without magnet, finding good agreement between theory and experiment.
- Secondly, the same frequency gap values were measured with the coaxial immersed in the hollow magnet. No discharge was found for any of these cases, in concordance with the theoretical predictions.
- Magnet mitigation behavior is quite similar to the solenoid case (the empirical condition of mitigation for values above the range $f_c/f \in [0.7, 1]$ is roughly fulfilled)

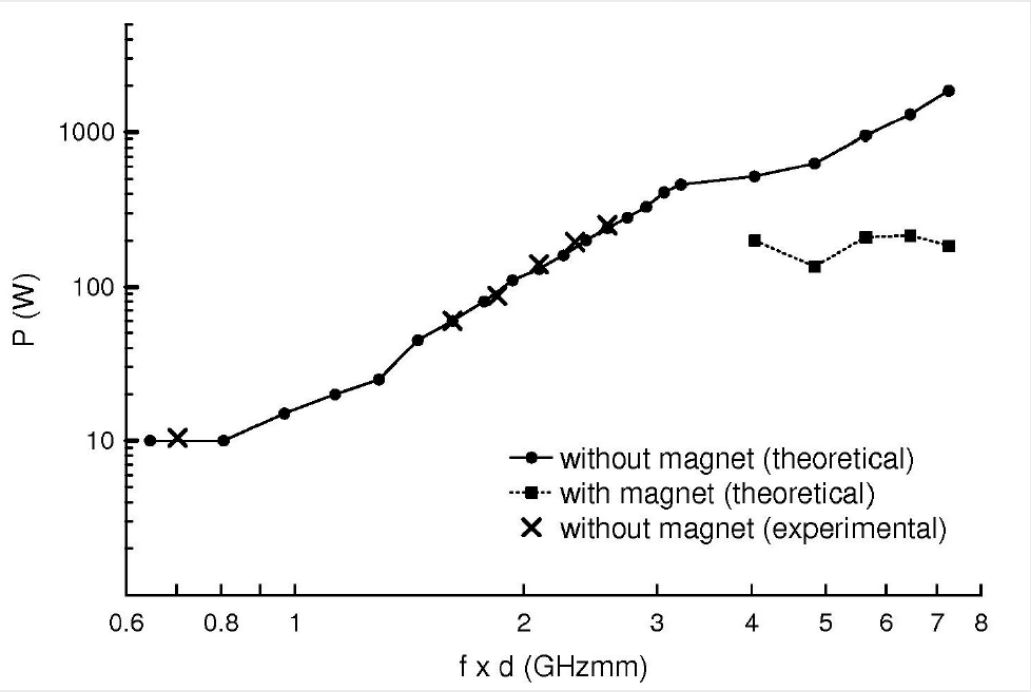

IV. Results

Permanent magnet: non-uniform DC magnetic field (III)

In order to understand the multipactor physics with the magnet it is examined the magnetic field pattern, the electron motion equations and trajectories

Differential equations of motion

$$\frac{dv_r}{dt} = -\frac{e}{m_e}\left[E_{RF}(\vec{r},t) + E_{sc}(\vec{r},t) - B_{RF}(\vec{r},t)v_z + B_{ext,z}(\vec{r})v_\phi\right]$$
$$\frac{dv_\phi}{dt} = -\frac{e}{m_e}\left[-B_{ext,z}(\vec{r})v_r + B_{ext,r}(\vec{r})v_z\right]$$
$$\frac{dv_z}{dt} = -\frac{e}{m_e}\left[-B_{ext,r}(\vec{r})v_\phi + B_{RF}(\vec{r},t)v_r\right]$$

With the assumptions $B_{ext,r} \ll B_{ext,z}$, $B_{RF} \ll B_{ext}$, $E_{sc} \approx 0$

The previous equations can be approximated in the following way

$$\frac{dv_r}{dt} \approx -\frac{e}{m_e}\left[E_{RF}(\vec{r},t) + B_{ext,z}(\vec{r})v_\phi\right]$$
$$\frac{dv_\phi}{dt} \approx \frac{e}{m_e}B_{ext,z}(\vec{r})v_r$$
$$\frac{dv_z}{dt} \approx \frac{e}{m_e}B_{ext,r}(\vec{r})v_\phi$$

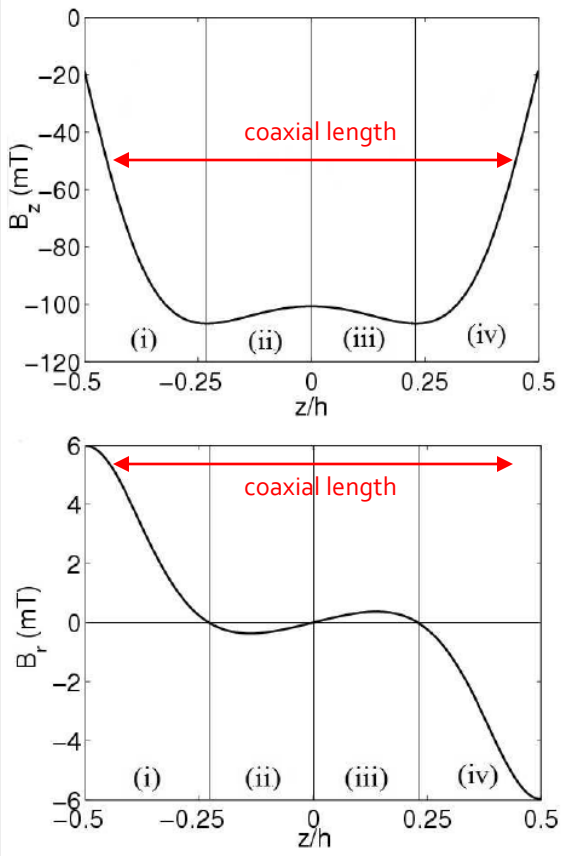

h is the magnet height

IV. Results

Permanent magnet: non-uniform DC magnetic field (IV)

An electron immersed in a DC magnetic field tends to spin around the magnetic field flux lines [1]:

$$\vec{\omega}_c = \frac{e}{m_e}\vec{B}$$

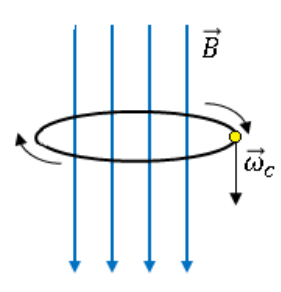

For an axial DC magnetic field oriented along -z, the electron will spin clockwise → $v_\phi < 0$

[1] R. K. Wangsness, Electromagnetic Fields, 2nd ed. New York, NY, USA: Wiley, 1986.

Despite in our case there is a radial RF electric field, we can still assume the electron will spin clockwise:

The axial acceleration is given by $$\frac{dv_z}{dt} \approx \frac{e}{m_e} B_{ext,r}(\vec{r}) v_\phi$$

There are four different zones according to sign of $B_{ext,r}$

- Zones (i) and (iii) : $B_r > 0$, $v_\phi < 0$ → $dv_z/dt < 0$
- Zones (ii) and (iv) : $B_r < 0$, $v_\phi < 0$ → $dv_z/dt > 0$

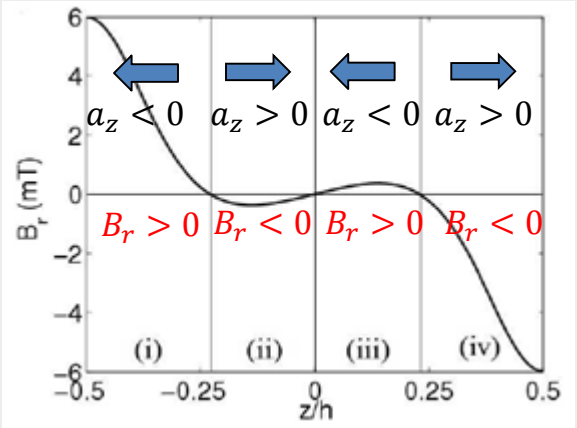

Electrons in zones (i) and (iv) are pushed out the coaxial and cannot contribute to the multipactor process

IV. Results

Conclusions

- It has been demonstrated the capability of using an uniform axial DC magnetic field for inhibiting the multipactor discharge in a coaxial transmission line .
- Multipactor discharge can be suppressed at any RF frequency provided a strong enough axial DC magnetic field is applied.
- As a rule of thumb the minimum magnetic field for ensure mitigation must fulfill that $f_c/f \in [0.7, 1]$
- Besides, it has been found that the non uniform axial magnetic field generated by means of a neodimium permanent magnet can also suppress the discharge.
- For the hollow magnet prototype analyzed the multipactor mitigation behavior is very similar to the uniform axial magnetic field case and the aforementioned rule of thumb ($f_c/f \in [0.7, 1]$) can still be applied.

IV. Results

Publications

[1] D. González-Iglesias, A. M. Pérez, S. Anza, J. Vague, B. Gimeno, V. E. Boria, D. Raboso, C. Vicente, J. Gil, F. Caspers, L. Conde, "Multipactor in a coaxial line under the presence of an axial DC magnetic field", *IEEE Electron Device Letters*, vol. 33, no. 5, pp. 727-729, May 2012.

[2] D. González-Iglesias, A. M. Pérez, S. Anza, J. Vague, B. Gimeno, V. E. Boria, D. Raboso, C. Vicente, J. Gil, F. Caspers, L. Conde, "Multipactor mitigation in coaxial lines by means of permanent magnets", *IEEE Transactions on Electron Devices*, vol. 61, no. 12, pp. 4224-4231, Dec. 2014.

Multipactor in ridge waveguides

IV. Results

Ridge waveguides

Ridge and multi-ridge waveguide sections are widely employed for constructing band-pass and low-pass filters devoted to space telecommunication applications. In this section:

- Multipactor susceptibility charts will be computed for several typical ridge waveguide topologies
- A simple method for multipactor prediction in structures containing ridge waveguide sections will be presented

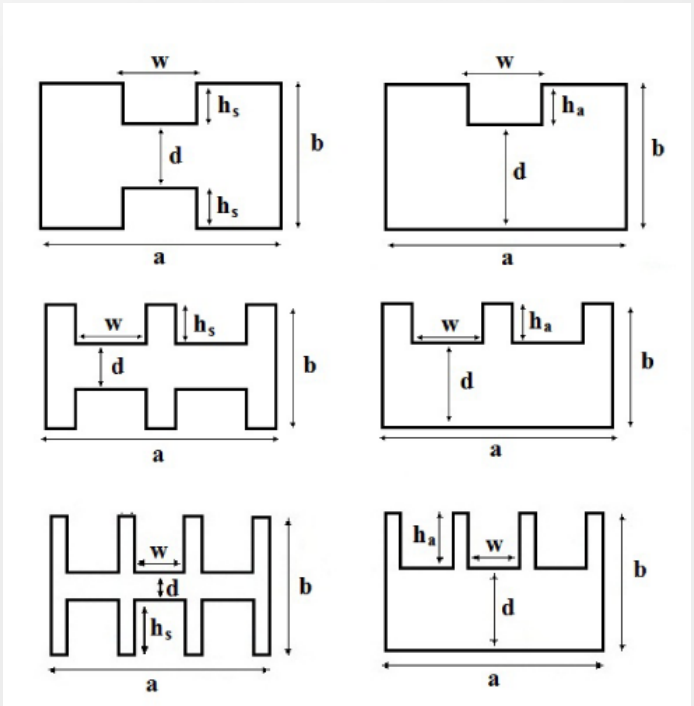

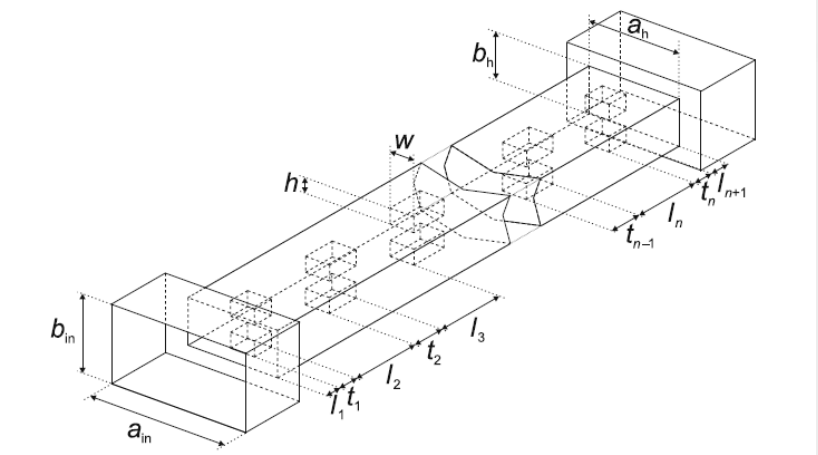

Symmetrical evanescent mode ridge waveguide filter topology

a is the waveguide width

b is the waveguide height

d is the gap between ridges or ridge and waveguide

w is the ridge width

h is the ridge height

IV. Results

Multipactor susceptibility charts

Several multipactor susceptibility charts have been computed by means of the commercial software FEST3D [1] for a wide range of cases of practical interest.

The standard WR-75 rectangular waveguide has been taken as the housing dimensions for the ridge waveguides.

The ridge waveguides are assumed to be silver-plated with the following SEY parameters W_1 = 30 eV, W_{max} = 165 eV, δ_{max} = 2.22

Equivalent voltage for susceptibility charts is computed integrating the RF electric field along the ridge gap:

$$V_{eq} = \left| \int_0^d \vec{E} \cdot \overrightarrow{dl} \right|$$

$\overrightarrow{dl}$ differential element parallel to the gap direction

[1] FEST3D, www.fest3d.com

RF electric field pattern in ridge waveguides

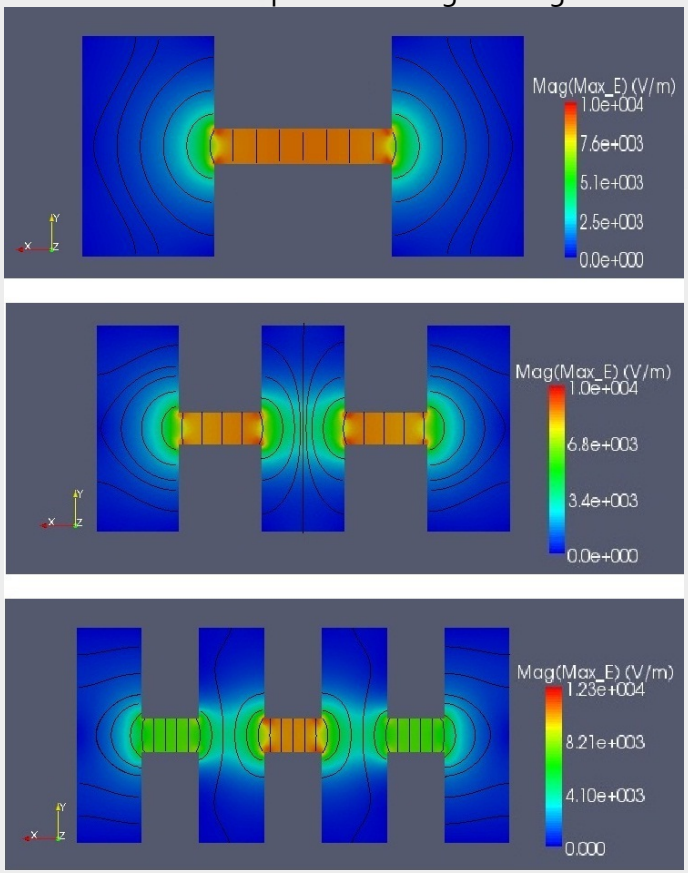

IV. Results

Multipactor susceptibility charts (II)

Study of the variation of multipactor voltage threshold with the ridge width (in all cases the gap is d = 0.5 mm):

ridge

- It is observed that the narrower the ridge the higher the multipactor threshold, but only slight variations are noticed

Double-ridge

- This phenomenon is due to that low values of w/a allow electrons escaping from the gap region so an extra voltage is needed to compensate these electron losses

Multi-ridge

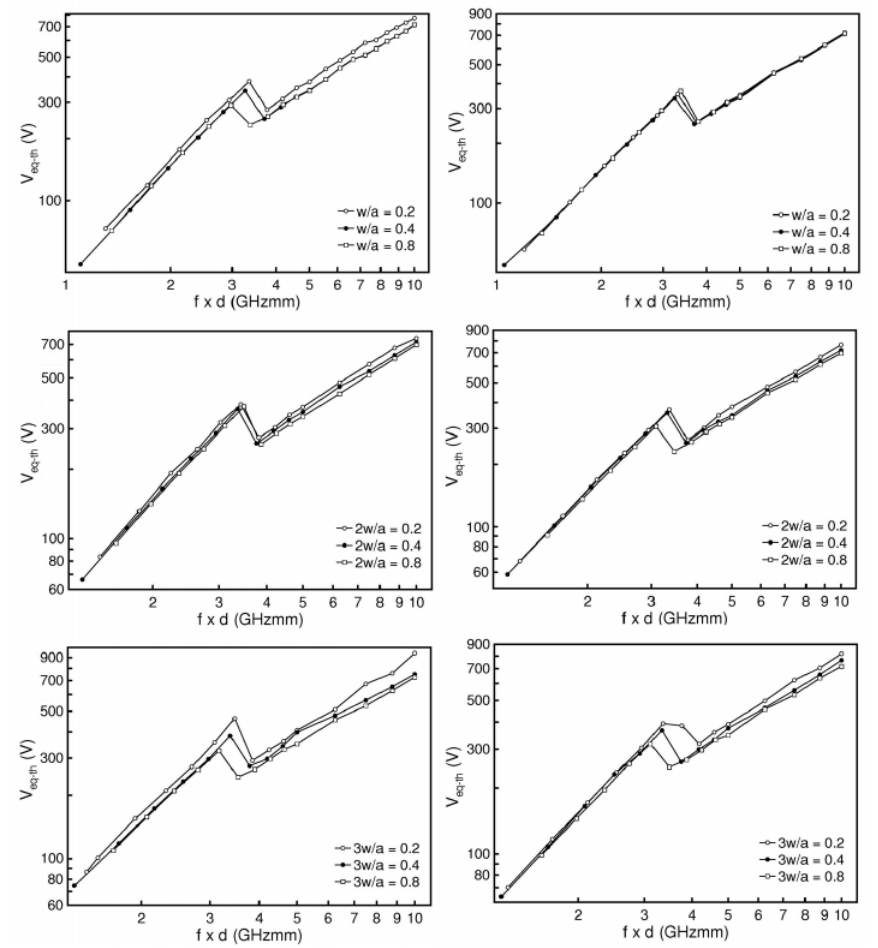

symmetrical asymmetrical

IV. Results

Multipactor susceptibility charts (III)

The phenomenon of electrons escaping from the gap zone was already reported in [1] and [2], and becomes more important when the ridge width is similar or below the gap length.

Ridge symmetrical waveguide with d = 0.5 mm

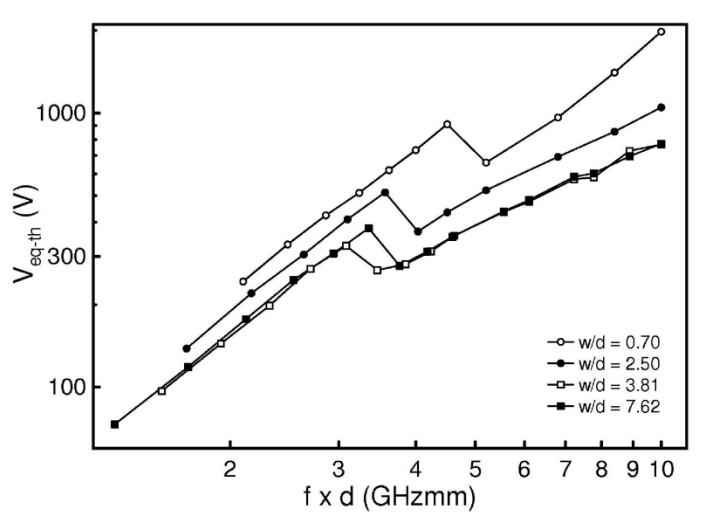

Electrons leave the gap zone due to two different mechanisms:

- Fringing RF electric field effect
- Random drift due to the component transverse to the gap of the initial velocity of the secondary electrons

Fringing RF electric field at the edges of the ridge

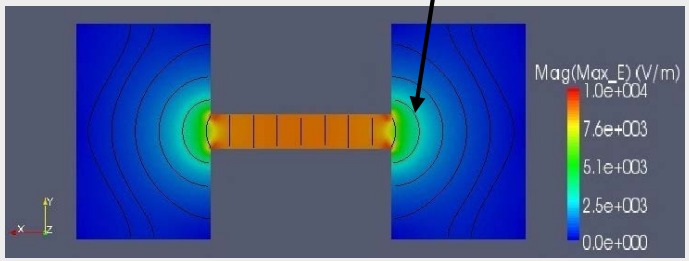

[1] D. Wolk, C. Vicente, H.L. Hartnagel, M. Mattes, J.R. Mosig, D. Raboso, “An investigation on the effect of fringing fields on multipactor breakdown”, 5th International Workshop on Multipactor, Corona and Passive Intermodulation, Sept. 2005.

[2] V. E. Semenov, E. Rakova, R. Udiljak, D. Anderson, M. Lisak, and J. Puech, “Conformal mapping analysis of multipactor breakdown in waveguide irises”, *Physics of Plasmas*, vol. 15, 033501, 2008.

IV. Results

Multipactor susceptibility charts (IV)

Study of the variation of multipactor voltage threshold with the gap length:

Ridge w/a = 0.4

Double-ridge 2w/a = 0.4

- Very little variations of the multipactor threshold are observed within the gap range explored

Multi-ridge 3w/a = 0.4

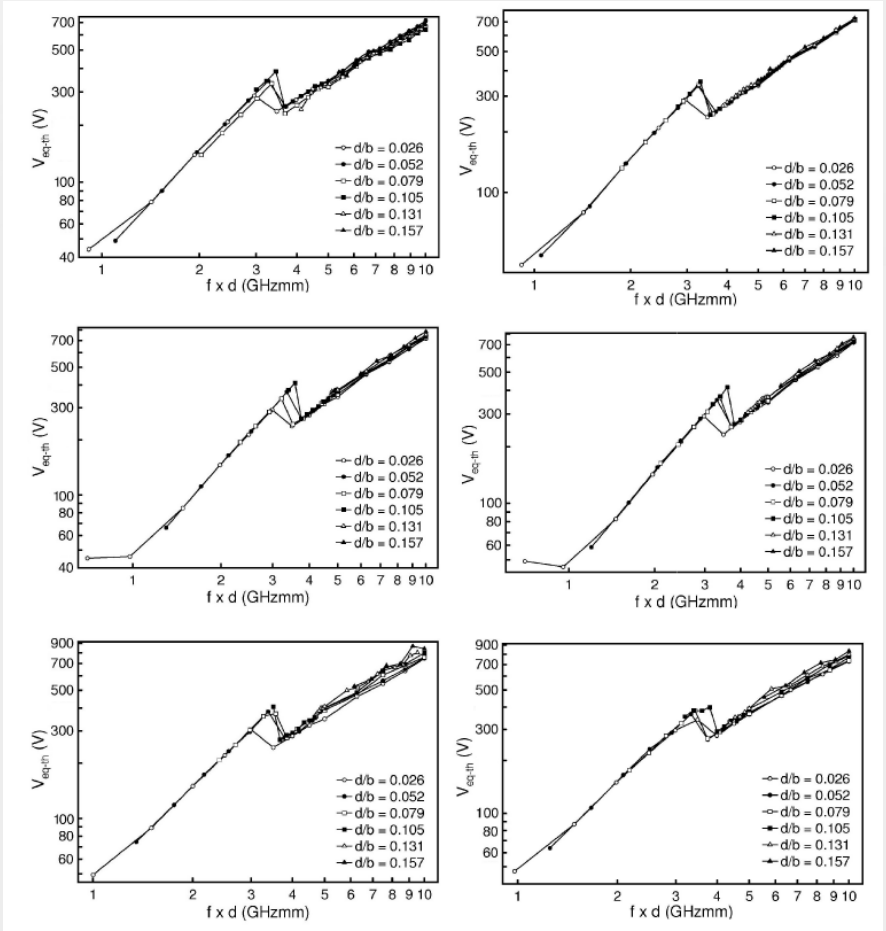

symmetrical asymmetrical

IV. Results

Multipactor prediction using susceptibility charts

The following method allows predicting the multpactor threshold in devices containing ridge waveguide sections by using the previous susceptibility charts:

1. It is required the computation of the RF electromagnetic field pattern of the whole structure (for example, using FEST3D).

2. The equivalent voltage is calculated by integrating the RF electric field for each of the ridge waveguide sections.

3. The highest equivalent voltage V'_{eq} is selected, the multipactor discharge will appear first at that ridge section.

4. In the multipactor susceptibility charts it is searched the case (frequency gap product, waveguide and ridge dimensions) that most fits with the aforementioned ridge section, and the multipactor voltage threshold is obtained $V_{eq\text{-}th}$

5. Multipactor power threshold at the input port of the device can be obtained with the following expression:

$$P_{th} = \left| \frac{V_{eq-th}}{V'_{eq}} \right|^2 P_{in}$$

P_{in} is the power at the input port of the device assumed to obtain the RF electromagnetic field pattern of the structure

IV. Results

Multipactor prediction using susceptibility charts (II)

Example I: Evanescent mode filter [1]

- Input and output port implemented in a WR-137 waveguide (b_{in} = 34.85 mm , a_{in}= 15.80 mm)
- RF frequency, f = 9.78 GHz
- Frequency gap, f x d = 3.08 GHzmm
- The most similar case in the susceptibility charts is the curve for w/a = 0.4, d/b = 0.026, with a threshold of $V_{eq\text{-}th}$ = 310 V

Summary of the multipactor analysis

Ridge	V'_{eq} (V)	P_{pred} (W)	P_{FEST3D} (W)
5	105.4	8.65	9.09

Filter dimensions

a_h	6.790 mm
b_h	5.275 mm
w	3.050 mm
h	2.480 mm
d	0.315 mm
$l_1 = l_6$	0.250 mm
$t_1 = t_5$	0.901 mm
$l_2 = l_5$	7.785 mm
$t_2 = t_4$	1.411 mm
$l_3 = l_4$	8.278 mm
t_3	1.411 mm

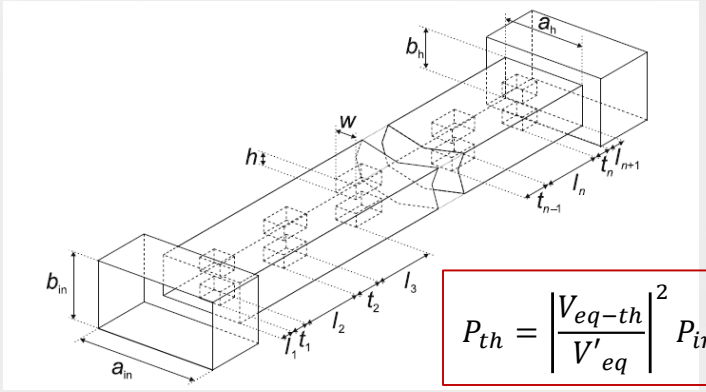

$$P_{th} = \left|\frac{V_{eq-th}}{V'_{eq}}\right|^2 P_{in}$$

Scheme of the symmetrical evanescent mode ridge waveguide filter analyzed

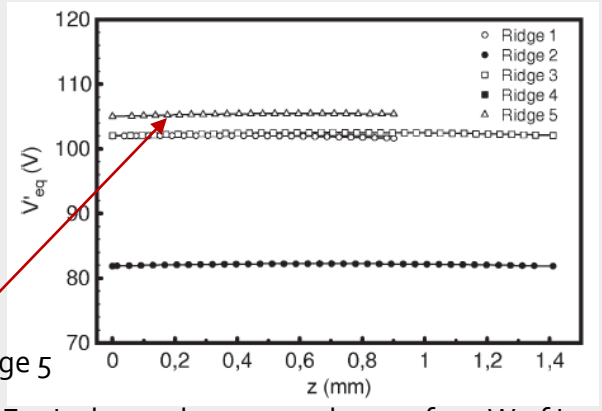

Discharge is foreseen at ridge 5

Equivalent voltage over the gap for 1 W of input power

[1] P. Soto et al. , "Performance analysis and comparison of symmetrical and asymmetrical configurations of evanescent mode ridge waveguide filters", Radio Science, vol. 44, RS6010, doi:10.1029/2008RS004034, 2009.

IV. Results

Multipactor prediction using susceptibility charts (III)

Example II: High-power S-band filter [1]

- Input and output port implemented in a waveguide with b_{in} = 6.4516 mm , a_{in}= 72.1360 mm)
- RF frequency, f = 2.78 GHz
- Frequency gap, f x d = 6.71 GHzmm
- The filter is made of copper, W_1 = 35 eV, δ_{max} = 2.3 , W_{max} = 165 eV
- From the susceptibility chart is the threshold is $V_{eq\text{-}th}$ = 530 V

Scheme of the five-ridge symmetrical waveguide

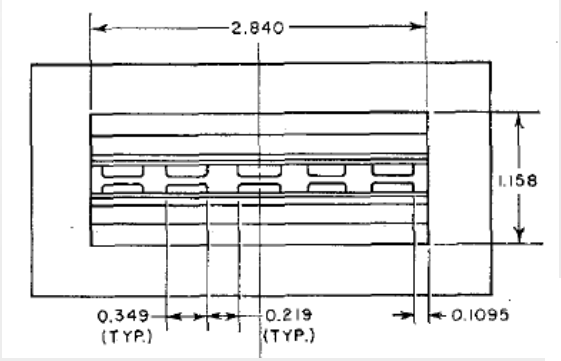

$$P_{th} = \left|\frac{V_{eq-th}}{V'_{eq}}\right|^2 P_{in}$$

Multipactor char for five-ridge symmetrical waveguide

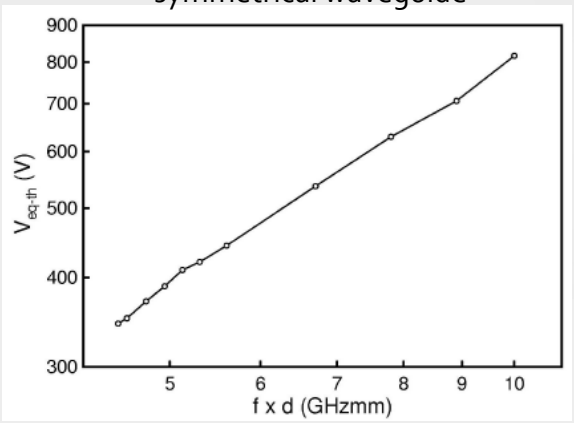

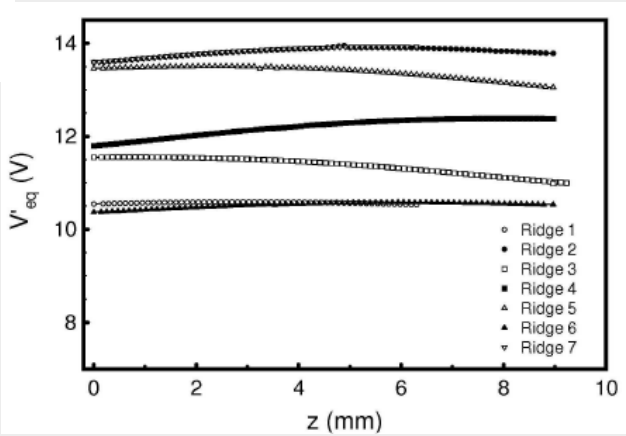

Equivalent voltage over the gap for 1 W of input power

Summary of the multipactor analysis

Ridge	V'_{eq} (V)	P_{pred} (W)	P_{FEST3D} (W)
7	13.921	1449	1532

[1] H. Guthart, "A high-power S-band filter," IRE Trans. Microw. Theory Tech., vol. 10, no. 2, pp. 148–149, Mar. 1962.

IV. Results

Multipactor prediction using susceptibility charts (IV)

Comparison between the multipactor the results predicted with the susceptibility charts for ridge waveguides and those from ECSS Multipactor Tool for parallel-plate waveguides

Component	P_{charts} (W)	P_{ECSS} (W)	Difference (dB)
Evanescent mode filter	8.65	3.44	4.0
High-power S-band filter	1449	676	3.3

- It is found that the results extracted from the parallel-plate waveguide approximation is rather conservative when applied to geometries that differ from such ideal case
- Significant increases of 4.0 and 3.3 dB in the power handling capabilities for the above filters arise when considering the ridge multipactor susceptibility charts

View of the ECSS Multipactor Tool version 1.1

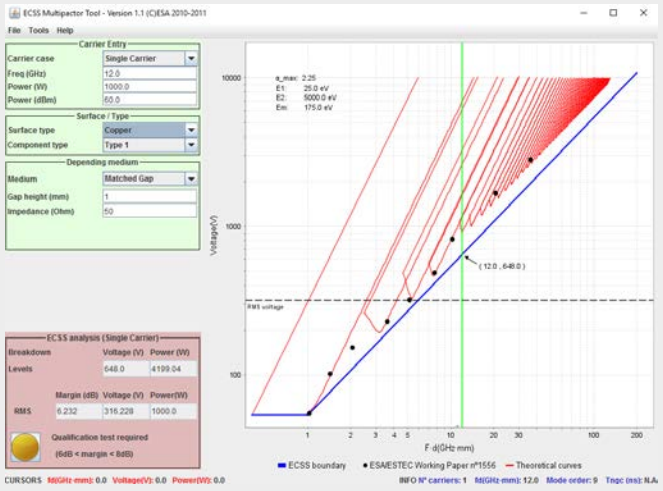

[1] Space Engineering: Multipacting Design and Test. Noordwijk, ESA Publ. Div., May 2003, ECSS-20-01A, edited by ESA-ESTEC

IV. Results

Conclusions

- Multipactor susceptibility charts have been computed for several ridge and multi-ridge waveguides .
- An approximate method based on the susceptibility charts is presented for predicting the multipactor voltage threshold in devices containing ridge and multi-ridge waveguides sections.
- The results of such approximate method are applied to a evanescent mode filter and a high power S-band filter finding good agreement when comparing with results from numerical simulations.
- Using the ridge and multi-ridge susceptibility charts allows to increase RF power handling capability of the device with regard to the use of the ECSS susceptibility charts for parallel-plate waveguides.

IV. Results

Publications

[1] D. González-Iglesias, P. Soto, S. Anza, B. Gimeno, V. E. Boria, C. Vicente, J. Gil, "Multipactor susceptibility charts for ridge and multiridge waveguides", *IEEE Transactions on Electron Devices*, vol. 59, no. 12, pp. 3601-3607, Dec. 2012.

Multipactor with digitally modulated signals

IV. Results

Most of the multipactor studies consider single-carrier harmonic signals whereas realistic signals employed in space telecommunications are multi-carrier and digitally modulated.

In this section, it is analyzed the multipactor RF voltage threshold in a coaxial transmission line excited by a single-carrier digital modulated signal

To reach this aim the following points are considered:

1. Theory of digital modulated signals
2. Multipactor simulations with the effective electron code (basic modulation scenarios)
3. Analysis of multipactor with RF pulsed signals
4. Coarse method for multipactor prediction with arbitrary digital modulated signals
5. Multipactor simulations with the individual electron code (complex modulation scenarios)

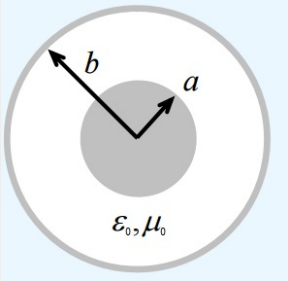

Cross section of a coaxial line

IV. Results

Theory of digital modulations

A digital modulated signal allows to transmit a bit sequence encoded as a certain combination of symbols of the modulation scheme.

Each symbol has a predefined duration in the transmitted signal denoted by T_s, typically this value is given in terms of the ξ factor, which is the ratio between the symbol duration and the RF carrier period

$$\xi = \frac{T_s}{T}$$

There are many ways to modulate digitally a carrier signal:

- The phase of the RF carrier signal can be switched among a certain number of values between different symbols, e.g. phase-shift keying (PSK)
- Both the phase and amplitude of the RF carrier can be varied between symbols, e. g. : quadrature amplitude modulation (QAM) or amplitude and phase-shift keying (APSK).

Example: BPSK

$$V(t) = V_0 \cos(2\pi f t + \theta_n(t))$$

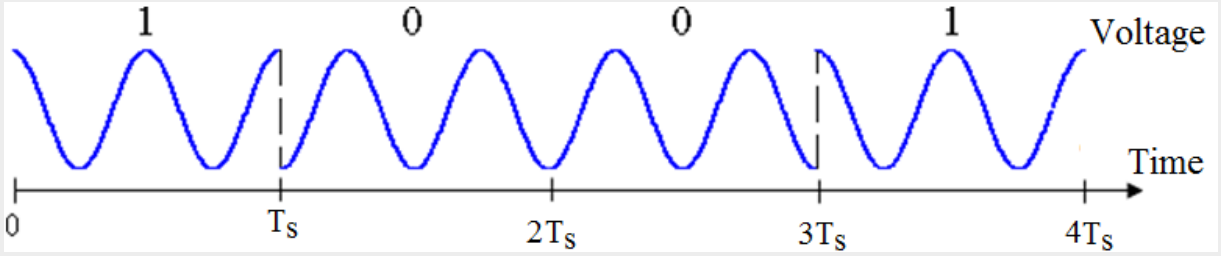

$\theta_n = \pi$ if the bit is "0"

$\theta_n = 0$ if the bit is "1"

IV. Results

Theory of digital modulations (II)

Any arbitrary digital modulated signal can be expressed as:

$$V(t) = V_0 A(t) \cos(2\pi f t + \theta(t))$$

A(t) and θ(t) are the symbol amplitude and phase, respectively, which change from symbol to symbol

Alternatively, any arbitrary digital modulated signal can be expressed in terms of the I/Q data in the following form:

$$V(t) = V_0 [I(t) \cos(2\pi f t) - Q(t) \sin(2\pi f t)]$$

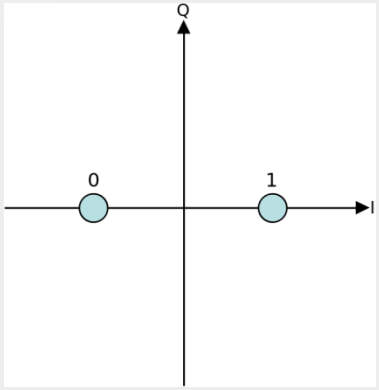

BPSK (M=2)

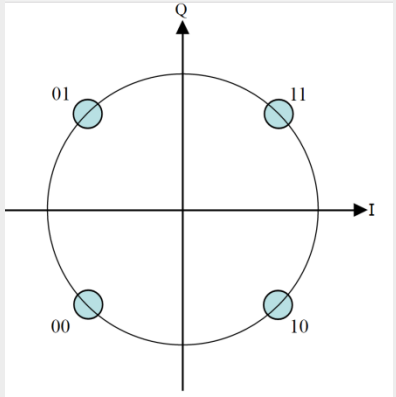

QPSK (M=4)

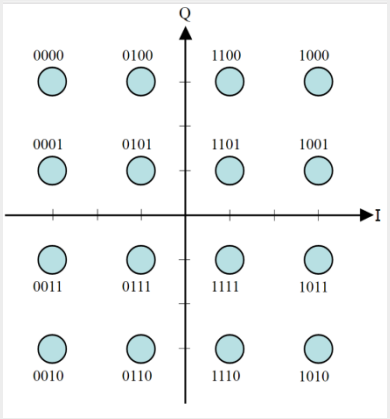

16-QAM (M=16)

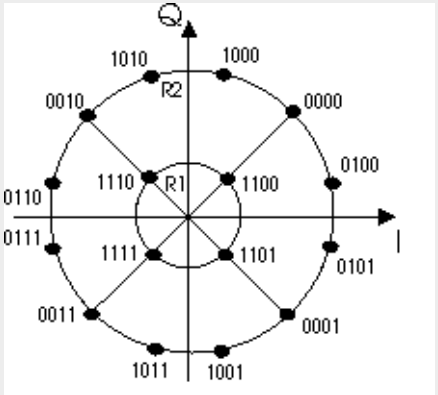

16-APSK (M=16)

IV. Results

Theory of digital modulations (III)

After the modulation of the RF carrier, in order to smooth transitions between symbols, a filtering process is applied to the signal. A typical choice is the use of the Root Raised Cosine filter (RRC).

RRC filter $$g_{rrc}(t) = \frac{4\Gamma}{\pi\sqrt{T_s}} \frac{\cos\left(\frac{(1+\Gamma)\pi t}{T_s}\right) + \frac{1}{\frac{4\Gamma t}{T_s}} \sin\left(\frac{(1-\Gamma)\pi t}{T_s}\right)}{1 - \left(\frac{4\Gamma t}{T_s}\right)^2}$$

Roll-off factor $0 \leq \Gamma \leq 1$

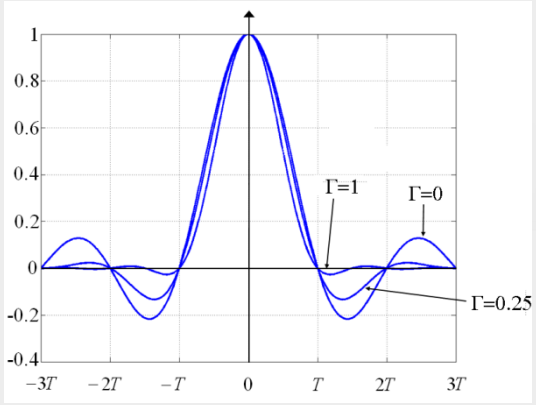

The digital modulated signal after filtering process is given by

$$V(t) = V_0 \sum_{n=-\infty}^{+\infty} g(t - nT_s) A_n \cos(2\pi f t + \theta_n)$$

Hence, the final shape of the digital modulated signal depends mainly on:

- The ξ factor
- The transmitted symbol sequence
- The filter type

Example: BPSK signal before (above) and after (below) a filtering with Γ = 0.2 RCC. Symbol sequence "10…", ξ = 5

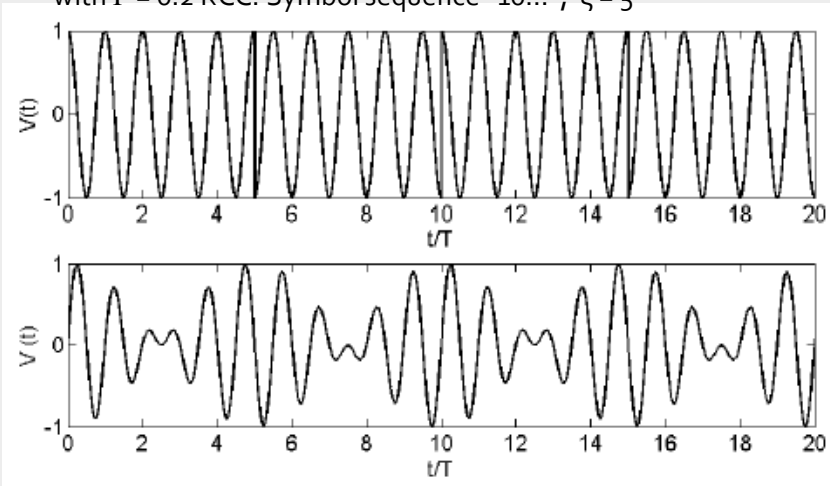

IV. Results

Multipactor simulations with the effective electron code

BPSK without filtering: It is shown the multipactor RF voltage threshold normalized to the multipactor threshold of the unmodulated (harmonic) signal

- ✓ Transmitted bit sequence "10…"
- ✓ No filtering: the phase varies 180º at the symbol transition (T_s)

It is observed that:

- ➢ Modulation affects the multipactor voltage threshold, specially for $\xi < 30$
- ➢ Different behaviors depending on the f x d value: with low f x d normalized threshold raises up, with medium-high f x d normalized threshold diminishes

Inner conductor radius → a = 1.515 mm
Outer conductor radius → b = 3.490 mm
Gap → d = b-a = 1.975 mm
Impedance→ Z = 50 Ω

Material → Copper
W_1 = 25 eV
W_{max} = 175 eV
δ_{max} = 2.25

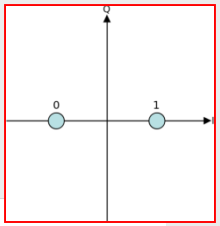

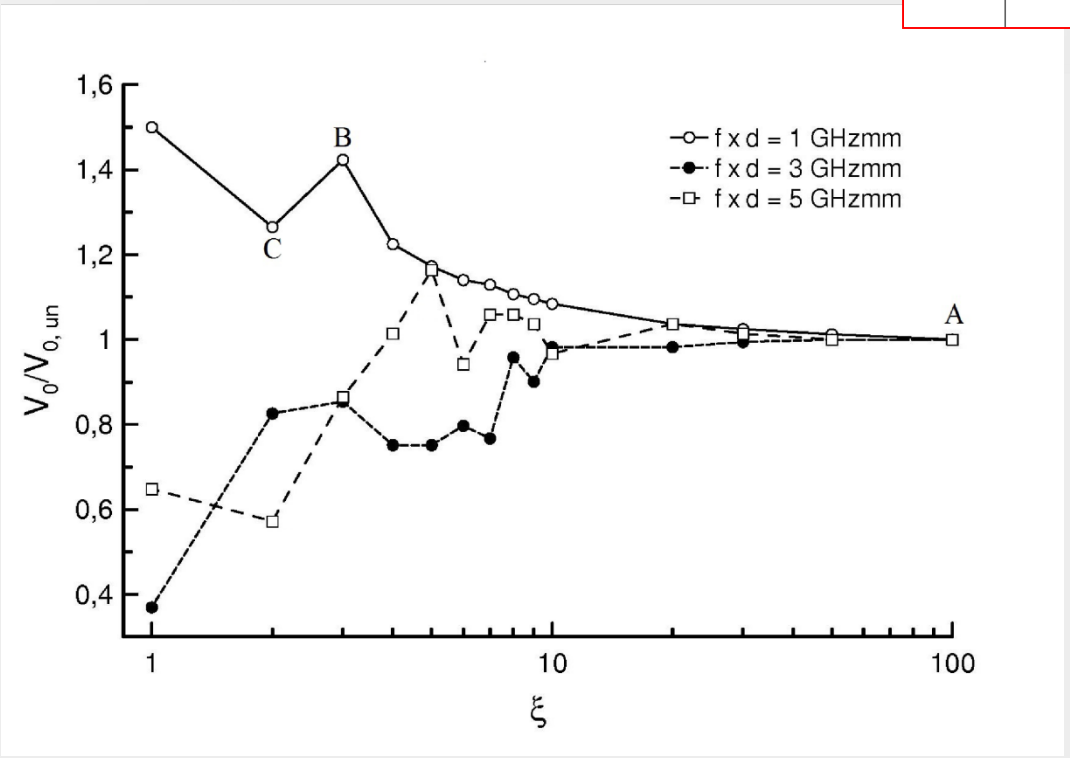

$$\xi = \frac{T_s}{T}$$

$\longrightarrow$ Time symbol
$\longrightarrow$ RF carrier period

IV. Results

Multipactor simulations with the effective electron code (II)

BPSK without filtering: The electron trajectories are analyzed at several points of the multipactor curve.

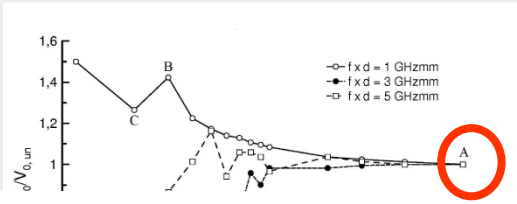

Point A

f x d = 1 GHzmm

$\xi = 100$

- Scenario very close to the unmodulated one (100 RF periods between successive phase shifts)

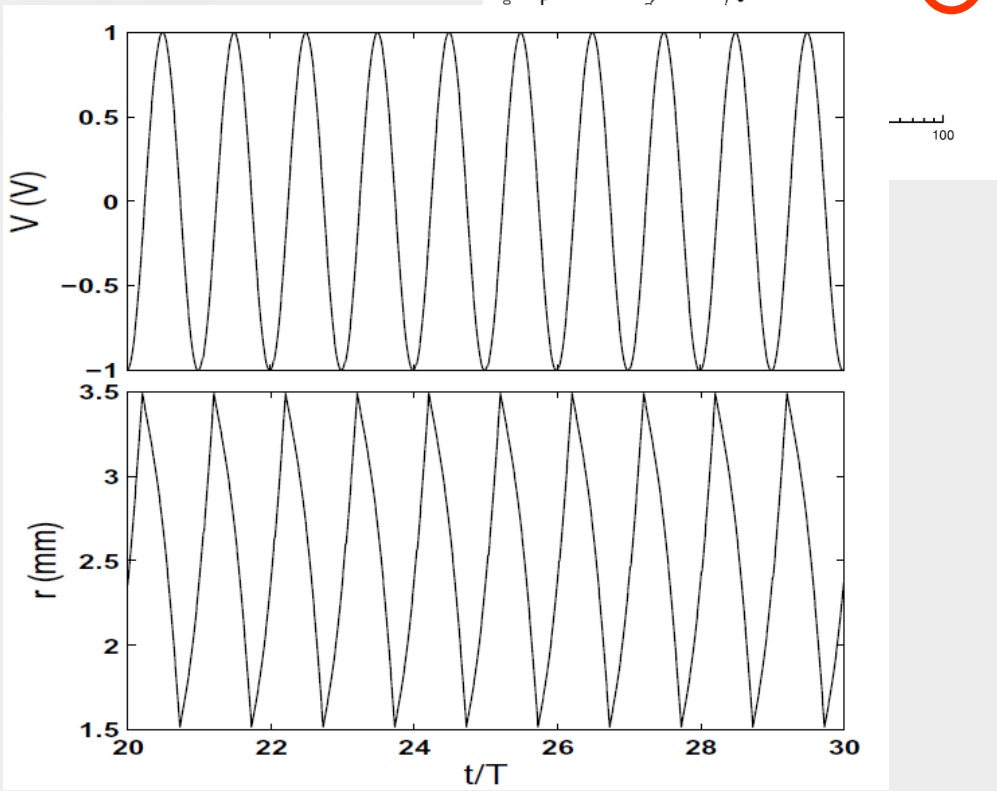

- Electron flight time between conductors:

From outer to inner → 0.5 T

From inner to outer → 0.5 T

Multipactor order → 1

IV. Results

Multipactor simulations with the effective electron code (III)

BPSK without filtering

Point B

$f \times d = 1$ GHzmm

$\xi = 3$

- Effective electron trajectory periodic with period equal to $2T_S$
- Complex trajectory: 10 impacts before repeating the sequence
- Flight time (in terms of T): 0.47 , 1.23, 0.36, 0.45, 0.46, 0.53, 1.18, 0.44, 0.38 y 0.5 → No estable multipactor order

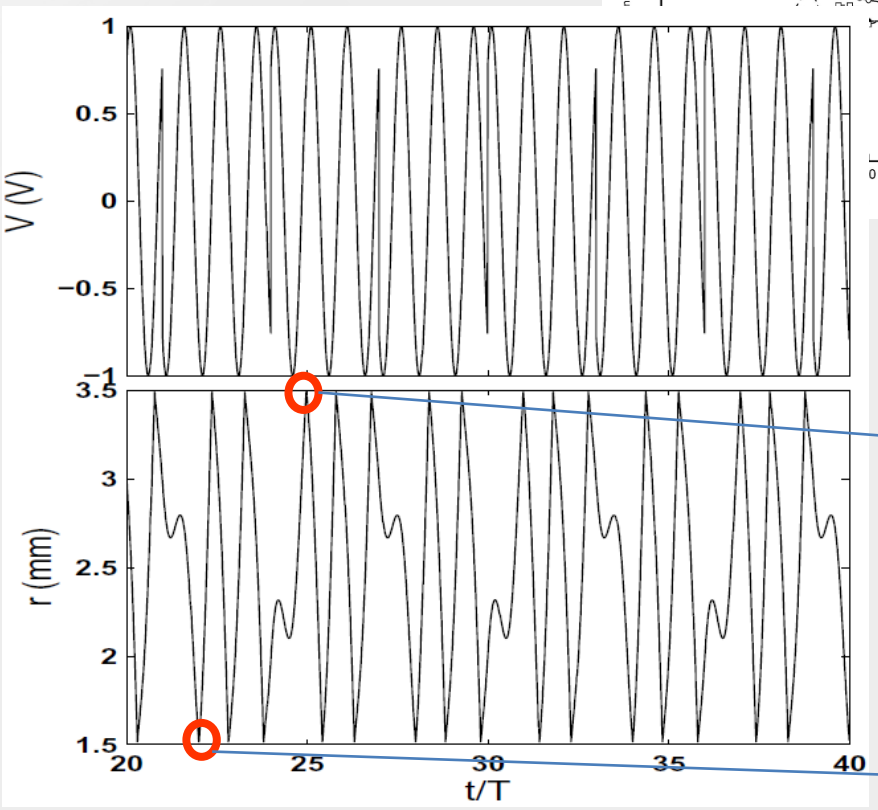

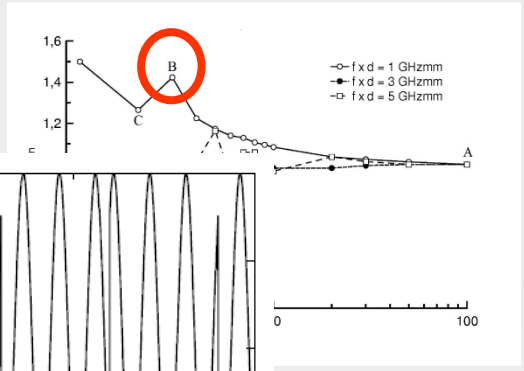

SEY below unity (δ<1) for these impacts

IV. Results

Multipactor simulations with the effective electron code (IV)

BPSK without filtering

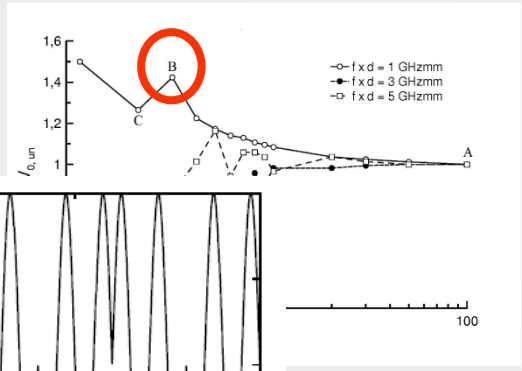

Point C

$f \times d = 1$ GHzmm

$\xi = 2$

- Effective electron trajectory periodic with period equal to 2Ts
- Trajectory more simple that in point C: 4 impacts before repeating sequence
- Flight time (in terms of T): 0.5, 0.5, 0.47 y 2.53

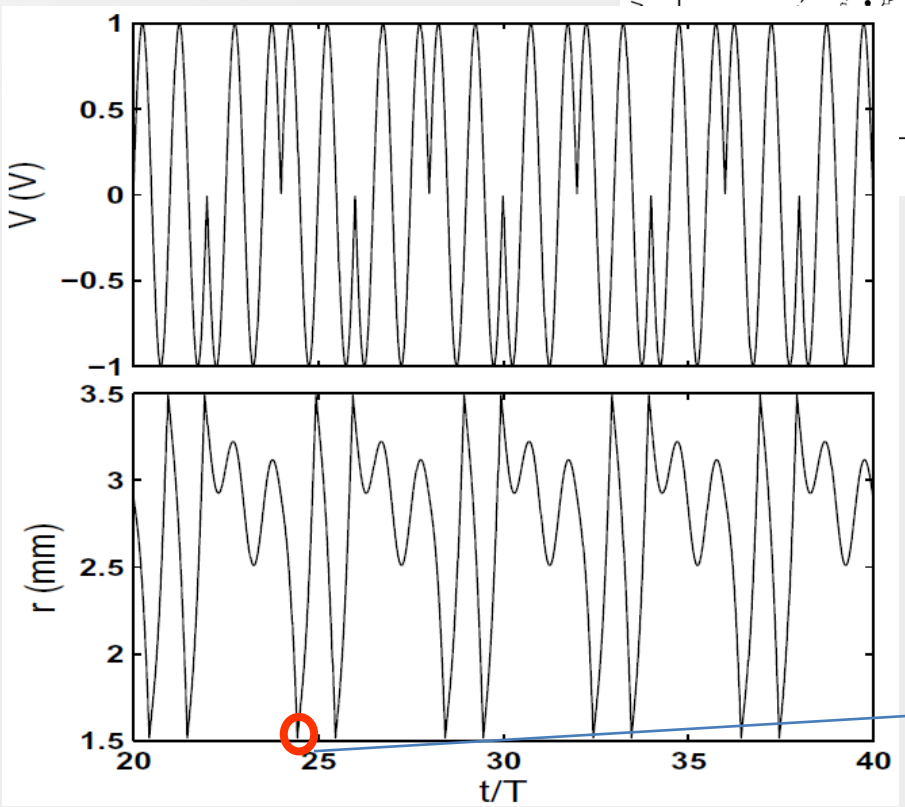

SEY below unity ($\delta<1$) for those impacts

IV. Results

Multipactor simulations with the effective electron code (V)

BPSK with RRC filter: It is shown the multipactor RF voltage threshold normalized to the multipactor threshold of the unmodulated (harmonic) signal

- ✓ RRC filter, Γ = 0.25
- ✓ Transmitted bit sequence "101010…"

It is observed that:

- ➢ Different behavior with respect to the without filter case: the curves for different f x d values do not converge at ξ = 100
- ➢ For low f x d normalized threshold raises up as ξ diminishes, whilst with medium-high f x d the normalized threshold diminishes as ξ does

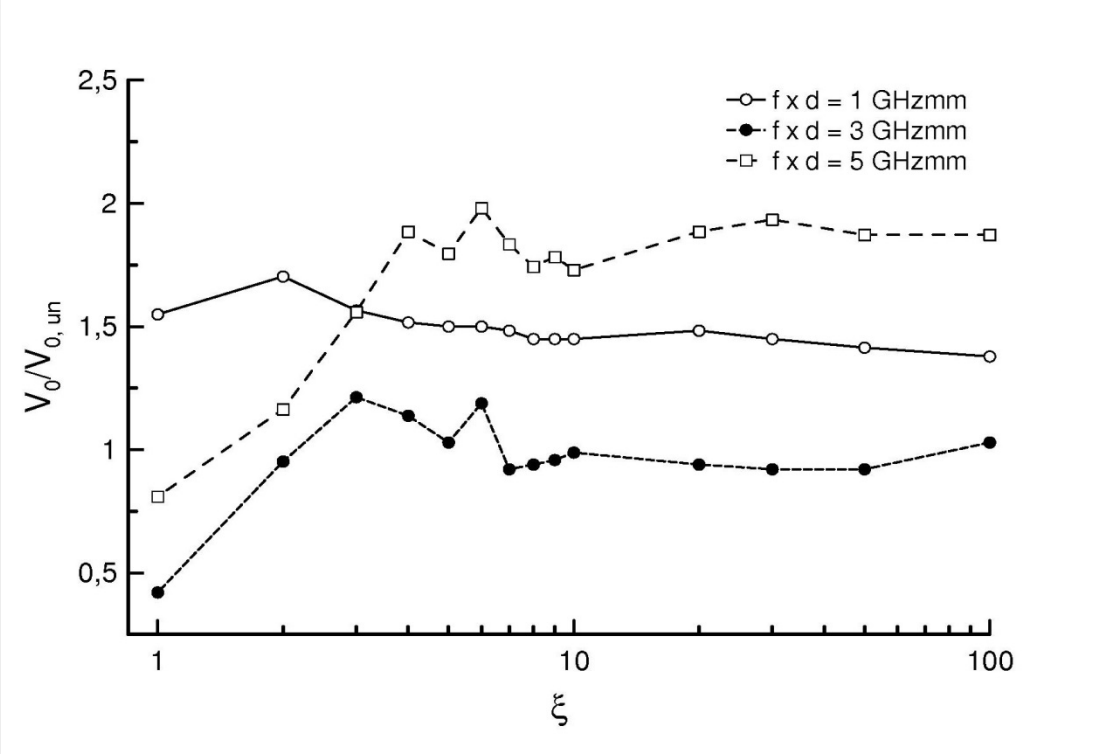

IV. Results

Multipactor simulations with the effective electron code (VI)

QPSK with RRC filter: It is shown the multipactor RF voltage threshold normalized to the multipactor threshold of the unmodulated (harmonic) signal

- ✓ RRC filter, Γ = 0.25
- ✓ f x d = 1 GHzmm
- ✓ Sequence "11011000…": phase shifts of 90º,180º,90º,180º…
- ✓ Sequence "11010010…": phase shifts of 90º between successive symbols

Seq. "11011000"

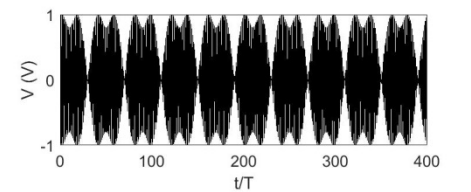

Seq. "11010010"

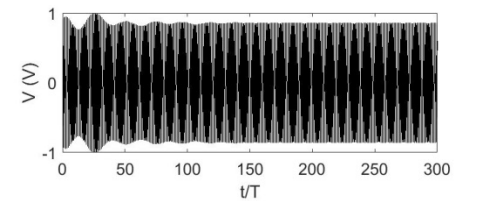

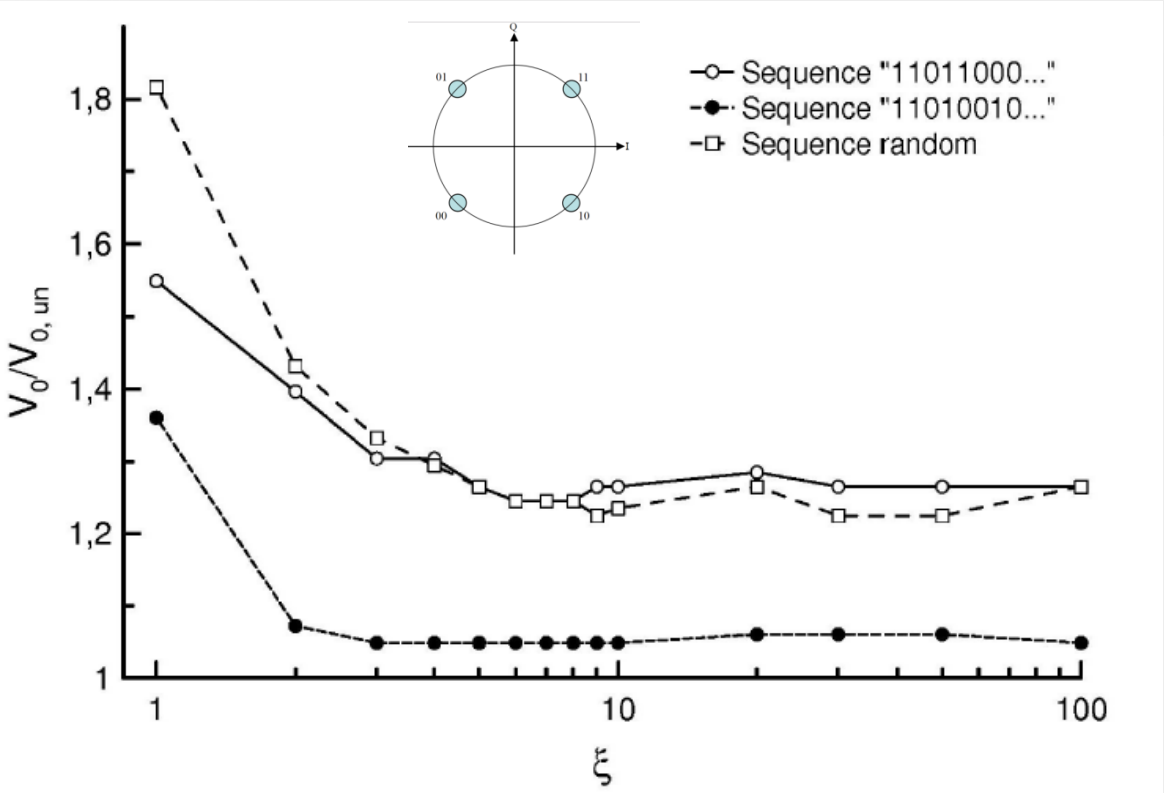

IV. Results

Multipactor simulations with the effective electron code (VII)

Experimental validation. It was carried out a multipactor experiment to validate some of the previous results presented

- ✓ BPSK
- ✓ without filtering
- ✓ f = 435 MHz , f x d = 0.859 GHzmm
- ✓ Transmitted bit sequence "10…"

It is observed:

- ➢ Good agreement between theoretical and experimental data

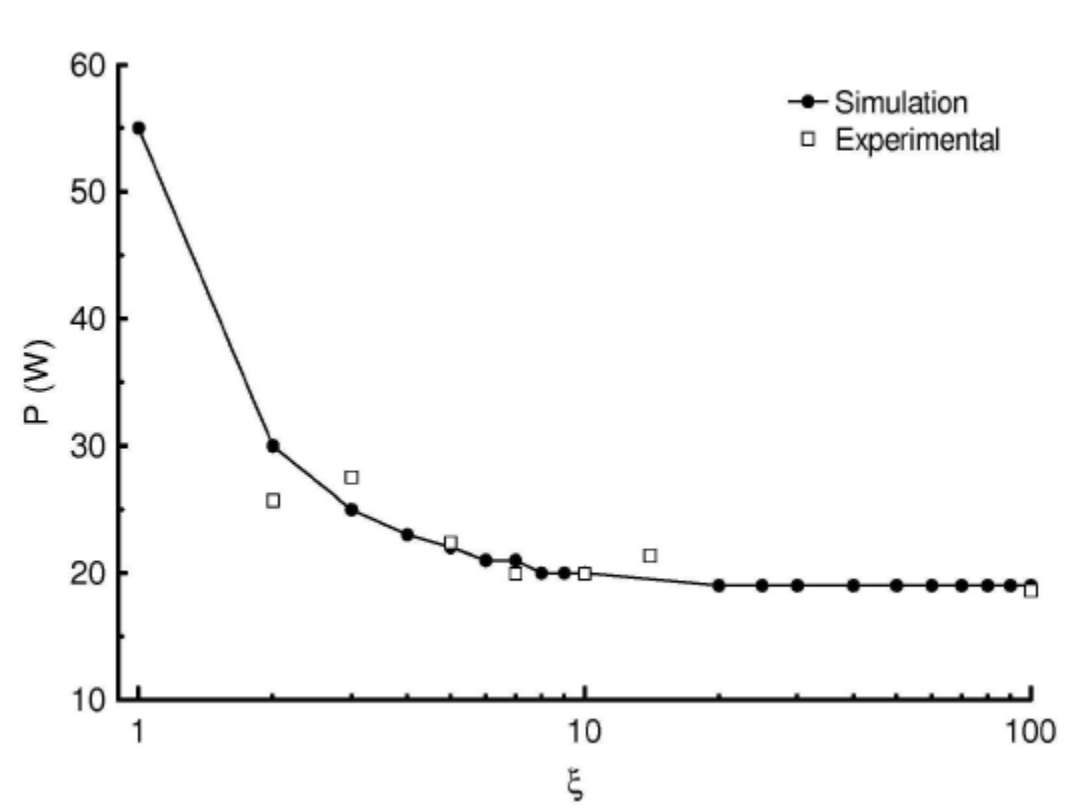

IV. Results

Analysis of multipactor with RF pulsed signals

The modulated signals analysed in the previous subsection correspond to simple academic cases (most of them were periodic), in such cases the selection of the multipactor discharge criterion is straightforward

QPSK ξ = 40 with RRC, Γ = 0.25, seq: “1110..”

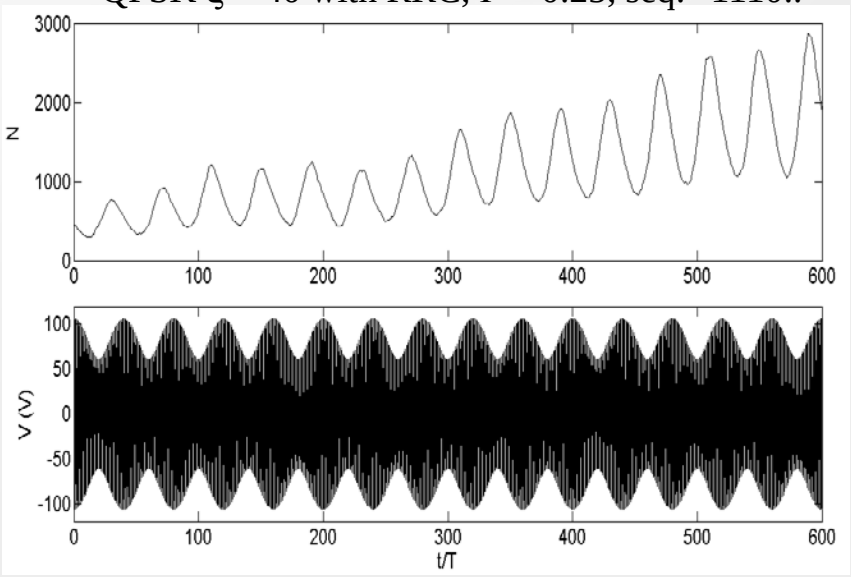

CW signal

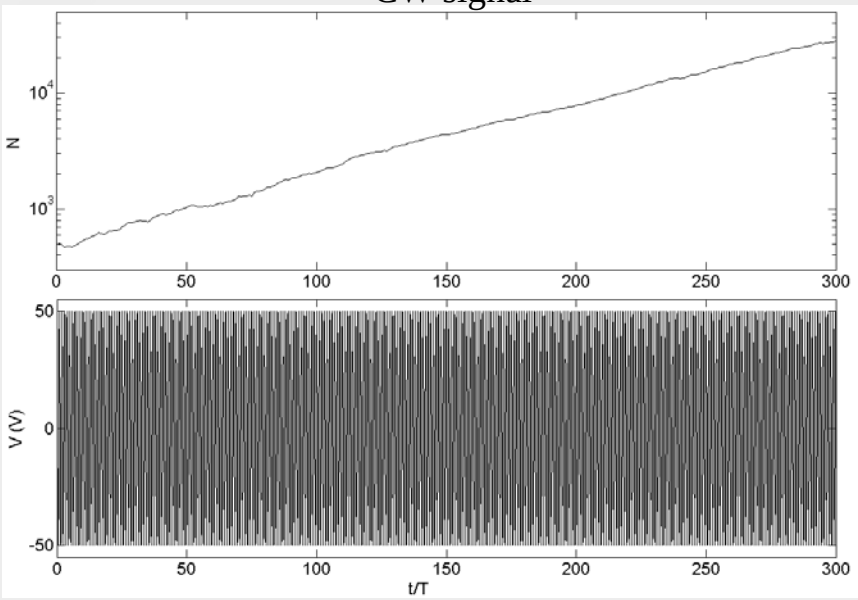

If it is observed an increase of the electron population with time, then the discharge will eventually occur sooner or later

IV. Results

Analysis of multipactor with RF pulsed signals (II)

However, realistic transmitted signals employed in telecommunication systems are far from the simplicity of the previous signals:

Telecommunication signal: 16APSK ξ = 40 with RRC Γ = 0.25

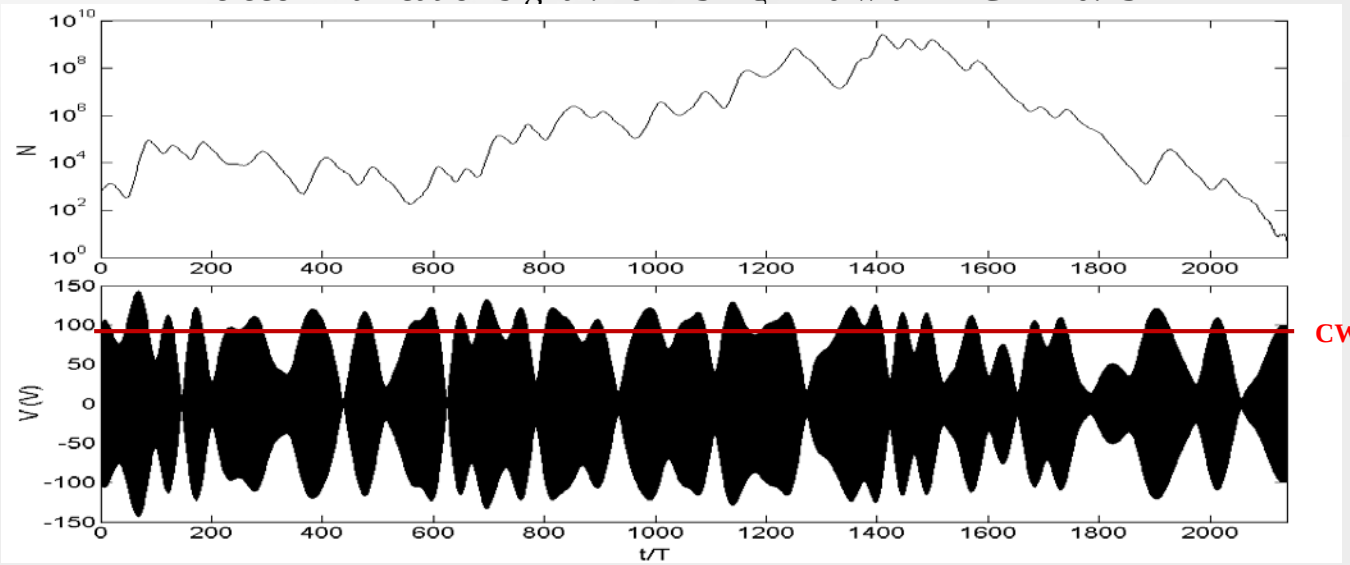

In this latter case, the multipactor criterion to decide if the discharge has been occurred is not evident. One question arises: *What is the minimum electron (density) population to trigger the multipactor discharge?*

IV. Results

Analysis of multipactor with RF pulsed signals (III)

What is the minimum electron (density) population to trigger the multipactor discharge?

The answer depends on the sensibility of the diagnostic methods implemented in the experimental set-up

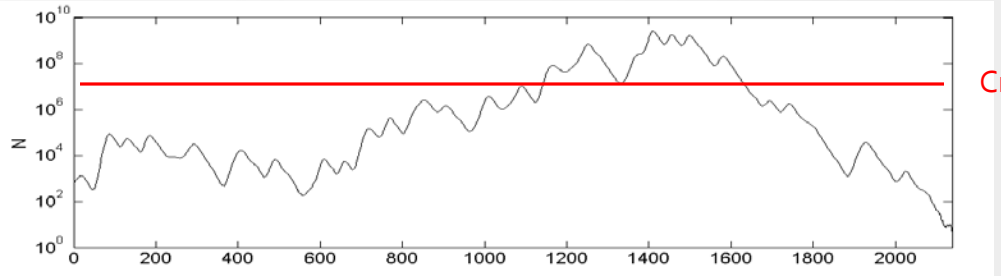

Critical discharge level?

Nulling system

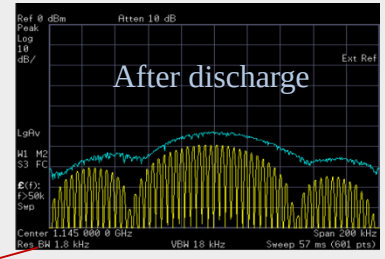

Several problems arise:

- There is no an unequivocal and quantitative definition of multipactor discharge
- There are no experimental data about the electron density (population) during the discharge

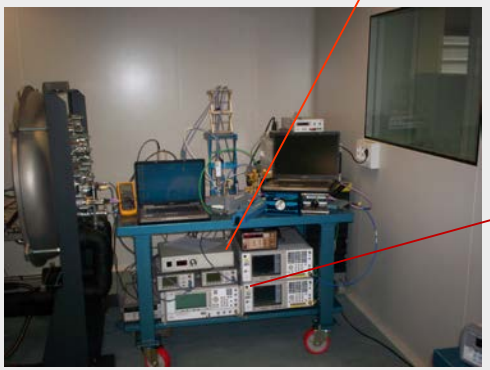

Partial view of a typical multipactor test-bed

IV. Results

Analysis of multipactor with RF pulsed signals (IV)

To overcome these inconveniences, we propose an indirect method to determine the electron density (population) during the discharge based on the study of the multipactor RF voltage threshold in RF pulsed signals.

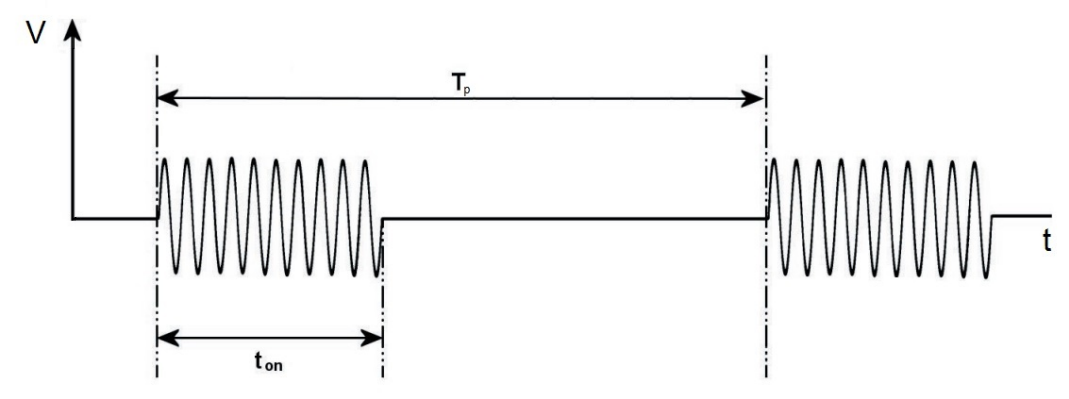

Scheme of a RF pulsed signal

- During the active part of the pulse (t_{on}) the signal is time-harmonic and the electron population will increase whenever the RF voltage amplitude exceeds the CW multipactor RF voltage threshold
- During the inactive part of the pulse the electron population will diminish since electrons are mainly absorbed by the walls
- If $t_{on} << T_p$ there will not be electron accumulation from one pulse to next, consequently only the active part of one individual pulse must be analyzed in the multipactor simulations

IV. Results

Analysis of multipactor with RF pulsed signals (V)

- The evolution of the electron population is obtained by means of the individual electron simulation code
- Assuming different values for the electron population at the discharge level (the multipactor crterion), it is obtained the multipactor RF voltage threshold curves for the RF pulsed signals
- From comparison with experimental measurements it is stated that the best fit is produced for $N_{max} = 10^{12}$
- This fact is in agreement with the theoretical results presented in [1]

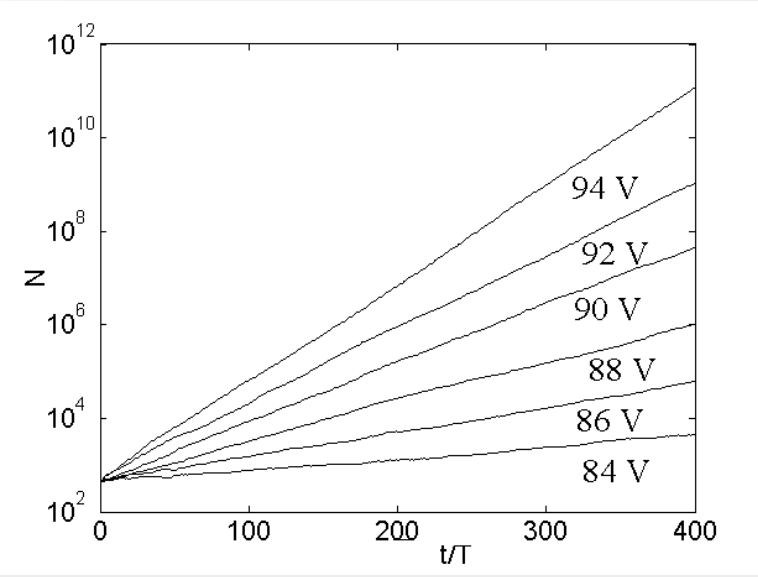

Number of electrons as a function of the normalized time

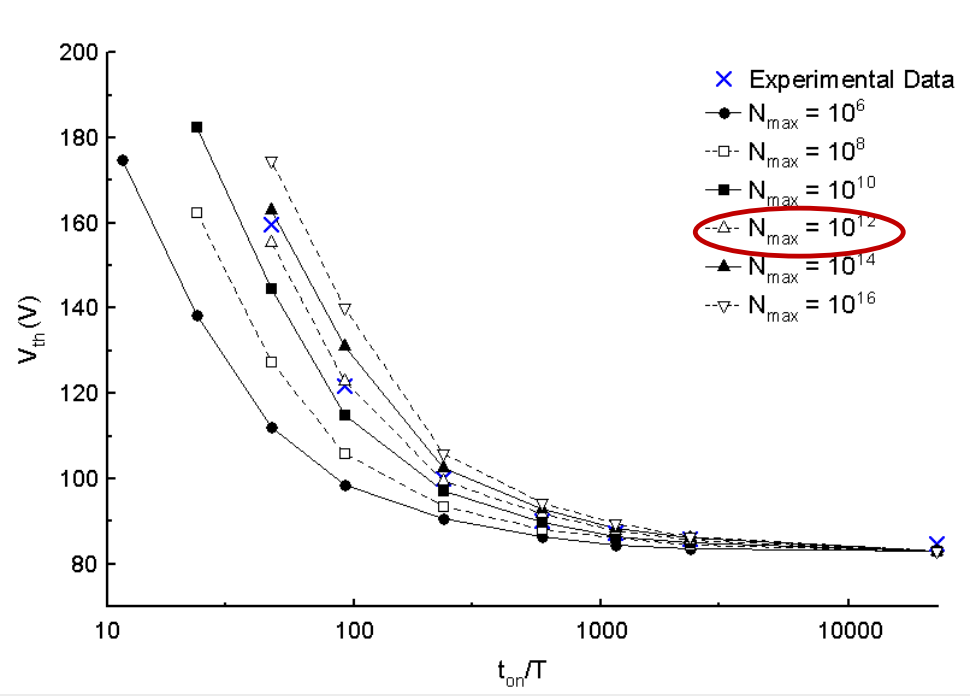

[1] E. Sorolla, A. Sounas, M. Mattes, "Space charge effects for multipactor in coaxial lines", *Physics of Plasmas*, vol. 22, 033512 (2015).

IV. Results

Coarse method for multipactor prediction

The coarse method is a procedure that allows to estimate the multipactor RF voltage threshold for digital modulated signals relying only in numerical simulations for the CW signal at the carrier frequency. Presents the advantage of being much faster than the numerical simulations (hours versus minutes).

This method is based on the electron growth model for parallel-plates with CW signal

N_0 , electron population at t = 0
$N(t_n)$ electron population after the *n*-th impact
δ_{av}, average SEY at the collisions
m multipactor order

$$N(t_n) = N_0 e^{\alpha t_n} \quad (1) \qquad \alpha = \frac{2f}{m} \ln \delta_{av} \qquad t_n = n\left(\frac{m}{2f}\right)$$

Time of the n-th impact

The following assumptions can be made:

I. Time can be assumed as a continuous variable since the time required for the onset of the discharge is much greater than the time between successive impacts

II. Signal envelope varies smoothly over the time interval between successive impacts of the electron (i.e. ξ>>1). This implies that the electron trajectories between two successive impacts are little disturbed due to the envelope change.

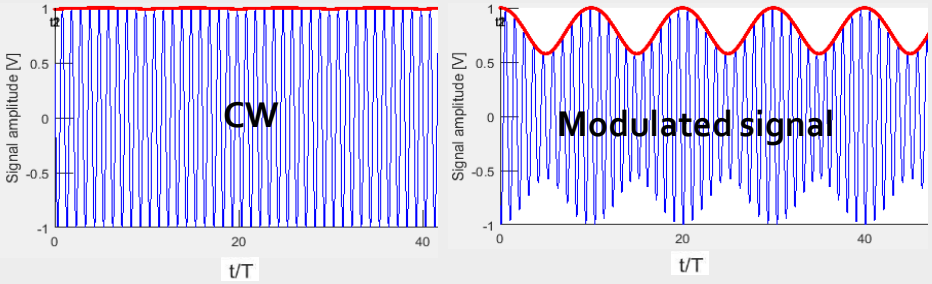

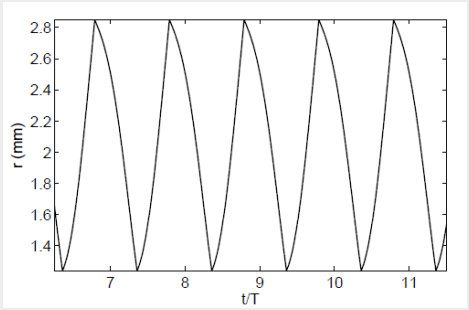

Electron resonant trajectory with m =1

IV. Results

Coarse method for multipactor prediction (II)

- Under assumption I the formula for the electron number with CW signals (1) can be differentiated:

$$N(t) = N_0 e^{\alpha t} \xrightarrow{\text{Differentiation}} \frac{dN}{N} = \alpha dt \quad (2)$$

- Assumption II implies that (1) and (2) are locally valid for modulated signals, but it has to be taken into account that now the growth factor α varies with time

$$\frac{dN}{N} = \alpha(t)dt \quad (3) \xrightarrow{\text{Integration}} \boxed{N(t) = N_0 exp\left(\int_0^t \alpha(t)dt\right) \quad (4)}$$

- Expression (4) constitutes the basis of the coarse method since it provides the time evolution of the electron population within the component.

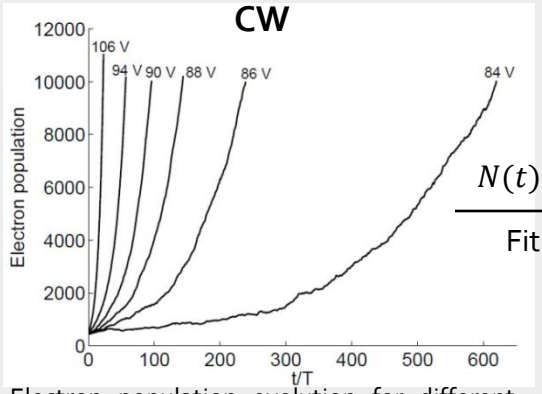

Electron population evolution for different values of the RF voltage amplitude

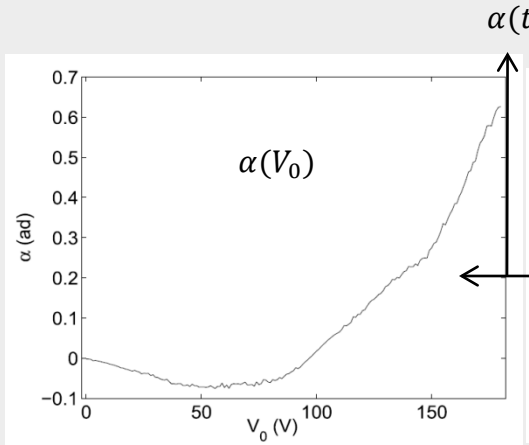

Value of the α factor for different RF voltage amplitudes

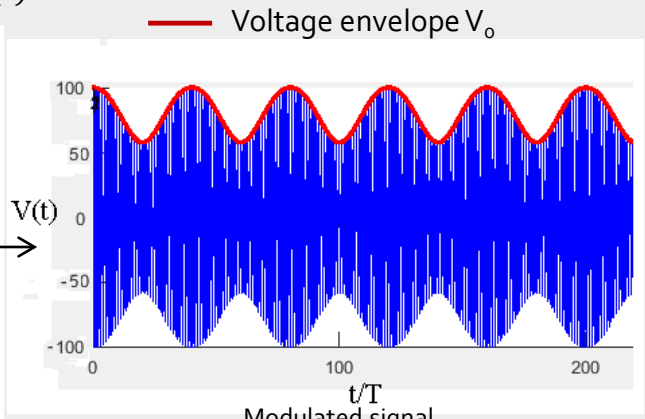

Modulated signal

IV. Results

”20-gap-crossing” rule

- Up to now, the standard adopted by the European Space Agency (ESA) for multicarrier multipactor design is based on the “20-gap-crossing” rule [1], which is used as an engineering “rule of thumb” for assessing the risk of multipactor breakdown.

- This rule states that “with a multi-carrier signal, multipactor events will be detectable whenever the power is maintained above the CW threshold for a time period about 20 gap crossings of the electron”.

Example:

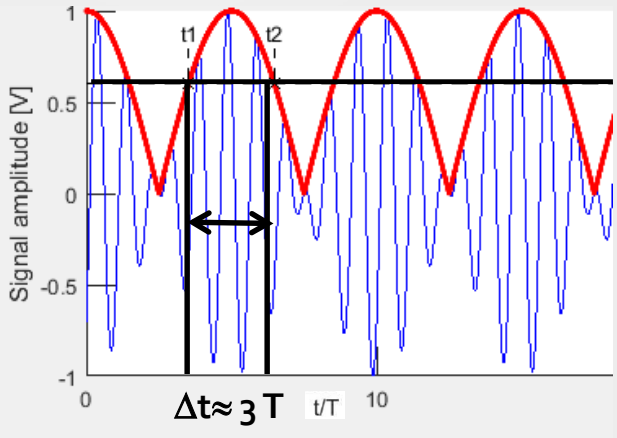

CW Voltage threshold

This signal will not trigger a multipactor discharge according to the “20-gap-crossing rule”

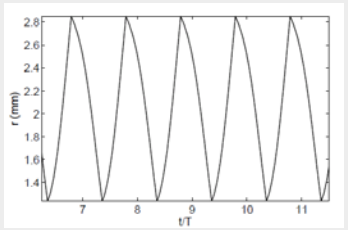

multipactor order m =1

½ T in crossing the gap once, 10T in crossing the gap 20 times 1

[1] ECSS Secretariat, “Multipaction design and test,” ESA-ESTEC Requirements & Standards Division, Noordwijk, The Netherlands, ESA-ESTEC, Tech. Rep. ECSS-E-20-01A, 2003.

IV. Results

Multipactor simulations with the individual electron code

Theoretical and experimental results are based on the following parameters scenario:

- RF carrier frequency is 1.145 GHz.
- The dimensions and characteristics of the coaxial sample are:

  Inner conductor radius → a = 1.238 mm Gap → d = b-a = 1.612 mm

  Outer conductor radius → b = 2.850 mm Material → copper

  Impedance→ Z = 50 Ω

- The Furman and Pivi SEY parameters for copper are

  s = 1.539
  δ_m = 1.77
  W_m = 277 eV

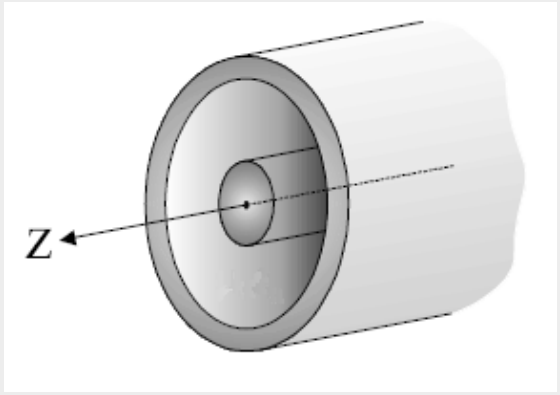

IV. Results

Multipactor simulations with the individual electron code (II)

In a first step, we consider QPSK digital modulated signals with simple periodic symbol sequence (Q and X sequences)

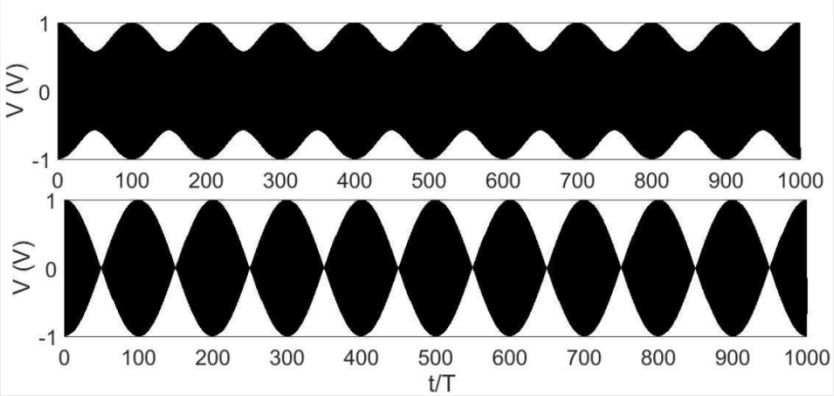

Voltage of the RF signals as a function of the time normalized to the RF period. Top: QPSK with Q sequence. Bottom: QPSK with X sequence. In both cases, ξ =100.

The multipactor RF voltage threshold for the modulated signals is expressed in dB

$$V_{th}(dB) = 20\log\left(\frac{V_{th}}{V_{th,CW}}\right)$$

$V_{th,CW}$ is the multipactor RF voltage threshold for the CW case

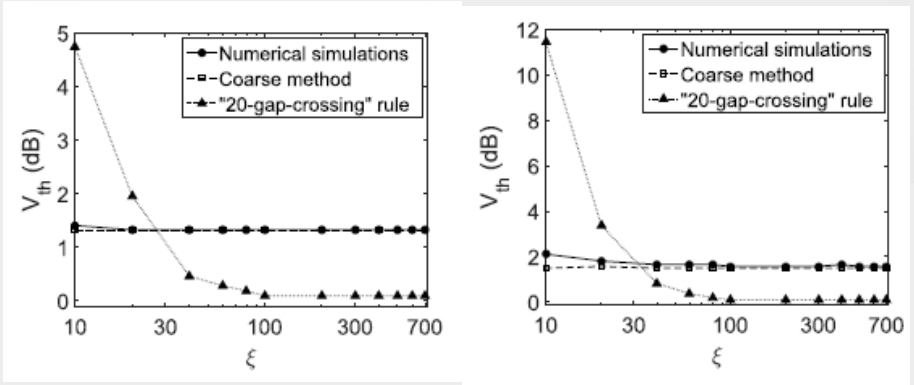

RF multipactor voltage threshold as a function of the ξ factor for Q (left) and X (right) sequences .

- It is found good agreement between results from numerical simulations and the coarse method.
- Significant discrepancies are found when comparing with the "20-gap-crossing" rule.
- The numerical simulations and the coarse method predict a slight increase in the multipactor RF voltage threshold for low ξ values.

IV. Results

Multipactor simulations with the individual electron code (III)

Next, we consider the case of realistic signal random sequences of symbols for QPSK, 16-APSK, 32-APSK, and 16-QAM digital modulations

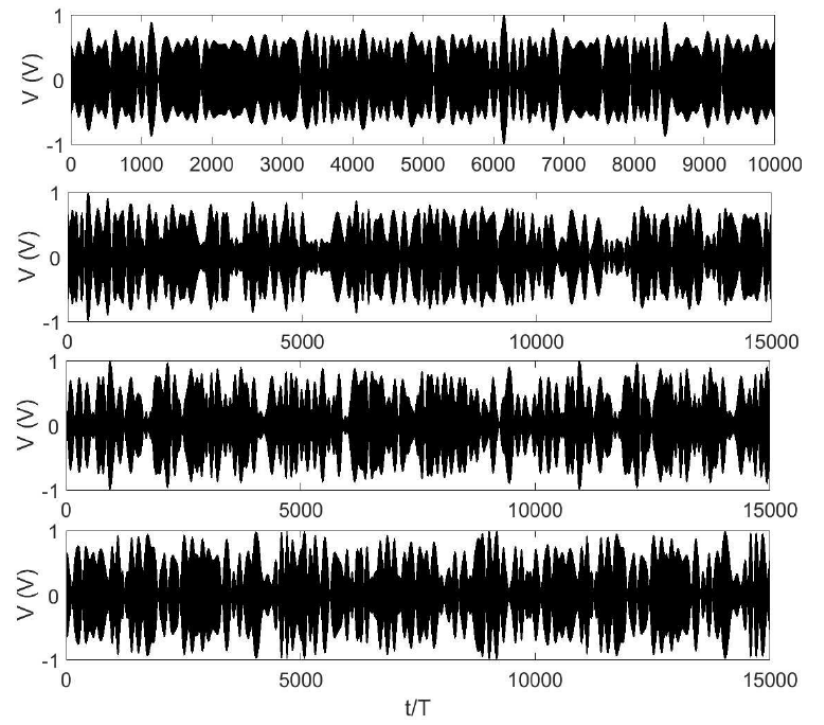

Voltage of the RF signals as a function of the time normalized to the RF period. Top to bottom: QPSK, 32-APSK, 16-APSK, and 16-QAM. In both cases, ξ =100.

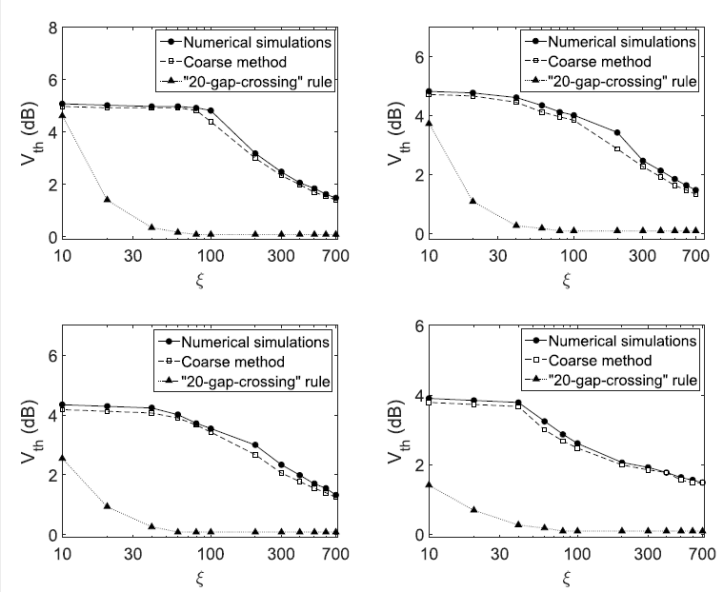

RF multipactor voltage threshold as a function of the ξ factor for the random sequences. From left to right and top to bottom: QPSK, 16-APSK, 32-APSK, and 16-QAM.

- It is found good agreement between results from numerical simulations and the coarse method but there are significant discrepancies with the "20-gap-crossing" rule.
- The numerical simulations and the coarse method predict a an increase in the multipactor RF voltage threshold for low ξ values.

IV. Results

Multipactor simulations with the individual electron code (IV)

Comparison with experimental results

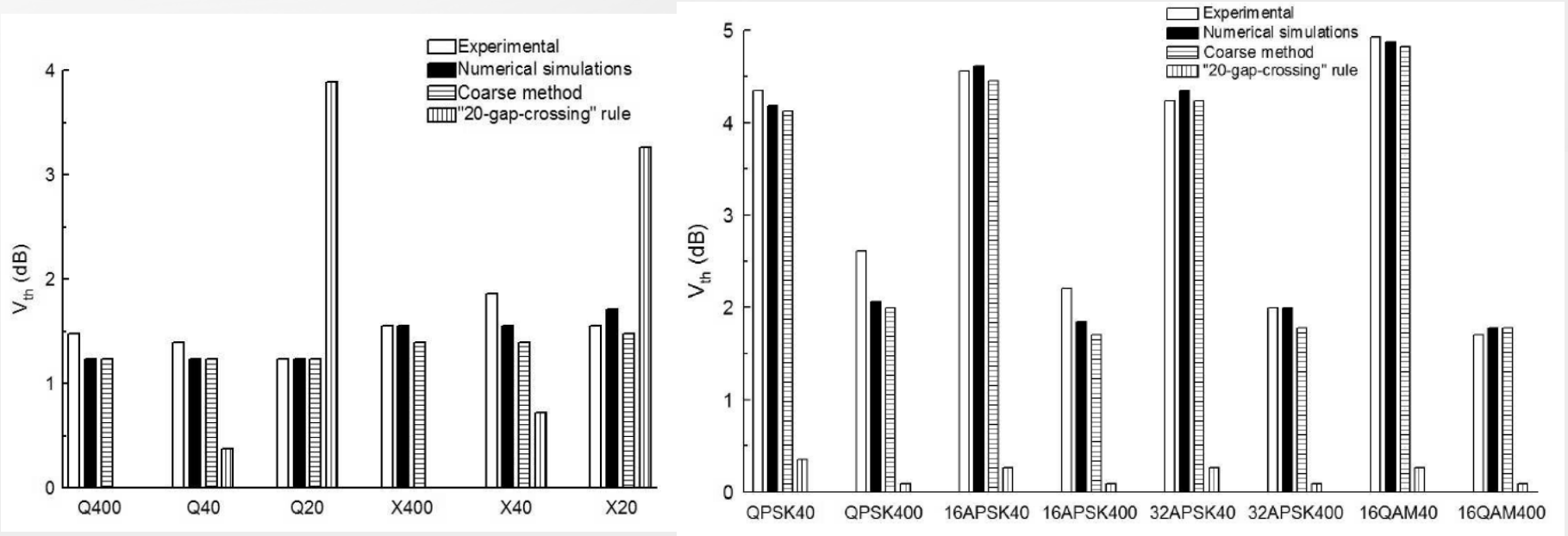

RF multipactor voltage threshold for different digital modulated signals. The number after the modulation indicates the ξ value.

- It is found good agreement between results from numerical simulations and the coarse method with the experimental data.
- Significant differences between the "20-gap-crossing" rule and the experimental results are found.

IV. Results

Conclusions

- Effect of digital modulated signals in the RF multipactor voltage threshold for a coaxial transmission line has been studied.
- Besides the numerical simulations, a fast coarse method for multipactor prediction with modulated signals is presented.
- Several digital modulation schemes (QPSK, 16-APSK, 32-APSK, 16-QAM) have been considered for different transmitted symbol sequences and different ξ values.
- Theoretical results from the numerical simulations and the coarse method are in agreement with the experimental data.
- Significant discrepancies have been found between the ESA standard "20-gap-crossing" rule and the experimental results

IV. Results

Publications

[1] D. González-Iglesias, M. P. Belloch, Ò. Monerris, B. Gimeno, V. E. Boria, D. Raboso, V. E. Semenov, "Analysis of multipactor effect using a Phase-Shift Keying single-carrier digital modulated signal", *IEEE Transactions on Electron Devices*, vol. 60, no. 8, pp. 2664-2670, Aug. 2013.

[2] D. González-Iglesias, Ò. Monerris, M. E. Díaz, B. Gimeno, V. E. Boria, D. Raboso, "Experimental analysis of the multipactor effect with RF pulsed signals", *IEEE Electron Device Letters*, vol. 36, no. 10, pp. 1085-1087, Oct. 2015.

[3] D. González-Iglesias, Ó. Monerris, B. Gimeno, M. E. Díaz, V. E. Boria, P. M. Iglesias, "Multipactor RF breakdown in coaxial transmission lines with digitally modulated signals", *IEEE Transactions on Electron Devices*, vol. 63, no. 10, pp. 4096-4103, Oct. 2016.

Multipactor in a ferrite-loaded waveguide

IV. Results

The main objective is the study of the multipactor effect in parallel-plate waveguides containing a magnetized ferrite slab:

- Computation of the multipactor RF voltage threshold for several representative cases.
- Detailed analysis of the electron trajectories and the multipactor regimes

Two different magnetization directions for the ferrite has been explored:

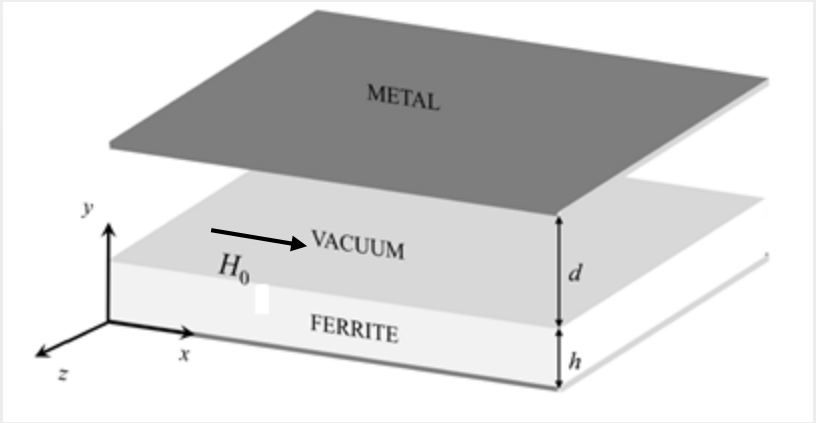

Parallel-plate waveguide partially loaded with a ferrite slab magnetized parallel to the ferrite slab direction by a static magnetic field.

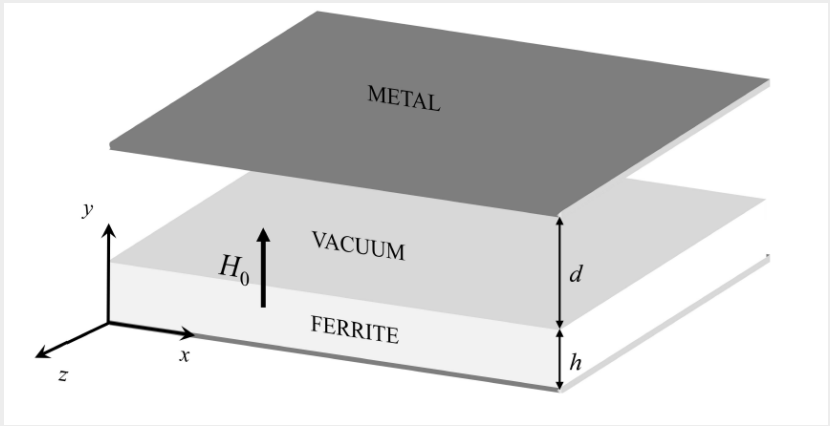

Parallel-plate waveguide partially loaded with a ferrite slab magnetized along the waveguide gap direction by a static magnetic field.

IV. Results

This work is aimed to be the first step towards the understanding of the multipactor phenomenon in most complex RF devices containing magnetized ferrites such as circulators, isolators and phase shifters.

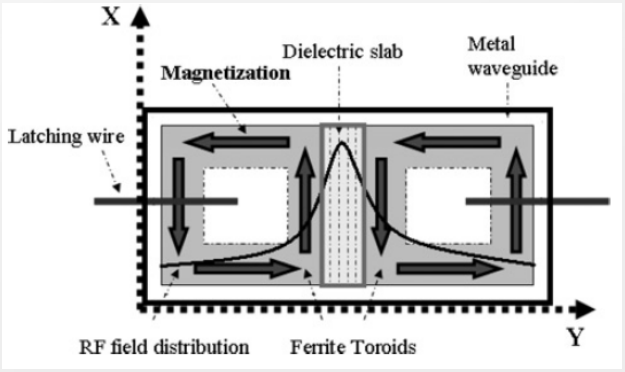

Scheme of a toroidal phase-shifter

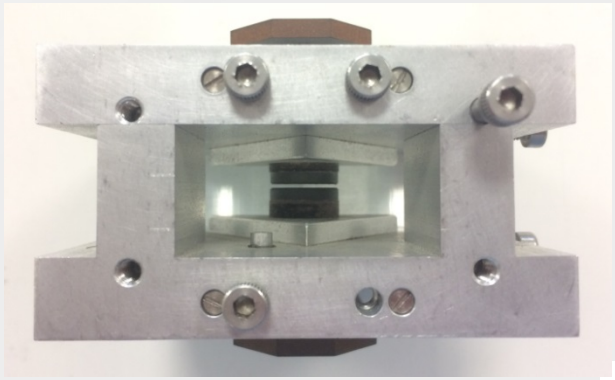

View of a ferrite junction circulator

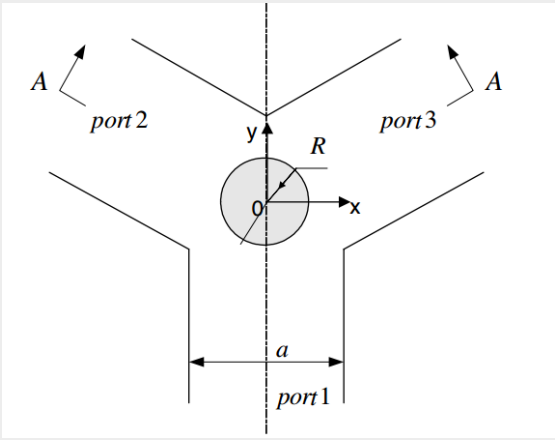

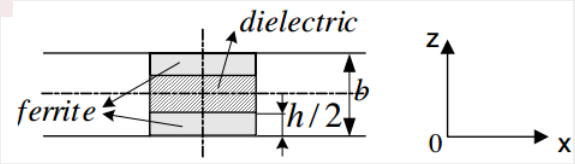

Scheme of a ferrite junction circulator

IV. Results

Case I: Ferrite magnetization parallel to the surface

- The external magnetic field employed to magnetize the ferrite slab is oriented in the *x*-direction.
- RF electromagnetic field is assumed to propagate along the possitive *z*-direction.
- An harmonic time dependence is implicitly assumed.
- Ferrites behave as ferrimagnetic materials when a DC magnetic field is applied. In this case, the magnetic anisotropy is described by the following permeability tensor:

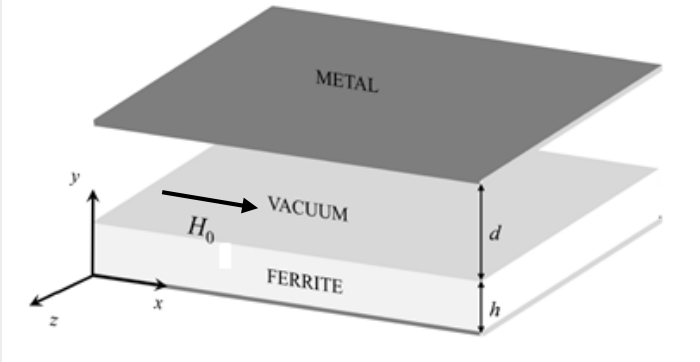

Case 1: Transversally parallel to the surface magnetized ferrite slab

$$\bar{\mu} = \begin{pmatrix} \mu_0 & 0 & 0 \\ 0 & \mu & j\kappa \\ 0 & -j\kappa & \mu \end{pmatrix}$$

$$\mu = \mu_0 \left(1 + \frac{\omega_0 \omega_m}{{\omega_0}^2 - {\omega_m}^2}\right)$$

$$\kappa = \mu_0 \frac{\omega \omega_m}{{\omega_0}^2 - {\omega_m}^2}$$

$$\omega_0 = \mu_0 \gamma H_0$$

$$\omega_m = \mu_0 \gamma M_s$$

$$\gamma = \frac{e}{m_e}$$

ω is the RF angular frequency

ω_0 is the Larmor frequency

ω_m is the saturation magnetization frequency

μ_0 is the vacuum magnetic permeability

γ is the gyromagnetic ratio of the electron

M_s is the saturation magnetization of the ferrite

IV. Results

Case I: Ferrite magnetization parallel to the surface

RF electromagnetic field computation

- In this case, the RF fields supported by the partially-loaded ferrite waveguide can be obtained analytically.
- Two families of electromagnetic field modes are found: TM^z (H_z = 0) and TE^z (E_z = 0).
- TE^z modes have no vertical electric field along the gap, so they are not suitable to hold a multipactor discharge. As a consequence, these modes will not be considered in this work.
- TM^z modes do have vertical electric field along the gap. The non-zero field components of such modes (in the vacuum region of the waveguide) are

Characteristic equation of TM^z modes $\longrightarrow$ $$\varepsilon_r k_1 \sinh(k_1 d)\cos(k_2 h) - k_2 \cosh(k_1 d)\sin(k_2 h) = 0$$

$$E_y(y,z,t) = \frac{V_0 k_1}{\sinh(k_1 d)}\cosh\left[k_1\left((d+h)-y\right)\right]\cos(\omega t - \beta z)$$

$$E_z(y,z,t) = -\frac{V_0 {k_1}^2}{\beta \sinh(k_1 d)}\sinh\left[k_1\left((d+h)-y\right)\right]\sin(\omega t - \beta z)$$

$$H_x(y,z,t) = -\frac{\omega \varepsilon_0}{\beta} E_y(y,z,t)$$

$${k_1}^2 \equiv \beta^2 - \omega^2 \mu_0 \varepsilon_0 \qquad {k_2}^2 \equiv \omega^2 \mu_0 \varepsilon_0 \varepsilon_r - \beta^2$$

ε_0 is the vacuum dielectric permittivity
ε_r is the relative dielectric permittivity of the ferrite
d is the separation between plates
β is the propagation factor
V_0 is the amplitude voltage

$$V_0 = \int_h^{d+h} E_y(y,0,0)\,dy$$

IV. Results

Case I: Ferrite magnetization parallel to the surface

The following partially filled ferrite waveguide was considered for multipactor simulations:

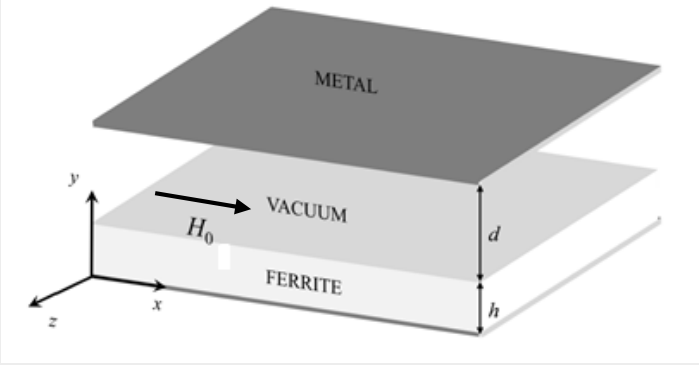

- Ferrite slab height, h = 3 mm
- Vacuum gap, d = 1 mm
- Saturation magnetization of the ferrite, M_S = 1790 Gauss
- Relative dielectric permittivity of the ferrite, ε_r = 15.5
- SEY parameters for the upper metallic waveguide wall (silver): W_1 = 30 eV , W_{max} = 165 eV , δ_{max} = 2.22
- The same SEY parameters are chosen for the ferrite surface
- Three different magnetization field values have been investigated, H_0 = 0 Oe, H_0 = 500 Oe, H_0 = 1000 Oe

IV. Results

Case I: Ferrite magnetization parallel to the surface

Multipactor susceptibility chart

- For H_0 = 0 Oe the ferrite exhibits no magnetic properties. Susceptibility chart is very similar to the classical metallic parallel-plate waveguide.
- For H_0 = 500 Oe and H_0 = 1000 Oe important variations in the multipactor voltage threshold regarding the H_0 = 0 Oe case are found.
- The multipactor discharge cannot appear below 1.3 GHzmm when Ho = 500 Oe. The same occurs below 2.4 GHzmm when H_0 = 1000 Oe.
- Electron trajectories are influenced by the ratio between the RF frequency and the cyclotron one.

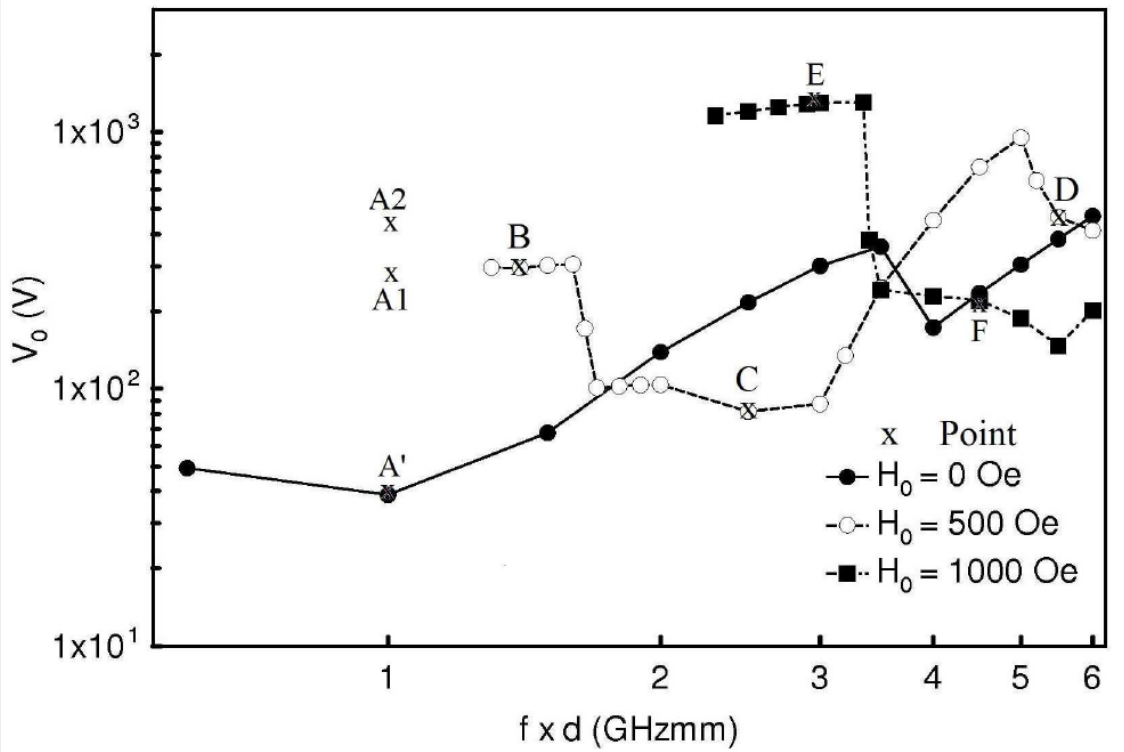

Multipactor voltage threshold as a function of the frequency gap value (gap remains fixed)

Cyclotron frequency $$f_c = \frac{1}{2\pi}\frac{e}{m_e}\mu_0 H_0$$

IV. Results

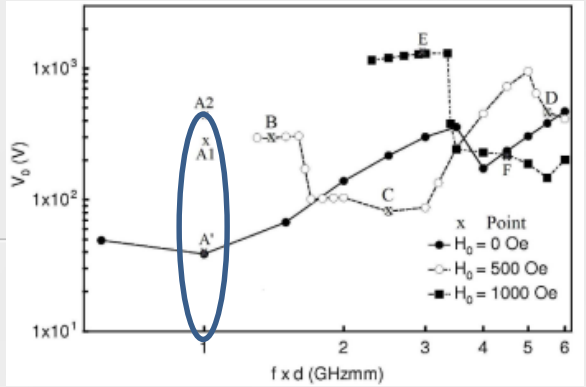

Case I: Ferrite magnetization parallel to the surface

Points A', A1, A2

f x d = 1 GHzmm

H_0 = 0 Oe

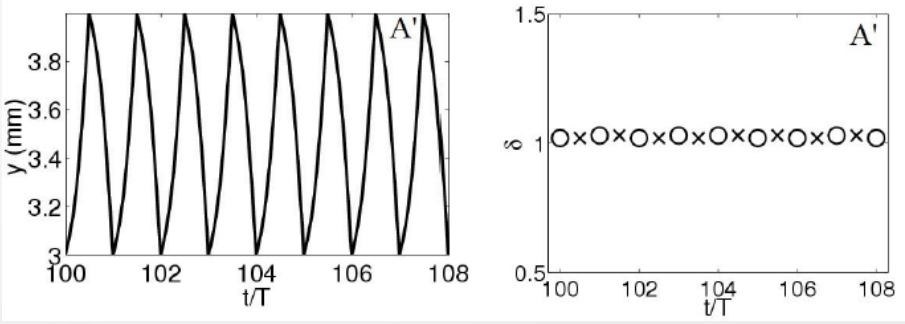

H_0 = 500 Oe

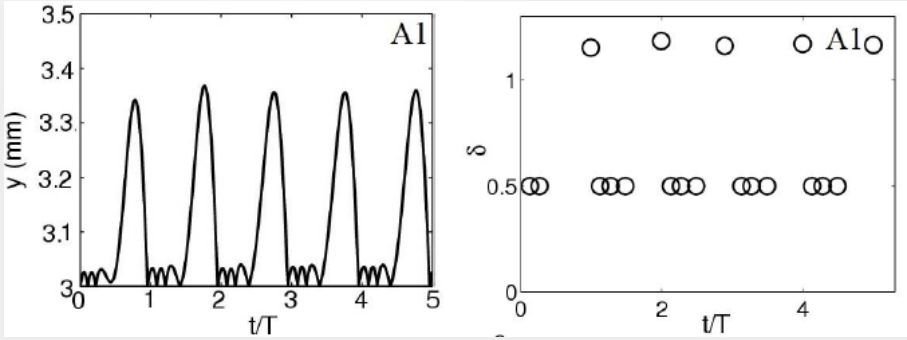

H_0 = 500 Oe

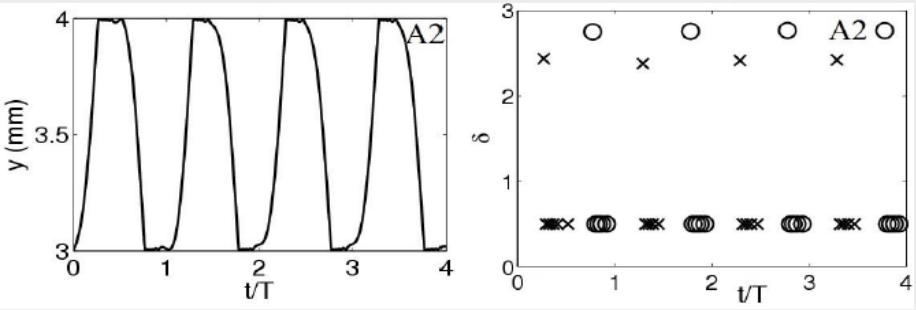

Point A':

- Double-surface multipactor discharge of order one.
- SEY slightly above the unity.

Point A1:

- No multipactor discharge.
- Single-surface electron trajectories are not synchronized with the RF electric field.
- Mean SEY below the unity.

Point A2:

- No multipactor discharge.
- RF voltage has increased regarding point A1.
- Double- and single-surface electron trajectories not synchronized with RF electric field.
- Mean SEY below the unity.

IV. Results

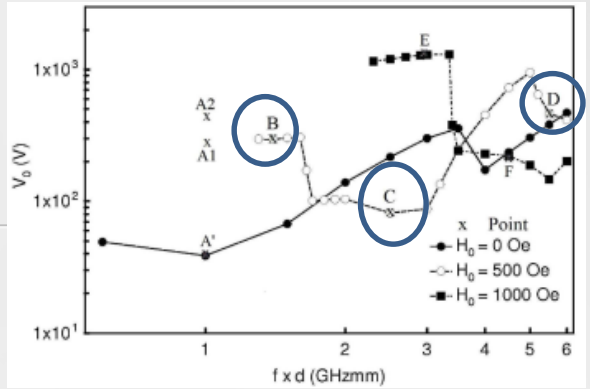

Case I: Ferrite magnetization parallel to the surface

Points B, C, D

H_0 = 500 Oe

fxd = 1.3 GHzmm

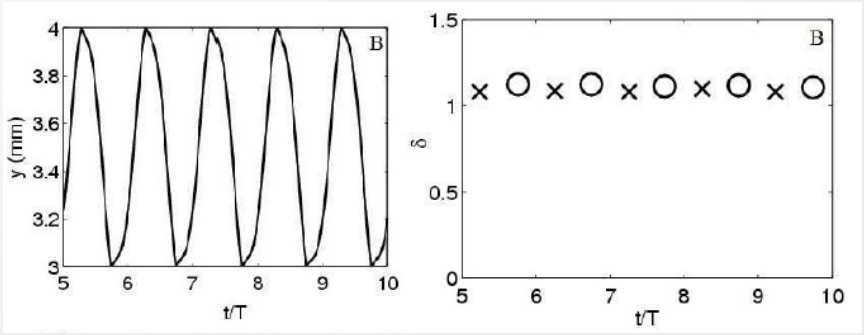

Point B:

- Double-surface multipactor of order one.
- SEY slightly above the unity.
- The ratio f_c/f increases regarding points A1 and A2, allowing higher flight time of the electron.

fxd = 2.5 GHzmm

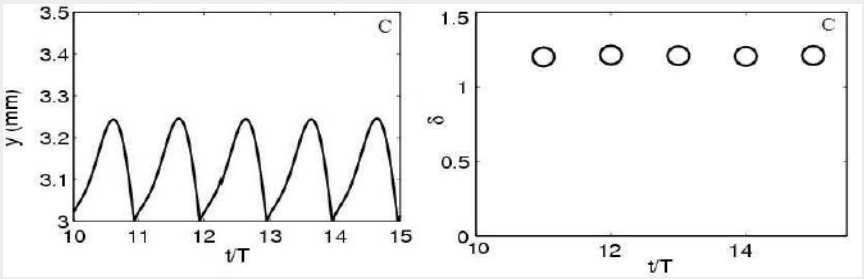

Point C:

- Single-surface multipactor of order two.
- SEY slightly above the unity.
- Multipactor voltage threshold has decreased regarding point B.
- Multipactor threshold value is below the H_0 = o Oe case.

fxd = 5.5 GHzmm

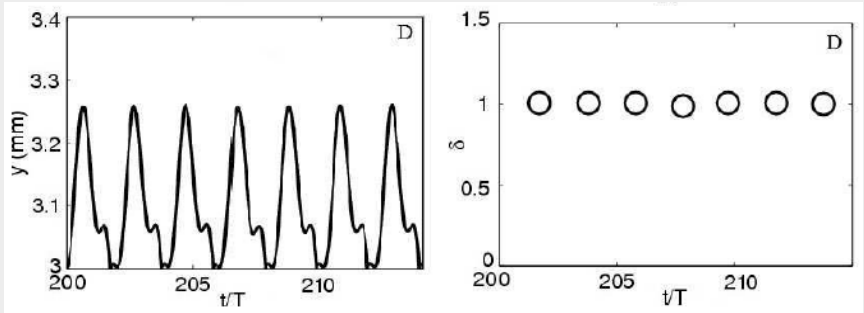

Point D:

- Single-surface multipactor of order four.
- SEY slightly above the unity.

IV. Results

Case I: Ferrite magnetization parallel to the surface

Points E, F

H_0 = 1000 Oe

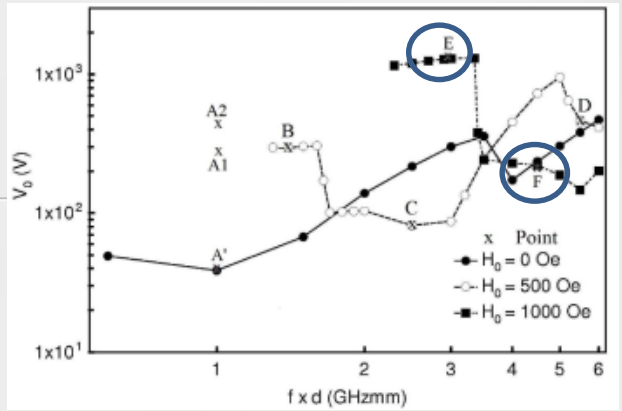

fxd = 2.7 GHzmm

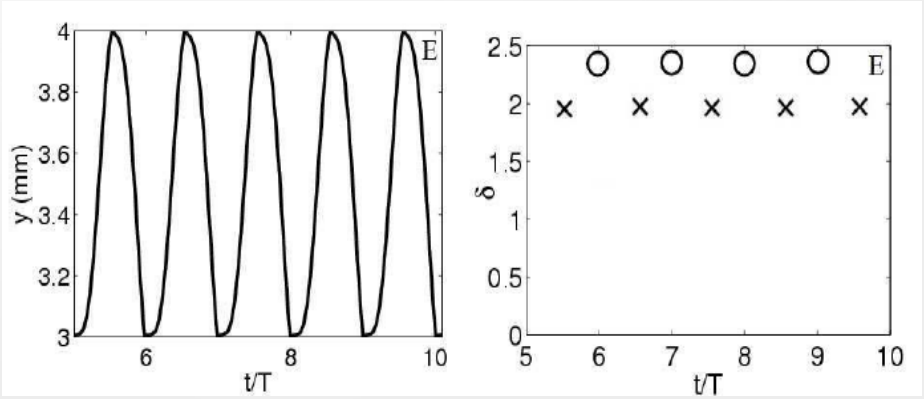

fxd = 4.5 GHzmm

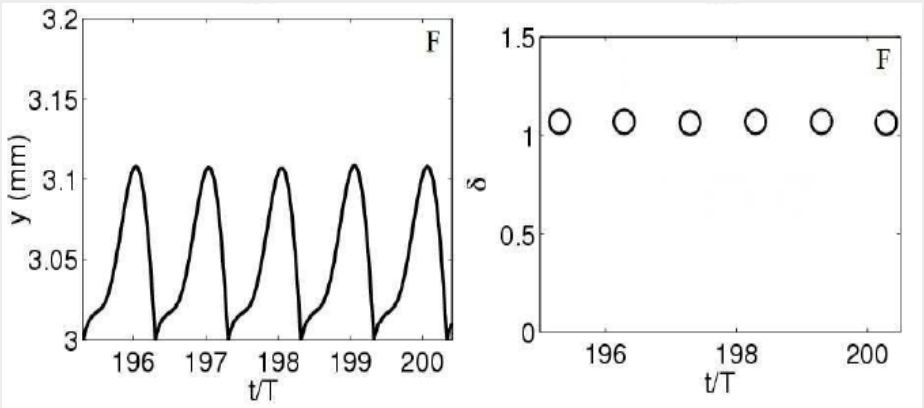

Point E:

- Double-surface multipactor of order one.
- SEY above the unity.

Point F:

- Single-surface multipactor of order two.
- SEY slightly above the unity.

- Note that there is a correspondence between points E, F and the points B, C; respectively.
- Actually, multipactor curve shape for cases H_0 = 1000 Oe and H_0 = 500 Oe are similar.
- These facts can be explained in terms of the f_c/f ratio: similar values of this quotient imply similar multipactor resonances.

IV. Results

Case II: Ferrite magnetization normal to the surface

- The external magnetic field employed to magnetize the ferrite slab is oriented in the *y*-direction.
- RF electromagnetic field is assumed to propagate along the positive *z*-direction.
- An harmonic time dependence is implicitly assumed.
- Ferrites behave as ferrimagnetic materials when a DC magnetic field is applied (H_0). In this case, the magnetic anisotropy is described by the following permeability tensor:

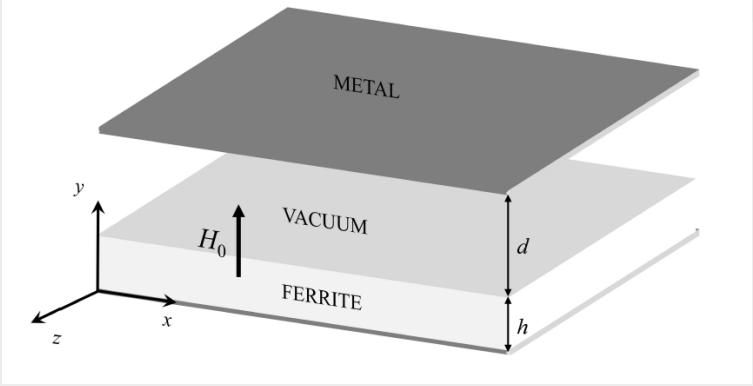

$$\bar{\mu} = \begin{pmatrix} \mu & 0 & -j\kappa \\ 0 & \mu_0 & j\kappa \\ j\kappa & 0 & \mu \end{pmatrix}$$

$$\mu = \mu_0 \left(1 + \frac{\omega_0 \omega_m}{{\omega_0}^2 - {\omega_m}^2}\right)$$

$$\kappa = \mu_0 \frac{\omega \omega_m}{{\omega_0}^2 - {\omega_m}^2}$$

$$\omega_0 = \mu_0 \gamma H_{ef}$$

$$\omega_m = \mu_0 \gamma M_s$$

$$H_{ef} = H_0 - M_s$$

$$\gamma = \frac{e}{m_e}$$

ω is the RF angular frequency

ω_0 is the Larmor frequency

ω_m is the saturation magnetization frequency

μ_0 is the vacuum magnetic permeability

γ is the gyromagnetic ratio of the electron

M_s is the saturation magnetization of the ferrite

H_{ef} is the effective magnetization field within the ferrite

IV. Results

Case II: Ferrite magnetization normal to the surface

RF electromagnetic field computation

There is no analytical solution in this case, hence a numerical method must be employed. Here we will use the Coupled Mode Method (CMM):

- Numerical method in the frequency domain, originally formulated by Schelkunoff, used for analyzing the electromagnetic wave propagation inside waveguides that contain any isotropic, anisotropic or complex medium.
- The EM field components in the loaded waveguide are expanded in terms of linear combinations of the components of the EM of an empty parallel plate waveguide (method of moments).
- Can be applied in both open and closed structures.
- Provides an approximated solution of the propagation problem inside the waveguide:
  - Propagation constants
  - Profile of the electromagnetic field components

IV. Results

Case II: Ferrite magnetization normal to the surface

The following partially filled ferrite waveguide was considered for multipactor simulations:

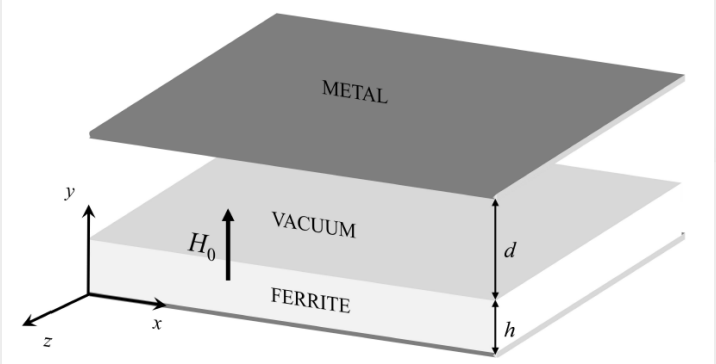

- Waveguide height, $d+h$ = 10.16 mm (WR-90 rectangular waveguide)
- Saturation magnetization of the ferrite, M_S = 1806 Gauss
- Relative dielectric permittivity of the ferrite, ε_r = 15
- SEY parameters for the ferrite slab are W_1 = 19 eV , W_{max} = 289 eV , δ_{max} = 2.88
- The same SEY parameters are chosen for the upper metallic wall
- The external magnetization field is H_0 = 3000 Oe, thus H_{ef} = 1194 Oe $\quad H_{ef} = H_0 - M_s$
- The propagation of the fundamental mode is assumed

IV. Results

Case II: Ferrite magnetization normal to the surface

Propagation factor for the fundamental mode of the parallel-plate ferrite loaded waveguide

Propagation factor

$$\Gamma = Re(\Gamma) + jIm(\Gamma)$$

$$\vec{E}(\vec{r}) = \vec{E}_0(x,y)e^{-\Gamma z} = \vec{E}_0(x,y)e^{-Re(\beta)z}e^{-j\,Im(\beta)z}$$

- The fundamental mode is propagative within the explored frequency range (0.5-20.0 GHz)
- At 3.34 GHz (Larmor frequency) it is observed a sharp variation in the propagation factor due to the gyromagnetic resonance

$$\omega_0 = \mu_0 \gamma H_{ef}$$ Larmor frequency

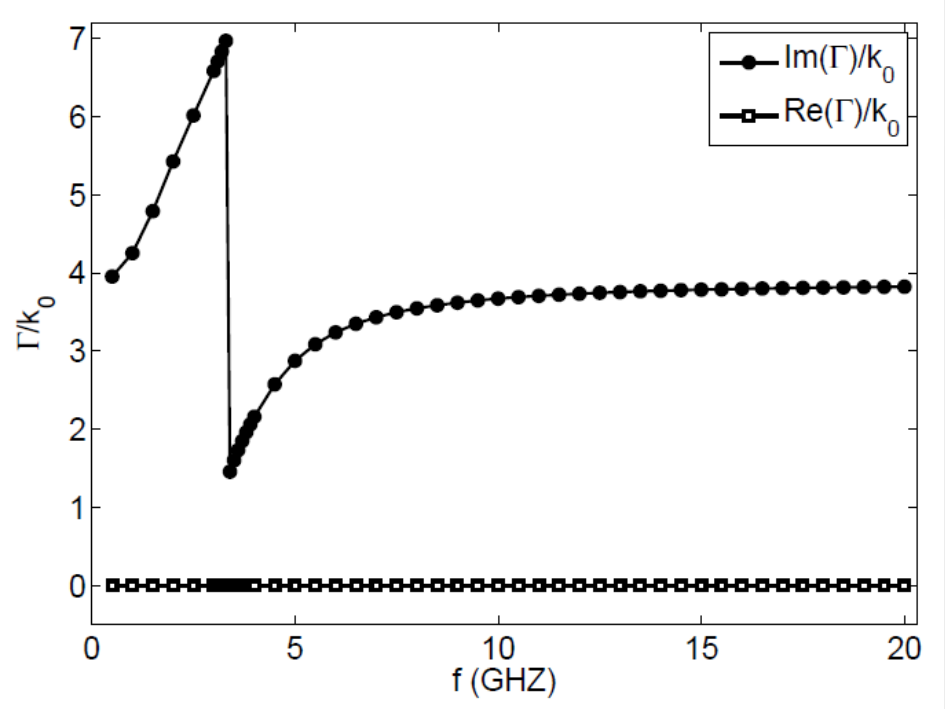

$$k_0 = \frac{\omega}{c}$$

Real and imaginary parts of the propagation factor for a ferrite loaded waveguide with d = 1 mm as a function of the RF frequency

IV. Results

Case II: Ferrite magnetization normal to the surface

Multipactor RF voltage threshold as a function of the frequency-gap product for several waveguides

- It is varied the gap and the ferrite height but with the constraint d+h = 10.16 mm
- The without ferrite case represents a classical metallic parallel-plate waveguide with no external magnetization field.

At the view of the results:

- ➢ There is notorious difference in the multipactor RF voltage threshold between the without ferrite case and the ferrite-loaded waveguides.
- ➢ The difference between the without ferrite and the ferrite cases increases with the frequency gap value.
- ➢ It is found that the bigger the gap the higher the discrepancies with the without ferrite case. For d = 0.2 mm waveguide the maximum difference is 6.5 dB, for the d = 1.0 mm is 26 dB, and for the d = 2 mm case is 35 dB.

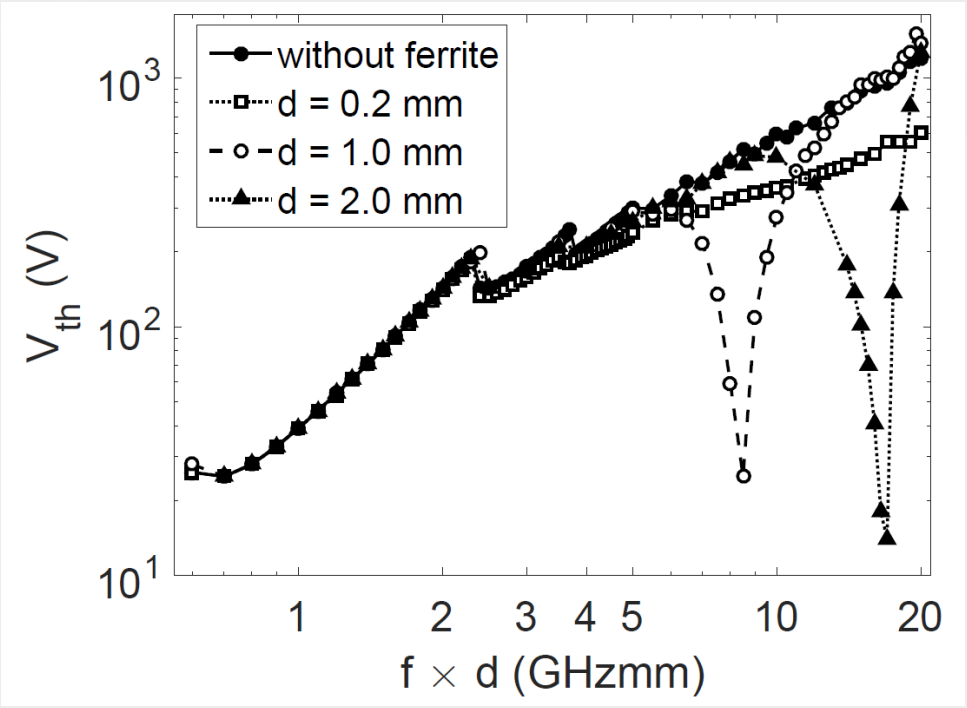

IV. Results

Case II: Ferrite magnetization normal to the surface

In order to get a better understanding of the multipactor RF voltage threshold curves, it is crucial to analyze:

RF electromagnetic fields (spatial distribution, scale analysis of the different components)
Electron dynamics (find resonant electron trajectories and multipactor order)

Explicitly, the equations of motion for the effective electron (at the early stages of the electron multiplication when $\vec{E}_{sc} \approx 0$ and $\vec{E}_{pol} \approx 0$) are

$$\frac{dv_x}{dt} = \frac{e}{m_e}\left[-E_{RF,x} + \left(B_0 + B_{RF,y}\right)v_z - B_{RF,z}v_y\right]$$

$$\frac{dv_y}{dt} = \frac{e}{m_e}\left[-E_{RF,y} - B_{RF,x}v_z + B_{RF,z}v_x\right]$$

$$\frac{dv_z}{dt} = \frac{e}{m_e}\left[-E_{RF,z} + B_{RF,x}v_y - \left(B_0 + B_{RF,y}\right)v_x\right]$$

The analysis of the RF magnetic field components revealed that the terms in the form $v_i\, B_{RF,j}$ have very little influence in the electron dynamics.

In fact, they can be removed from the differential equations of motion

IV. Results

Case II: Ferrite magnetization normal to the surface

With regard to the RF electric field components, it is found that they are in the same magnitude order and, as a consequence, none of them can be neglected in the equations of motion

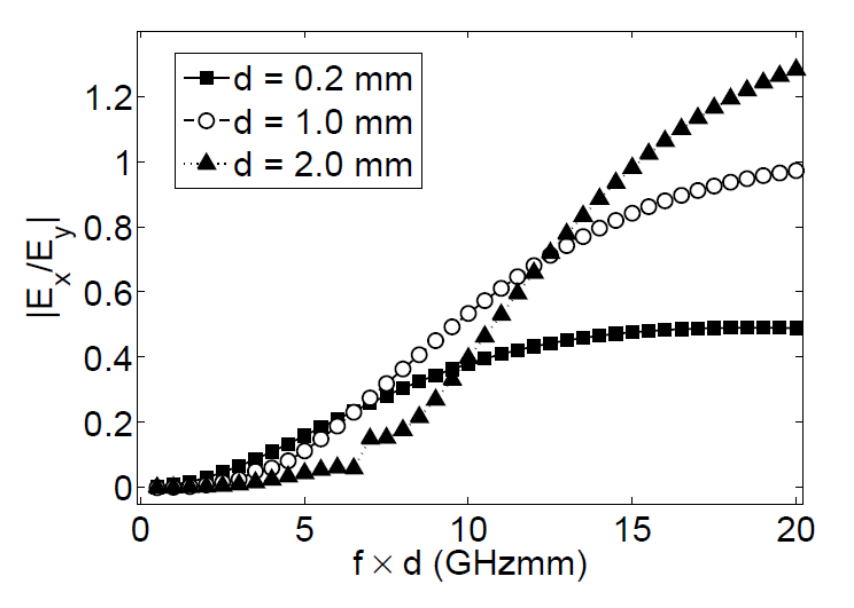

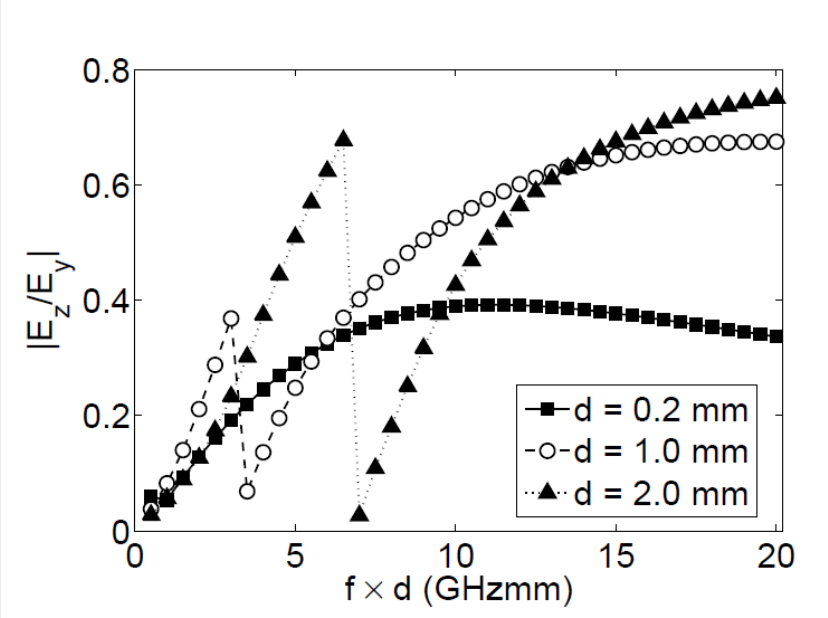

Left (right): quotient between the maximum absolute value along the gap of the $E_{RF,x}$ ($E_{RF,z}$) and $E_{RF,y}$ components for the ferrite loaded waveguides.

- In most of the cases the E_{RFy} component is greater than E_{RFx} and E_{RFz}.
- E_{RFx}/E_{RFy} and E_{RFz}/E_{RFy} quotients tend to increase with the frequency gap product, and the higher the gap the higher the increase of the quotients is.

IV. Results

Case II: Ferrite magnetization normal to the surface

Back to the simplified equations of motion, they can be expressed in the following form:

$$\frac{dv_x}{dt} \approx \omega_c v_z - \frac{e}{m_e} E_{RF,x} \cos(\omega t + \phi) \quad (1)$$

$$\frac{dv_y}{dt} \approx -\frac{e}{m_e} E_{RF,y} \cos(\omega t + \phi) \quad (2)$$

$$\frac{dv_z}{dt} \approx -\omega_c v_x - \frac{e}{m_e} E_{RF,z} \sin(\omega t + \phi) \quad (3)$$

- y-equation becomes decoupled from the x and z coordinates
- In fact, y-equation becomes the corresponding one to the well-known classical case without ferrite
- The effect of the static field H_0 is to spin the electron orbits in the xz-plane

$\omega_c = \frac{e}{m_e}\mu_0 H_0$ cyclotron angular frequency $\quad \omega = 2\pi f$ RF angular frequency $\quad \phi$ RF field phase

Manipulating (1) and (3):

$$\frac{d^2 v_x}{dt^2} + {\omega_c}^2 v_x = A_1 \sin(\omega t + \phi) \quad (4)$$

$$\frac{d^2 v_z}{dt^2} + {\omega_c}^2 v_z = A_2 \cos(\omega t + \phi) \quad (5)$$

$$A_1 = \frac{e}{m_e}\left(E_{RF,x,0}\omega - E_{RF,z,0}\omega_c\right)$$

$$A_2 = \frac{e}{m_e}\left(E_{RF,x,0}\omega_c - E_{RF,z,0}\omega\right)$$

(4) and (5) can be analytically solved provided if spatial uniformity of the RF field is assumed

$$v_x = \frac{A_1}{{\omega_c}^2 - \omega^2}\sin(\omega t + \phi) - \frac{A_1 \sin\phi}{{\omega_c}^2 - \omega^2}\cos(\omega_c t) - \frac{A_2 \cos\phi}{{\omega_c}^2 - \omega^2}\sin(\omega_c t) \quad (6)$$

$$v_z = \frac{A_2}{{\omega_c}^2 - \omega^2}\cos(\omega t + \phi) - \frac{A_2 \cos\phi}{{\omega_c}^2 - \omega^2}\cos(\omega_c t) + \frac{A_1 \sin\phi}{{\omega_c}^2 - \omega^2}\sin(\omega_c t) \quad (7)$$

- It is assumed zero initial x and z velocities
- (6) and (7) are valid except for $\omega = \omega_c$
- The amplitude of the oscillatory terms is maximum in the neighborhood of $\omega = \omega_c$

IV. Results

Case II: Ferrite magnetization normal to the surface

Thus, there is a maximum kinetic energy gain for v_x and v_z in the neighborhood of the cyclotron resonance and, as a consequence, there is a minimum in the multipactor RF voltage threshold

d = 0.2 mm, f_c = 8.4 GHz, f_c x d = 1.68 GHzmm

d = 1.0 mm, fc = 8.4 GHz, fc x d = 8.4 GHzmm

d = 2.0 mm, fc = 8.4 GHz, fc x d = 16.8 GHzmm

Sharp minimums in the RF multipactor voltage threshold due to the cyclotron resonance

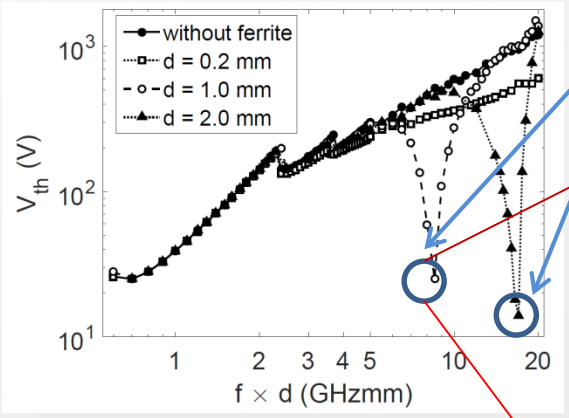

- It is a noticeable increase in the amplitude of the v_x and v_z in the successive oscillations
- In v_y is not observed such an amplitude increment
- Trajectory in the xz-plane is very similar to those of an electron in a cyclotron accelerator

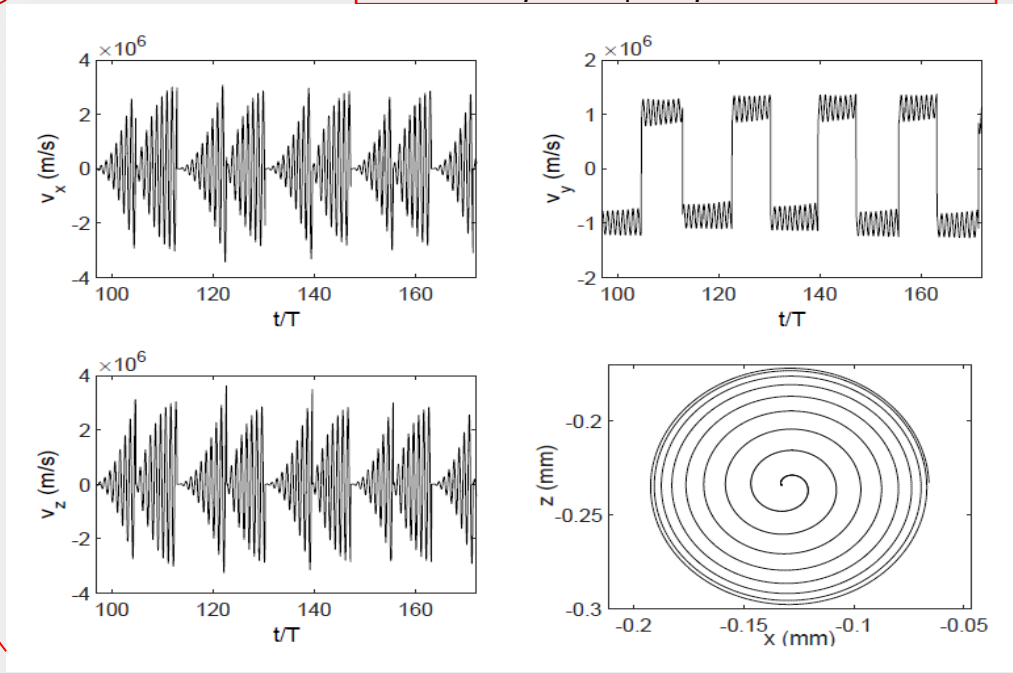

From left to right, and up to down: effective electron velocity components as a function of the time normalized to the RF period (T), and xz-plane electron trajectory. All for a ferrite waveguide with d = 1 mm, f x d = 8.5 GHzmm, V_0 = 25 V

IV. Results

Case II: Ferrite magnetization normal to the surface

However, it is notorious that the multipactor RF voltage minimum was not observed for the case of d = 0.2 mm waveguide

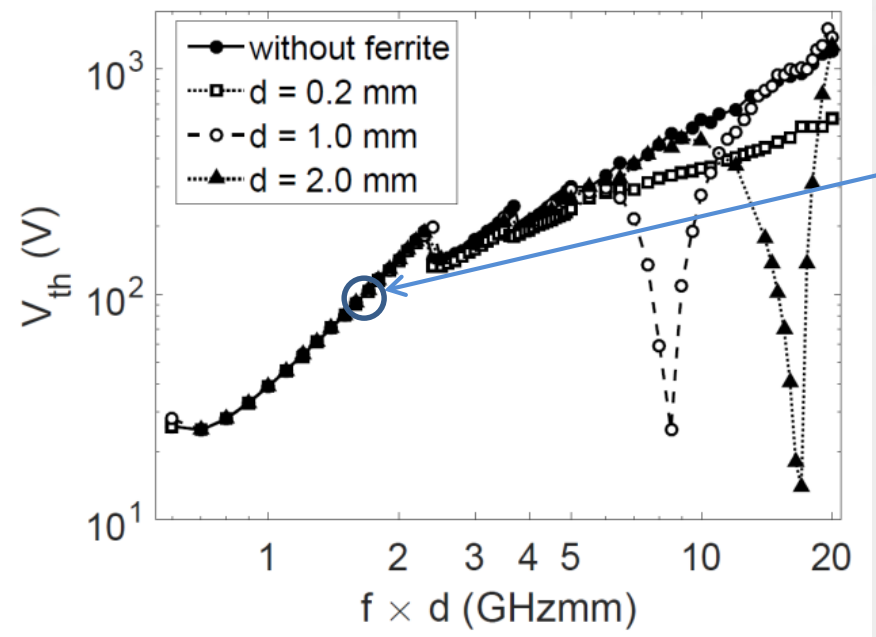

cyclotron resonance

d = 0.2 mm, f_c = 8.4 GHz, f_c x d = 1.68 GHzmm

To understand this point, it is required to recall at some aspects of the classic multipactor theory for parallel-plate waveguides

IV. Results

Case II: Ferrite magnetization normal to the surface

- As argued before, the y-equation of motion, in first approximation, becomes the same that the classical parallel-plate case (without ferrite nor external magnetic field)
- Consequently, double-surface electron resonant modes will appear in the ferrite-loaded waveguide.
- Note that the higher is the frequency gap, the higher is the order of the modes available
- Despite the classical parallel-plate waveguide, in the ferrite case, there is an acceleration in the xz-plane due to the cyclotron resonance effect (which is maximum when $\omega = \omega_c$)
- In the case d = 0.2 mm, the cyclotron resonance occurs at very low f x d, consequently only low order modes are available (with short time between successive impacts), thus no substantial gain in the transverse plane kinetic energy is obtain and the multipactor voltage threshold cannot be reduced

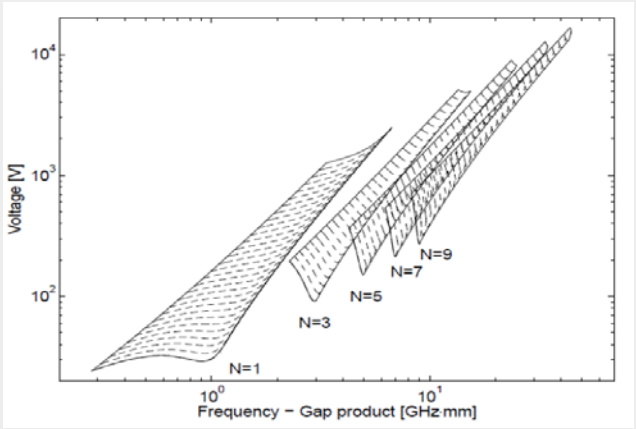

Multipactor resonant modes for the classic metallic paralell-plate waveguide

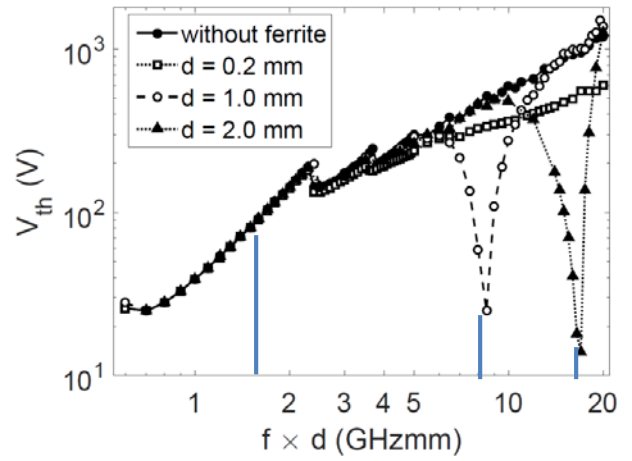

d = 0.2 mm, f_c x d = 1.68 GHzmm
d = 1.0 mm, f_c x d = 8.4 GHzmm
d = 2.0 mm, f_c x d = 16.8 GHzmm

IV. Results

Case II: Ferrite magnetization normal to the surface

For completeness, the multipactor RF voltage threshold curve for a big gap ferrite slab with d = 5.0 mm is computed

- Again it appears a sharp minimum in the multipactor RF voltage threshold for the cyclotron resonance
- It is worth mentioning that the typical frequency gap region at which the multipactor is explored does not exceed the 10 GHzmm
- For higher values than 10 GHzmm, the multipactor RF voltage threshold becomes very high (with regard to the typical working voltage levels of communication satellite devices)
- However, with ferrite devices, it is shown that the multipactor RF voltage can drop to very low values even for very high frequency values at which the discharge should not be expected
- As a consequence, detailed multipactor analysis of ferrite components are required in order to prevent the discharge

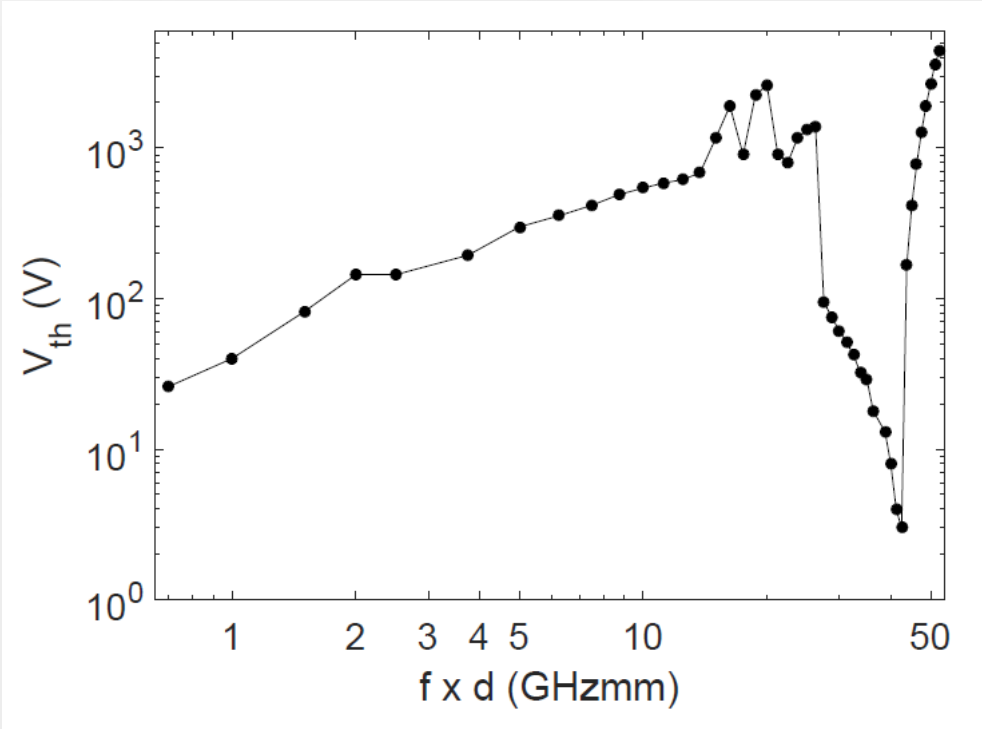

d = 5.0 mm, f_c = 8.4 GHz, f_c x d = 42 GHzmm

IV. Results

Case II: Ferrite magnetization normal to the surface

Finally, it has been analyzed the case of having different SEY coefficients for the ferrite and the metal surface

SEY parameters for silver,

$W_1 = 30$ eV, $W_{max} = 165$ eV, $\delta_{max} = 2.22$

SEY parameters for ferrite

$W1 = 19$ eV, $W_{max} = 289$ eV, $\delta_{max} = 2.88$

- It is observed slight difference between the two multipactor RF voltage threshold curves
- Multipactor RF voltage threshold tends to be higher in the ferrite and silver SEY case
- W_1 for silver is higher than for the ferrite and, consequently, more RF voltage amplitude is required in the former case to reach the multipactor threshold

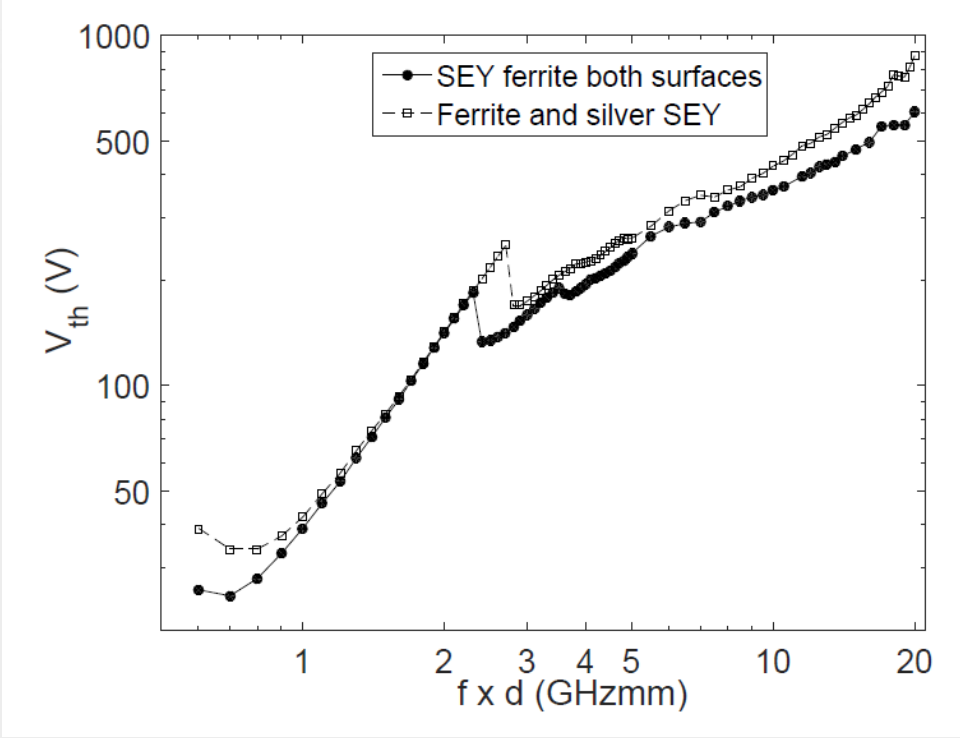

Multipactor RF voltage threshold as a function of the frequency gap for a ferrite waveguide with *d* = 0.2 mm, considering the same SEY properties for both surfaces and considering different SEY for ferrite and metal (silver) surfaces

IV. Results

Conclusions

- Multipactor effect in a parallel-plate waveguide containing a magnetized ferrite slab has been studied.

- Two different directions of magnetization (parallel and normal to the ferrite slab) have been considered, finding different behaviors in the multipactor susceptibility curves for each case.

- For the parallel magnetization case, it is found multipactor free zones for low frequency gap zones. For higher frequency gap values the multipactor discharge can appear even at voltage values below the classical parallel-plate case multipactor voltage threshold.

- For the normal magnetization case, the multipactor voltage threshold remains very similar to the classical parallel-plate case. However, as the frequency gap increases the multipactor voltage threshold tends to drop below the classical parallel-plate case, specially when the RF frequency is in the neighborhood of the cyclotron one.

IV. Results

Publications

[1] D. González-Iglesias, B. Gimeno, V. E. Boria, Á. Gómez and A. Vegas, "Multipactor effect in a parallel-plate waveguide partially filled with magnetized ferrite", *IEEE Transactions on Electron Devices*, vol. 61, no. 7, pp. 2552-2557, July 2014.

[2] D. González-Iglesias, Á. Gómez, B. Gimeno, Ó. Fernández, A. Vegas, F. Casas, S. Anza, C. Vicente, J. Gil, R. Mata, I. Montero, V. E. Boria, D. Raboso, "Analysis of multipactor RF Breakdown in a waveguide containing a transversely magnetized ferrite", *IEEE Transactions on Electron Devices*, vol. 63, no. 12, pp. 4939-4947, Dec. 2016.

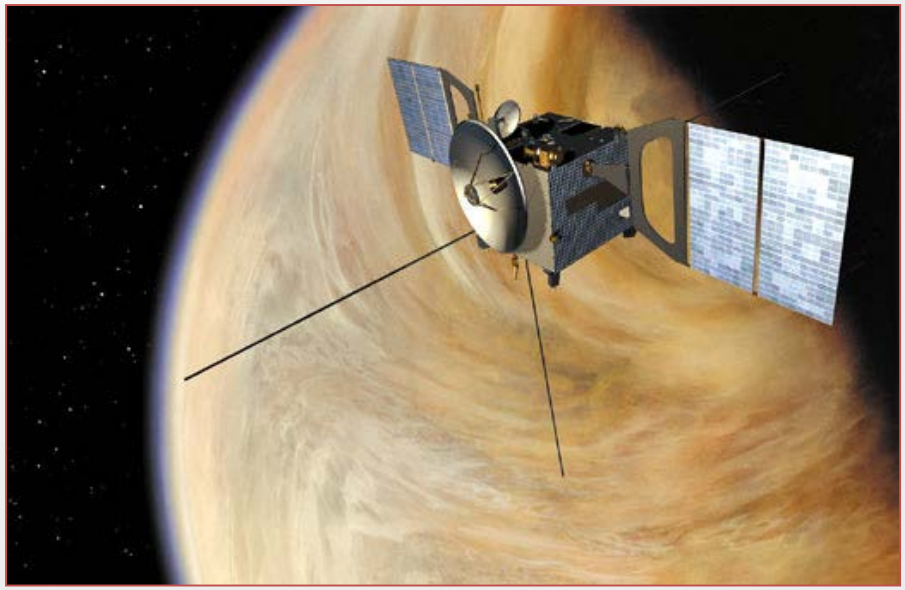

Thanks for your attention

IV. Results

Multipactor simulations with the effective electron code (V)

BPSK without filtering

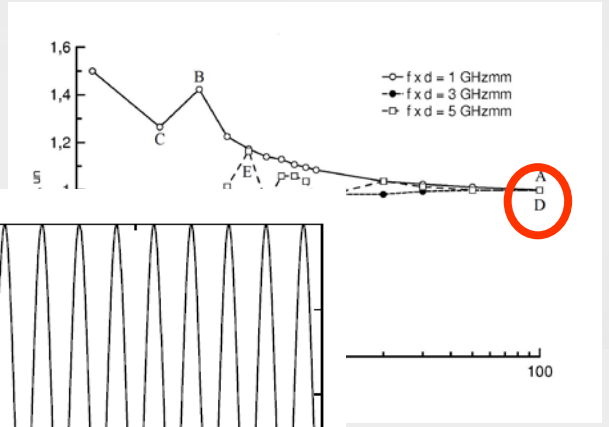

Point D

$f \times d = 5$ GHzmm

$\xi = 100$

- Scenario very close to the unmodulated one (100 RF periods between successive phase shifts)

- Flight time between conductors:

From inner to outer → 1.49 T

From outer to inner → 2,51 T

Multipactor order → 3 + 5

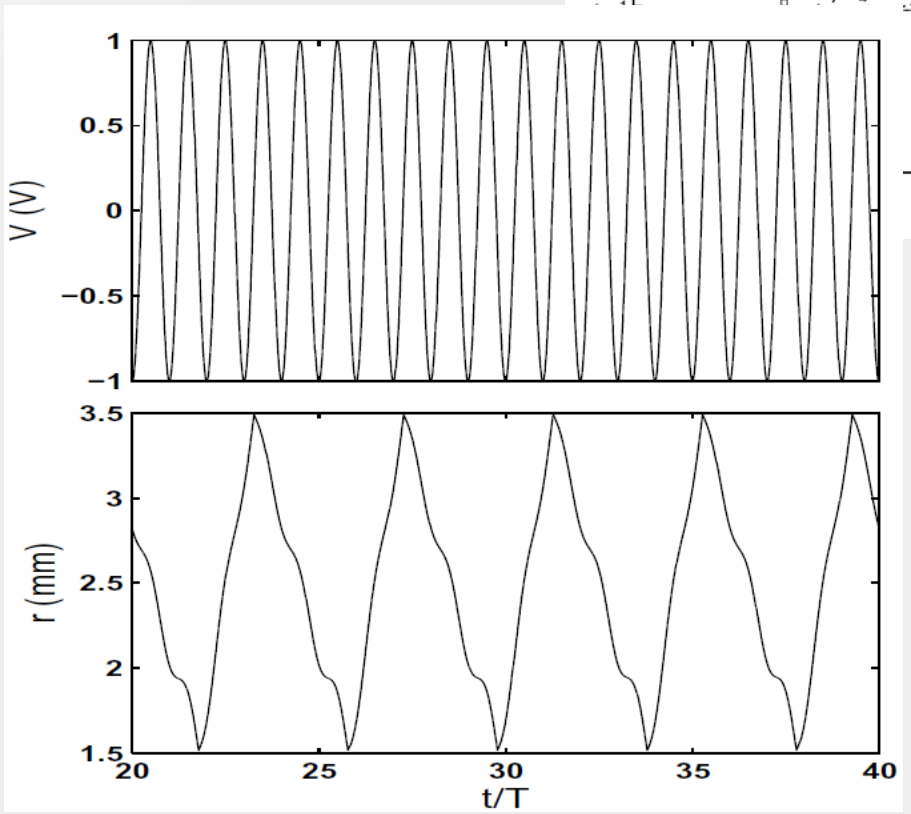

IV. Results

Multipactor simulations with the effective electron code (VI)

BPSK without filtering

Point E

$f \times d = 5$ GHzmm

$\xi = 5$

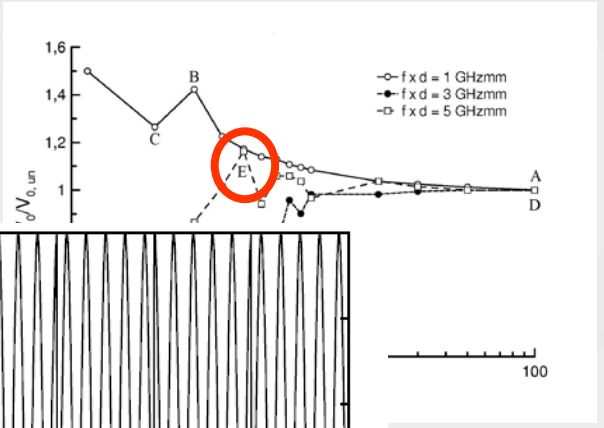

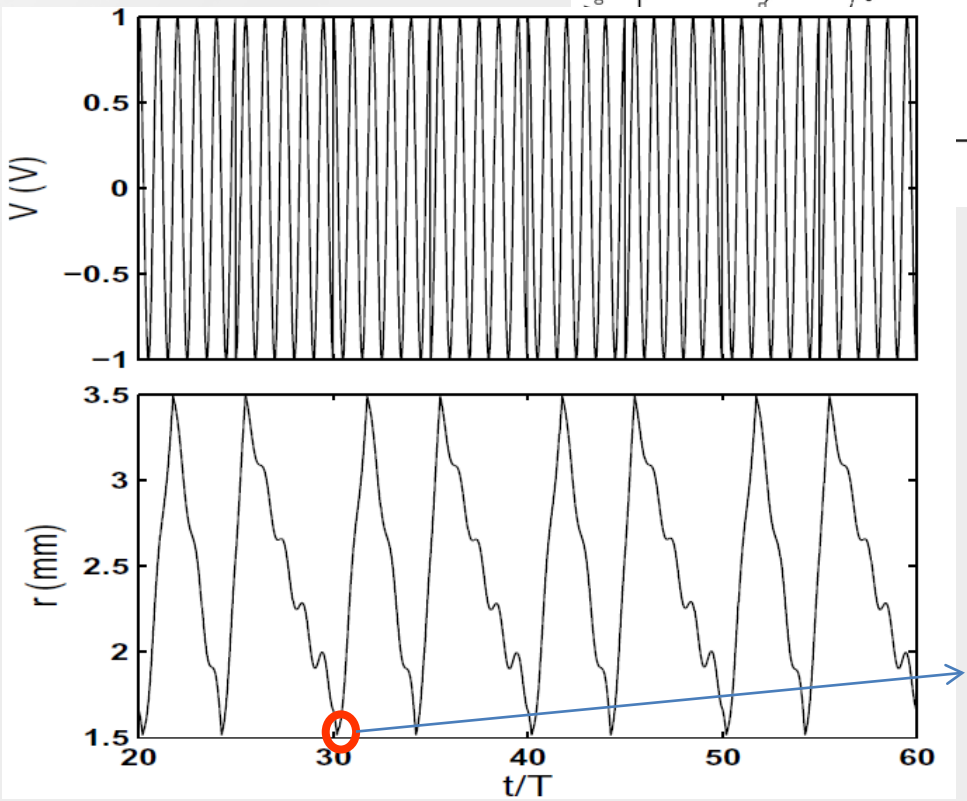

- Trajectory more complex than in point D: 4 impacts before repeating the sequence
- Flight times (in terms of T): 1.58, 2.47, 1.23, 4.72

SEY below unity ($\delta<1$) for these impacts

IV. Results

Multipactor simulations with the effective electron code (VII)

BPSK without filtering

Point F

$f \times d = 5$ GHzmm

$\xi = 2$

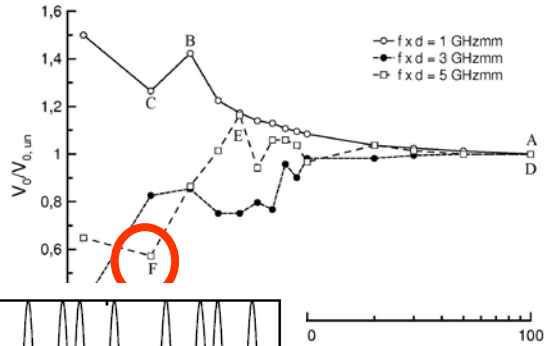

- Trajectory simple (similar to point D): 2 impacts before repeating the sequence

- Flight times between conductors:

From outer to inner → 2.16 T

From inner to outer → 1.84 T